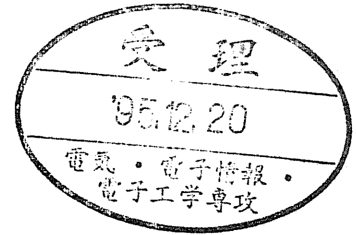

3·337

Studies of High Quality InP Layers Heteroepitaxially Grown on Si Substrates by Epitaxial Lateral Overgrowth

(横方向成長によるSi基板上の InP
ヘテロエピタキシーに関する研究)

A Thesis Presented to
the Graduate School of the University of Tokyo
in Partial Fulfillment of the Requirements
for the Degree of Doctor of Engineering

by

Shigeya Naritsuka

Dissertation Supervisor

Professor Tatau Nishinaga

Acknowledgments

The works described in this thesis have been carried out at the University of Tokyo, during the period from 1993 to 1995.

I greatly appreciate my dissertation supervisor, Professor Tatau Nishinaga for his guidance and support. His enthusiasm for the research has provide the motivation to undertake and complete this work. I learned from him not only the way of researching but also the attitude of mind to work and life. I would like to thank Dr. Masaaki Tanaka, associate professor in this laboratory, for his useful discussion and encouragements. The author would like to thank his thesis committee Professor K. Tada, Professor T. Kamiya, Professor K. Hoh and Professor Y. Arakawa, University of Tokyo for their time and input.

I am also very grateful to Dr. Xu-Qiang Shen for his interesting discussion and Ms. Masako Washiyama for the constant support and help. I am also indebted to my colleagues in Nishinaga laboratory for providing such good advice and collaborations. I am particularly grateful to Messers. Y.S.Chang, Yasuhiko Matsunaga, Hiroshi Kawano and Yuuichiro Matsuda for their experimental help.

I am very grateful to Drs. Hidefumi Mori and Masami Tachikawa, NTT Opto-electronics Laboratories for the growth of InP-coated Si substrates and their fruitful discussion. I also like to thank Dr. Takeshi Yamada, NTT Opto-electronics Laboratories for the useful discussion about the growth of MQW layers.

I would like to thank Dr. Wu-yih Uen, associate professor, Chung Yuan Christian Unversity, Taiwan for providing good advice and discussion.

Finally, I owe to considerable debts to my parents who encouraged me throughout these years. My deepest thank is to my wife for her continuing support and encouragement. My son and daughter gave me a lot of pleasure and challenging spirits for research.

Contents

1 Introduction **4**

1.1 Historical Background 6

1.2 Motivation of this Research 9

2 Epitaxial Lateral Overgrowth of InP on InP Substrates **13**

2.1 Introduction 13

2.2 Substrate Preparation 14

2.3 LPE Growth System 16

2.4 ELO by LPE 17

2.5 ELO of InP on (001) InP Substrates 19

2.6 Sn doping to improve ELO ratio 22

2.7 ELO of InP on (111) InP Substrates 24

2.8 Dislocations in ELO Layers 26

2.9 Summary 27

3 Epitaxial Lateral Overgrowth of InP on InP-coated Si Substrates **55**

3.1 Introduction 55

3.2 Modification of ELO for InP-coated Si Substrate 56

3.3 ELO of InP on InP-coated Si Substrates 58

3.4 Doping Effects 62

3.5 Dislocations in ELO layers 63

3.6 Summary 65

4 **Characterization by Spatially Resolved Photoluminescence** **87**

4.1 Introduction 87

4.2 SRPL Measurement 89

4.3 SRPL of InP ELO on InP Substrates 89

4.4 SRPL of InP ELO on InP-coated Si Substrates 91

4.5 SRPL of MQW 94

4.6 Stress Calculation by Finite Element Method 95

4.7 Microchannel Epitaxy 99

4.8 Summary 101

5 **Conclusions** **125**

A **Critical Width for Michrochannel** **129**

B **Heteroepitaxial ELO of InP on InGaAs Layers** **13** Printer

Chapter 1

Introduction

The advances which have been made in epitaxial growth processes recently have been truly remarkable. Not only bulk crystallization but also epitaxy[1] has been studied vigorously. A lot of new epitaxial techniques have been developed, such as molecular beam epitaxy (MBE)[2], metalorganic chemical vapor deposition (MOCVD)[3], migration-enhanced epitaxy (MEE)[4], atomic layer epitaxy (ALE)[5] and etc. Using these techniques various kinds of materials have been grown homoepitaxially or heteroepitaxially. Heteroepitaxy means a epitaxial growth of a material which differs from a substrate used for the growth. Lattice matched heteroepitaxial growth systems, such as AlGaAs growth on GaAs, InGaP growth on GaAs and InGaAsP growth on InP, have been used in very wide fields of applications and various kinds of devices, for examples, high electron mobility transistor (HEMT)[6], heterobipolar transistor (HBT)[7] and laser diode[8] are being fabricated to make our daily lives comfortable. Heteroepitaxy is not only limited in lattice-matched systems but also has a wide field of lattice-mismatched systems. Lattice-mismatched heteroepitaxy, in particular highly mismatched heteroepitaxy (HM^2) is one of the very interesting subjects in crystal growth, which is a main subject of this thesis. To perform HM^2, a lot of difficulties should be overcome. The main three difficulties are as follows.

The first difficulty comes from the difference in the crystal structure between a grown layer and a substrate. III-V material growth on Si has this kind of difficulty.

Namely, III-V material has zinc blende structure while Si has diamond structure. In other words, III-V materials are polar semiconductors, which consist of two kinds of atoms, while Si is a non polar semiconductor, which consists of one kind of atoms. Consequently antiphase domains (APDs) are produced in the grown III-V layer because the diamond structure does not show which atoms should come to a crystal site in the III-V layer.

The second difficulty comes from the difference in the lattice constants between the grown layer and the substrate, which produces stress in the grown layer. Misfit dislocations are introduced when the strain energy exceeds a critical value for the formation[9]. On the other hand, the stress in the grown layer changes the growth mode from Frank-van der Merwe to Stranski-Krastanov or Volmer-Weber. Therefore, layer by layer growth mode can not be maintained under stress and 3-dimensional islands of the grown material are formed on the surface of the substrate during growth. Twins or stacking faults are produced on the facets formed on the 3-dimensional islands or at the boundary where two 3-dimensional islands meet to each other. Therefore a lot of dislocations and defects are produced in the grown layers.

The third difficulty comes from the difference in the thermal expansion coefficient between the grown layer and the substrate. Stress is produced due to the difference in the thermal expansion coefficient during the cooling process after growth. The stress causes misfit dislocations and threading dislocations in the grown layers. A part of this stress remains after the cooling process. It is reported that residual strain in GaAs and InP layers grown on a Si substrate is respectively about 1.5×10^{-3} and 0.4×10^{-3}[10]. On the other hand, it is reported that more than 10^6 cm^{-2} dislocations are generated in a GaAs layer on a Si substrate during the cooling process even if the dislocation density is 10^4 cm^{-2} at the growth temperature[11].

These difficulties should be overcome to grow heteroepitaxial layers with excellent characteristics sufficient for device fabrications. To tide over these difficulties a lot of researches and methods are proposed. We will describe the works in

more detail in the following section. After the break-through of these difficulties, excellent HM^2 can be realized.

HM^2 will open a large application field. Opto-electronic integrated circuit (OEIC) is one of the example. For instance, GaAlAs lasers can be fabricated on a Si LSI chip. HM^2 also provides new substrates, which can not be obtained by ordinary bulk crystallizations. The characteristic of a GaAlAs HEMT is improved by using an InGaAs channel. The InGaAs channel can be grown without residual stress and dislocations on a InGaAs substrate, which is difficult to be obtained by an ordinary bulk crystallization. Moreover, HM^2 offers large freedom to device design. Various kinds of materials will be grown on one substrate by HM^2. For example, InGaAsP lasers, GaAs HEMTs, InGaP red diodes, InGaAlAs green diodes and GaN blue diodes can be grown on a Si VLSI to form a new system.

1.1 Historical Background

The way for HM^2 was cut through by the GaAs growth on Si substrates. The combination of GaAs and Si overcomes a weak point of Si which can not emit light because it is an indirect semiconductor. The GaAs growth on Si has been extensively investigated by many researchers since the success of the growth may realize OEICs. Some of the major difficulties in the GaAs growth on Si have been solved by the proposal of the two-step growth process[12]. In the two-step growth process the growth is initiated at low temperature and subsequent growth is performed at a higher (normal) growth temperature. A low growth temperature of around 300 °C leads to good coverage of the Si substrate and less formation of 3-dimensional islands but the quality of the initial buffer layer is not good at this temperature. The quality of the initial buffer layer is improved by subsequent high temperature growth. The two-step growth process is effective to overcome partly the second difficulty of the lattice mismatch of 4 %. The poor crystalline quality of the initial buffer layer contributes to release the stress and to reduce the dislocation density in the grown layer. On the other hand, the first difficulty, that

is, polar semiconductor growth on non-polar semiconductor, is eliminated by using an As prelayer and a high temperature thermal treatment of a misoriented (001) Si substrate with the two-step growth process. Growth steps on a Si substrate with a few degrees of misorientation toward ⟨001⟩ are changed to double step by the high temperature treatment of more than 900 °C[13]. Combinational usage of a double step structure and As prelayer brings no APD formation. Moreover, the dislocation density of $10^8 \sim 10^9$ cm^{-2} given by the two-step growth process can be improved to 1.4×10^6 cm^{-2} using a super lattice buffer layer and a thermal cyclic annealing[14]. Nonetheless the third difficulty has not been solved yet. The third difficulty concerns with a material constant itself. Therefore it is hard to solve the difficulty, which determines the lower limit of dislocation density of 10^6 cm^{-2} at present.

InP growth on Si is also studied though the large lattice mismatch of 8 % makes it more difficult to be grown. InP is one of the most important materials for opto-electric and microwave devices. Lasers fabricated on InP substrates can be used to minimize light loss from optical fibers[15]. In 1986 Yamamoto et al. grew a single domain InP layer on Si at the first time[16]. Then the buffer layers of GaAs[17], ZnSe[18] and GaAs/strained layer superlattice (SLS) buffer[19] were studied to improve the crystallinity. The lowest dislocation density achieved is about 5×10^6 cm^{-2}, which is almost determined by the difference in the thermal expansion coefficients between InP and Si[20].

InP layers grown on Si substrates are more suitable for the fabrication of optical devices such as laser diodes than GaAs layers grown on Si substrates because dislocations in InP layers, which deteriorate the characteristics of optical devices, are less movable than those in GaAs layers during the device operation. Moreover, the residual stress in InP layers grown on Si is less than that in GaAs layers grown on Si[10].

InP-based laser diodes, photodiodes and solar cells have been fabricated on Si substrates[21~25]. In particular an InGaAsP laser diode reported by Sugo et al.[26] was one of the most successful ones. This laser diode showed excellent

life characteristics but its DC characteristics were still inferior to those of diodes fabricated on InP substrates. This is probably because of the high density of generated dislocations and the residual stress. Further crystallinity improvement is necessary to realize performance and reliability levels high enough to enable commercial applications.

As we have shown, the dislocation density and the residual stress, which are still high for the realization of commercial devices, in III-V layers grown on Si substrates are mainly determined by the difference in the thermal expansion coefficient between III-V materials and Si. To overcome this difficulty several methods are proposed, for examples, low temperature growth[27], low temperature growth by migration enhance epitaxy (MEE)[28], patterned growth[29], conformal growth[30], epitaxial lateral overgrowth (ELO)[31]. Among these methods, ELO has biggest potential for III-V growth on Si because dislocation-free III-V layers are possibly produced using ELO. Then, we will describe about ELO in the following.

Growth of LPE are carried out under the condition close to thermodynamic equilibrium and has therefore the following advantages: (1) defect free material; (2) high ratio of lateral growth width to vertical growth thickness, hereafter this ratio is called "ELO ratio"; (3) large overgrowth width. High ELO ratio and wide overgrowth are realized mainly from a strong anisotropy of growth in LPE. Namely, low growth rates in (111) directions result in a preferential development of (111) plane. Suzuki and Nishinaga used Sn solutions for Si ELO[32]. They reported on the overgrowth around the $\langle 110 \rangle$ and $\langle 112 \rangle$ direction; ELO ratio of 50:1 was obtained[32]. The ELO technique was also applied to the growth of GaAs and GaP alloy[33~35] but there is no study about InP ELO. On the other hand, it has been shown that a drastic decease of dislocation density is possible even for a heteroepitaxy system with large lattice mismatch such as GaAs on Si where GaAs-coated Si substrate was used instead of Si substrate itself to prevent meltback during LPE[31, 36, 37]. This encourages us to use the ELO technique for the growth of InP on InP-coated Si substrate to obtain high quality InP layers on Si

with low dislocation density. As ELO technique is a kind of the patterned growth, reduction of residual stress in the ELO layers is also expected. Hence, it can be said that ELO is a promising technology to overcome the last major difficulty left for the III-V materials growth on Si substrates.

1.2 Motivation of this Research

To improve the performance of InP-based devices grown on Si substrates, ELO technique was applied to the growth of InP layers on Si substrates. ELO has excellent capabilities for improving the quality of InP layers grown on Si substrates by reducing dislocation density down to a dislocation-free level and by releasing residual stress. These two advantages are commonly demanded for other III-V materials grown on Si substrates. The difference in the thermal expansion coefficient between III-V materials and Si substrates is the major problems in the growth of III-V materials on Si substrates, which brings high dislocation density and residual stress in the grown layer. Therefore, the application of ELO technique is useful to solve the problems and to obtain high quality III-V layers on Si substrates.

Firstly, in chapter 2 an InP ELO by LPE is studied entirely since this is the first study about the application of ELO technique to the growth of InP layers. In chapter 3, using this ELO technique, InP growth on InP-coated Si substrates is investigated to improve the crystallinity of the grown layers. ELO is expected to make a break-through to the limits of the existing technique. In chapter 4, the optical properties of the grown layers are characterized by using specially resolved photoluminescence (SRPL) . The residual stresses are also evaluated using SRPL. The stress simulation by finite element method (FEM) is conducted to understand these SRPL results. Finally in chapter 5, conclusions are given.

Bibliography

[1] L.Royer, Bull. Soc. franç. min., **51** (1928) 7.

[2] A.Y.Cho and J.R.Arthur, *Progress in Solid State Chemistry*, Vol.10, Pergamon (1975) p.157.

[3] H.M.Manasevit, Appl. Phys. Lett. **12** (1968) 156.

[4] Y.Horikoshi, M.Kawashima and H.Yamaguchi, Jpn. J. Appl. Phys. **25** (1986) L868.

[5] T.Suntola and J.Anston, US patent 4058430, 197.

[6] T.Mimura, S.Hiyamizu, T.Fujii and K.Nanbu, Jpn. J. Appl. Phys. **19** (1980) L225.

[7] H.Kroemer, RCA Rev. **18** (1957) 332.

[8] I.Hayashi, M.B.Panish, P.W.Foy and S.Sumski, Appl. Phys. Lett. **17** (1970) 326.

[9] R.People and J.C.Bean, Appl. Phys. Lett. **47** (1985) 322.

[10] M.Sugo, N.Uchida, A.Yamamoto, T.Nishioka and M.Yamaguchi, J. Appl. Phys. **65** (1989) 591.

[11] M.Tachikawa and H.Mori, Appl. Phys. Lett. **56** (1990) 2225.

[12] M.Akiyama, Y.Kawarada and K.Kaminishi, Jpn. J. Appl. Phys. **23** (1984) L843.

[13] R.Kaplan, Surf. Sci. **93** (1980) 145.

[14] H.Okamoto, Y.Watanabe, Y.Kadota and Y.Ohmachi, Jpn. J. Appl. Phys. **26** (1987) L1950.

[15] For example: S. M. Sze, *Physics of Semiconductor Devices, 2nd ed.* (Wiley, New York, 1981) p.704.

[16] A.Yamamoto, N.Uchida, and M.Yamaguchi, Optoelectronics Devices and Tech. **1** (1986) 41.

[17] A.Seki, F.Konushi, J.Kakimoto, T.Fukushima and M.Koba, Jpn. J. Appl. Phys. **26** (1987) L1587.

[18] M.K.Lee, D.S.Wuu, H.H.Tung, J.H.Chang and Y.F.Lin, Appl. Phys. Lett. **53** (1988) 107.

[19] M.Sugo, M.Yamaguchi and M.M.AL-Jassim, J. Crystal Growth, **99** (1990) 365.

[20] M.Tachikawa, T.Yamada, T.Sasaki, H.Mori and Y.Kadota, Jpn. J. Appl. Phys. **34** (1995) L657.

[21] D. G. Deppe, N. Holonyak, Jr., D. W. Nam, K. C. Hsieh, G. S. Jackson, R. J. Matyi, H. Shichijo, J. E. Epler and H. F. Chung, Appl. Phys. Lett. **51** (1987) 637.

[22] T. Egawa, H. Tada, Y. Kobayashi, T. Soga, T. Jimbo and M. Umeno, Appl. Phys. Lett. **57** (1990) 1179.

[23] J. Paslaski, H. Z. Chen, H. Morkoc and A. Yariv, Appl. Phys. Lett. **52** (1988) 1410.

[24] W. Dobbelaere, J. De Boeck, P. Heremans, R. Mertens, G. Borghs, W. Luyten and J. Van Landuyt, Appl. Phys. Lett. **60** (1992) 3256.

[25] Y. Itho, T. Nishioka, A. Yamamoto and M. Yamaguchi, Appl. Phys. Lett. **49** (1986) 1614.

[26] M. Sugo, H. Mori, Y. Itoh and Y. Sakai, *Ext. Abstr. 1992 Int. Conf. on Solid State Devices and Materials* (Japan Society of Applied Physics, Tsukuba,1992) P656.

[27] Z.Liliental-Weber, W.Swider, K.M.Yu, J.Kortright, F.W.Smith and A.R.Calawa, Appl. Phys. Lett. **58** (1991) 2153.

[28] K.Nozawa, Y.Horikoshi, Jpn. J. Appl. Phys., **30** (1991) L668.

[29] R.J.Matyi, H.Shichijo, T.M.Moore and H-L. Tsai, Appl. Phys. Lett. **51** (1987) 18.

[30] D.Pribat, V.Provendier, M.Dupuy, P.Legagneux and C.Collet, Jpn. J. Appl. Phys., **30** (1991) L431.

[31] Y.Ujiie and T.Nishinaga, Jpn. J. Appl. Phys., **28** (1989) L337.

[32] Y. Suzuki and T. Nishinaga, Jpn.J.Appl.Phys. **28** (1989) 440.

[33] T. Nishinaga, T. Nakano and S. Zhang, Jpn.J.Appl.Phys. **27** (1988) L964.

[34] S. Zhang and T. Nishinaga, J.Cryst.Growth **99** (1990) 292.

[35] S. Zhang and T. Nishinaga, Jpn.J.Appl.Phys. **29** (1990) 545.

[36] S. Sakawa and T. Nishinaga, J.Cryst.Growth **115** (1991) 145.

[37] S. Sakawa and T. Nishinaga, Jpn.J.Appl.Phys. **31** (1992) L359.

Chapter 2

Epitaxial Lateral Overgrowth of InP on InP Substrates

2.1 Introduction

For performing Epitaxial Lateral Overgrowth (ELO), a substrate is covered with a mask, for example SiO_2 and Si_3N_4. An opening in the protection mask is used as a seed for growth. On the other hand, it is well known that LPE has a great advantage of precise control of interface supersaturation. This allows us to get a high lateral to vertical growth velocity ratio without any polycrystal growth on the protection mask. Therefore, the lateral overgrowth from the seed in the protection mask is performed by LPE. As shown in the schematic illustration of ELO structure given in fig.2.1, this protection mask prevents the propagation of the dislocations from the substrate to the lateral overgrowth layer. Hence, ELO layers have fewer dislocations than the substrate and, in principle, dislocation-free regions can be obtained in the overgrown regions. Moreover, top surface of ELO layer is formed by a certain crystal face, which is atomically flat. Therefore, ELO by LPE is able to provide atomically flat epitaxial layers with few dislocations. The ELO of GaAs on Si substrate has been studied and suitable growth conditions for ELO were investigated [1~3]. ELO is also applicable for the fabrication of semiconductor on insulator structure which is indispensable for the realization of high speed devices

and 3-dimensional ICs. Therefore ELO is expected to open a new and useful field in crystal growth.

InP is one of the most important materials for optoelectric and microwave devices since lasers fabricated on InP substrates can emit the light suffered minimum loss from optical fibers [4]. Hence, the needs for InP in optical-fiber communication have rapidly been increased and various kinds of devices on InP substrates were investigated [5~11]. In the present work, the ELO technique was applied to grow InP in order to obtain a high-quality crystal by decreasing dislocation density and to fabricate a semiconductor on insulator structure by using a SiO_2 mask.

In this chapter, the principle of ELO is described at first. Then, ELO growth by LPE is described. A systematic investigation of the InP ELO by LPE is also presented. Surface steps of ELO layer are studied and the role of surface steps in ELO growth is discussed. In addition, the reproducibility of ELO is investigated.

2.2 Substrate Preparation

InP wafers were cut into a rectangular shape (10mm×15mm) to use as a substrate for LPE. These InP wafers have dislocations, whose densities depend on their dopants. The dislocation density of InP wafers are as follows. InP wafers doped with Fe, S and Zn have dislocation densities of 1×10^5 cm^{-2}, 1×10^4 cm^{-2} and 7×10^3 cm^{-2}, respectively, which are commercially available. The dislocation density of Fe-doped InP wafer is rather high. Therefore, ELO is also useful in homoepitaxial growth of InP. Prior to the LPE growth, a SiO_2 film was deposited with organic liquid mainly consisting of SiO_2 (OCD, Tokyo Ohka Kogyo Co. Ltd.) which was coated by a spinner. The thickness of the organic liquid film was controlled to be around 1200~1500 Å by adjusting the revolution rate and time of the spin coating, which was chosen to be 6000 rpm for 30 seconds in our experiments. Then the film was baked at 450 °C for 30 min in the air to solidify the film into SiO_2. A pattern with line openings was cut in the SiO_2 film by a conventional photolithographic technique. The opening regions where the InP substrate is exposed were used as

the seeds for ELO. We will call these opening regions as "line seeds", hereafter. Three kinds of line seed patterns were used in this study. They are as follows: first, long parallel line seeds whose length and interval are 10~15 mm and 200 μm, respectively; second, short parallel line seeds whose length and interval are 50~700 μm and 200~556 μm, respectively; and the last, a star-like pattern which has line openings every 15 degrees.

After the photolithography, the photoresist coated on the seed pattern was completely removed using a remover (Stripper-10, Tokyo Ohka Kogyo Co. Ltd.). Then, the substrate was cleaned immediately. The following cleaning procedure was generally used: A substrate was washed ultrasonically in acetone for 5 minutes, in isopropanol for 5 minutes, and in Di H_2O for 5 minutes. After degreasing process, the substrate was dipped in H_2SO_4 for 2 minutes and etched in H_2SO_4:H_2O_2:H_2O(=5:1:1 in volume) for 30 seconds at 25 °C. Then, the substrate was dipped in Di H_2O five times and was blown with dry filtered nitrogen.

The choice of etchant is important in ELO and this decides whether the ELO is successful or not. Therefore, we must select the etchant carefully. At first, the candidates for the etchant were tested. They were HNO_3, H_2SO_4:H_2O_2:H_2O (3:1:1 by volume) and H_2SO_4:H_2O_2:H_2O (5:1:1 by volume). Then, ELO were performed using these etchants.

H_2SO_4:H_2O_2:H_2O (3:1:1 by volume) for 2 minutes at 70 °C was tried at first but the etching rate was so fast that the shape of a line seed could not be maintained. Figure 2.2 shows a damaged line seed with overetching. The InP substrate was also etched off around the line seed as shown in fig.2.2 (a). This shows an overetching which had a large underetching both sides of the line seed below the SiO_2 mask. As the result, SiO_2 masks bent down at both sides of the line seed as shown in fig.2.2 (b). Therefore, this etchant was turned out not suitable.

HNO_3 does not dissolve InP but it can clean the substrate surface by solving metals or other elements. After HNO_3 treatment, native oxide remains on the surfaces of InP substrates but this oxide are expected to be removed during the heat treatment before LPE growth. However, the reproducibility of this process

was not good. The grown layer sometimes shows mirror surface but in other times, a lot of dips appeared on the surface. These dips indicate that the removal of the native oxide was not sufficient. Therefore, this etchant also can not be used.

The third etchant is H_2SO_4:H_2O_2:H_2O (5:1:1 by volume). The etching rate was slower than that of first one. We used the etchant at 25 °C, which was low enough to decrease the etching rate. Consequently, the etching rate was decreased enough for maintaining the shape of line seeds as shown in fig.2.2 (c) and excess oxide layers were effectively removed off.

High quality (six 9's) indium weighted 3 grams in total was used as a solvent and InP single crystal was used as a source. The cleaning procedure for an InP source was similar to that for substrates except the last step for etching. In the case of an etching for the InP source, H_2SO_4:H_2O_2:H_2O (3:1:1 by volume) for 2 minutes at 70 °C was used. Then, InP source was dipped in Di H_2O for several times and then was blown with dry N_2.

2.3 LPE Growth System

After the cleaning process, the substrate was put in one of the shallow well in the base part of the graphite boat and an InP source was put in another well. During a saturation period, In melt which is contained in a well of a sliding part of the graphite boat is saturated with phosphorus dissolved from the InP source. The LPE growth apparatus is schematically demonstrated in fig.2.3. The growth occurs in a graphite boat inside a quartz tube and the tube was filled with highly purified H_2. Heating and cooling necessary for the epitaxial growth are programmed and done automatically by a programmable temperature controller system. The quartz tube is connected to an exchange chamber for substrates. The quartz tube and the exchange chamber can be evacuated by a rotary pump to change the ambient gas from air to H_2 effectively. The temperature of the graphite boat is measured by a thermocouple which is installed inside the graphite boat.

2.4 ELO by LPE

Using a schematic illustration of the ELO structure shown in fig.2.1, ELO can be explained as follows. One of the characteristics of LPE is its anisotropy in growth rate. Once the facet appears on the LPE layer, the growth rate in this orientation decreases greatly and the growth continues only on side surfaces which are atomically rough. When the facet has no screw dislocation, there is no growth step on the facet if there is no 2D nuclei. On the other hand, when screw dislocations exist intersecting the facet, the vertical growth %%[PrinterError: either paper empt steps emerged from screw dislocations. But, the growth rate is still much lower than that of rough surfaces. As the substrate surface is chosen (001) or (111)B face, the grown surface tends to be covered with a facet of (001) or (111)B face, which has a local minimum of surface energy. Then, the vertical growth rate is suppressed and lateral growth is enhanced.

The most of the threading dislocations in InP substrates will be intercepted by the SiO_2 film except those running through the line seed openings. Hence, in principle, an ELO layer without dislocation can be expected in the region outside the line seed openings.

Figure 2.4 shows the growth sequence of LPE. The In melt and the substrate are heated to 500~600 °C and are held for 1 hours to achieve enough saturation for the melt and also to evaporate the oxide on the substrate. Then, the temperature was cooled down by 0~4 °C with a cooling rate of 0.05~0.5 °C/min to achieve initial supercooling. Then the In solution was brought into contact with the substrate to start LPE growth. The cooling rate was kept constant during the LPE growth. InP layers with the thickness in the range of 1~40 μm have been grown.

An InP surface is not tough enough to endure such a high temperature environment before and after the LPE growth. The surfaces of InP substrates are degraded by the evaporation of phosphorus at high temperature. Therefore, a protection of the surfaces of InP substrates must be done to get mirror-like growth surfaces. We tried two types of surface protection methods, one was the protection

by using a part of the graphite boat and the other was the protection with an InP polycrystal wafer. The protection abilities of these methods were evaluated by a thermal treatment, in which InP substrates were kept at 600 °C for one hour and then the temperature was decreased at a rate of 0.3 °C/min for 30 minutes and finally quenched to room temperature. A thermal treatment without protection was also done as a reference. The results are as follows. The surface of an InP substrate without surface protection was degraded completely as shown in fig.2.5 (a). A lot of In droplets appeared on the surface and mirror-like flat regions were disappeared. When the graphite slider was used to cover the substrate, flat and mirror region appeared but there are still In droplets on the surface as shown in fig.2.5 (b). Best surface was obtained by the use of an InP polycrystal for the surface protection. Figure 2.5 (c) shows the InP surface that was free from damages protected by an InP polycrystal. Thereby we chose to use this protection method for all LPE growth. After growth, we also used a fan for rapid cooling of the substrate in order to minimize the thermal damage of the surfaces of grown layers.

Figure 2.6 shows the surface morphology of a (001) InP LPE layer which was grown by the above mentioned method. A mirror-like morphology was obtained. This mirror-like morphology indicates that the surface of the InP substrate was protected effectively during the growth. However, on the grown surface, small In droplets were left, after the melt was removed. HNO_3 was used to dissolve these droplets because HNO_3 dissolve only In but not InP. As a result, clean ELO surfaces were obtained. The time for the HNO_3 treatment was chosen as 30 minutes at room temperature.

To get large ELO ratio, it is important to optimize the supersaturation during the ELO growth. Figure 2.7 shows the well-known relationship between growth rate and supersaturation for LPE. The growth mode of LPE can be classified into 3 types. The growth by the first mode denoted by curve "A" in the figure occurs when the growth surface is atomically rough. In this mode, the incorporating rate of atoms is very fast because all the atoms arriving on the rough surface

are incorporated almost immediately. The growth rate of this mode is defined as R_{max}. The growth by the second mode denoted by curve "B", the rate of which is defined as R_{sp}, is carried out by the endless supply of steps from screw dislocations originated from substrate. The growth by the third mode denoted by curve "C", the rate of which is defined as R_{nucl} is taken place by two-dimensional nucleation, which is created under the condition of high supersaturation. In carrying out the ELO growth, the two-dimensional nucleation should be prevented by applying low supersaturation. In the present ELO, the growth in the normal direction is done by mode "B" where the screw dislocations from InP substrates supply growth steps. On the other hand, the lateral growth occurs in mode "A" since the side surfaces of the ELO layer become rough. From fig.2.7, it can be understood that by optimizing the super cooling, the difference in the growth rate between lateral and vertical growths can reach a maximum value. As a result, a large ELO ratio is obtained.

2.5 ELO of InP on (001) InP Substrates

(001) InP was chosen for substrates because {001} facets can easily appear during LPE, in other words, an ELO condition can be easily achieved on these substrates. Figure 2.8 shows a photograph of an ELO sample which was grown from In solution by using a star-like pattern on (001) InP substrate. The growth conditions and ELO parameters of the sample were as follows: the saturation temperature (T_s), the degree of supersaturation (ΔT), the cooling rate (R) and the growth time (t_g) are 550 °C, 4 °C, 0.3 °C/min, 30 min, respectively; star-like line seeds, width of line seeds 2.5 μm, length of line seeds 1 mm. The dependence of ELO on the orientation of the line seed can be easily seen from this figure. The width of ELO is the largest when the stripe was 15° and 30° off-oriented from the $\langle 110 \rangle$ and $\langle 010 \rangle$ directions or its equivalent orientations, while it is the smallest when the stripe was oriented just in the $\langle 110 \rangle$ and $\langle 010 \rangle$ direction or its equivalent orientations. The facets on the front edge of the ELO are identified as {111} and {001} planes by measuring the

angle of each plane to the substrate surface. The result indicates that the lateral growth was terminated by the formation of {111} and {001} facets in InP ELO as schematically illustrated in fig.2.9. In the same figure is given the orientation dependency of the lateral growth rate. An ELO stripe with ⟨011⟩ direction was terminated by $(\bar{1}11)$B and $(1\bar{1}1)$B facets on both sides and by a (010) facet on its end. On the other hand, an ELO stripe with ⟨010⟩ direction was terminated by (100) and $(\bar{1}00)$ facets on both sides and by a $(\bar{1}11)$B facet on its end. An ELO stripe with $\langle\bar{1}10\rangle$ direction was terminated by (111)A and $(\bar{1}\bar{1}1)$A facets on both sides and by a $(\bar{1}00)$ facet on its end. These facets also terminate the corner of ELO stripes which are off oriented from the ⟨110⟩ and ⟨010⟩ direction or its equivalent orientations. As shown in fig.2.9 ⟨110⟩ and ⟨010⟩ directions or their equivalent orientations have minimum lateral growth rate because of the facet formation and other directions show large lateral growth rate.

The lateral growth is governed by the density of steps supplied from screw dislocations and/or substrate misorientation. If there is no dislocation propagated from the substrate through the line seed opening, the steps are only supplied from the substrate misorientation. In this case, the vertical growth stops when (001) face is completed on the top surface of the ELO because no more growth steps are supplied. Figure 2.10 shows an InP ELO layer grown over a short line seed pattern with 200 μm in length and 6.5 μm in width. As shown in the figure it is found that a lot of line seeds have no ELO growth while some line seeds have thick ELO layers surrounded by {111} and {001} facets. The difference occurs depending on whether the line seed opening has dislocations or not. If there are dislocations with screw component inside of the line seeds, the steps will be supplied from them and the vertical growth becomes possible. If there is no dislocation, the vertical growth will be terminated when a facet is formed. When exactly oriented (001) InP substrate was used and there is no dislocation in window region, the thickness of ELO layer did not exceed that of the SiO_2 mask, therefore ELO could not spread over the mask. Some of the line seeds have a region where a small spread is seen at the edge of the line seed. This is probably because a small local misorientation

existed on the substrate[12].

According to the discussion about the line seed orientation, we have chosen the orientation 15° off from the $\langle 110 \rangle$ direction for the parallel line seeds. Figure 2.11 shows a photograph of InP ELO stripes grown in parallel on a (001) InP from In solution. The growth condition of this sample was as follows: T_s=600 °C, ΔT=4 °C, R=0.5 °C/min, t_g=120 min; width of line seeds 6.5 μm, length of line seeds 10 mm, period 200 μm. As is seen in fig.2.11, every growth front took an almost straight-line shape. Though the width of this layer is as large as 80~100 μm, the ELO ratio was not large. This is probably due to the fast cooling rate such as 0.5 °C/min. The relatively high supersaturation enhanced vertical growth rate. On the contrary, observation of the ELO layer by Nomarski differential interference contrast microscope (N-DICM) shows the presence of growth steps on the surface, whose intervals are more than ten micrometers. This means that the surface of the ELO layer is atomically flat.

Figure 2.12 shows one of the N-DICM photographs of the InP ELO layer. It was observed that a spiral step emerged from a screw dislocation. As N-DICM is so sensitive to surface roughness, a monolayer step can be detected by N-DICM. The shape of this spiral near the center is close to an oval, whose long axis lies in $\langle \bar{1}10 \rangle$ direction. The distances between steps are about 8.3 μm in $\langle \bar{1}10 \rangle$ direction and 6.7 μm in $\langle 110 \rangle$ direction. The steps perpendicular to $\langle 110 \rangle$ are thought to be "A" steps. "A" steps are more straight and have less kink sites than "B" steps. Therefore, "B" steps go faster than "A" steps because "B" steps have more density of kinks and can accept more atoms from the solution. This is the reason why the step distance shows anisotropy.

Figure 2.13 (a) and (b) shows a screw dislocation with the Burgers vector which is the twice and triple of ordinary one, respectively. These figures also show that the curvature of each spiral is almost equal. This is due to the following reason. The curvature of spirals is determined by the supersaturation of LPE growth as is well known by BCF theory. The supersaturation are almost equal since these spirals were grown very near to each other. On the other hand, fig.2.14 shows a

large separation between two steps, which is as large as 70 μm. Moreover, this sample shows the separation of up to 230 μm. The large separation indicates that the supply of steps is little in the area. Therefore, this ELO surface is atomically flat in such a large area. This is one of the characteristics of ELO. This figure also shows meniscus-lines which have opposite curvature to the surface steps. These meniscus-lines were formed when the solution was removed from the substrate.

Figure 2.15 shows an AFM (atomic force microscope) image of the ELO surface mentioned above. Two steps can be seen from this figure whose distance is about 3.5 μm. The distance is nearly equal to the step separation in the double spiral case. The cross section of this figure indicates that the height of these steps is monolayer. From this result, we can confirm that these steps are monolayer steps.

2.6 Sn doping to improve ELO ratio

In order to increase ELO ratio, we tried to use doping in ELO. Dopant produce a distortion around the dopant atoms on the surface in the crystal. When the dopant is incorporated at the step edge the distortion makes the propagation of steps difficult. As the propagation speed of steps becomes low, the vertical growth rate of ELO will be decreased and ELO ratio will be increased. We investigated the effect of doping on ELO. We chose Sn as a dopant because high Sn doping into InP is possible and n-type doping of Sn is also convenient for device fabrications. Sn shows strong segregation in LPE. The strong segregation may enhance the decrease of the step speed during the growth.

An In and Sn mixture was used as the solution for Sn doping. Doping level was studied by growing InP layers and measuring electrical properties with Hall measurements. Their growth conditions were as follows. T_s=550 °C, ΔT=1 °C, R=0.3 °C/min, t_g= 60 min. Sn:In=1:9 by volume was used as the solution. The cariier concentration (n) and the Hall mobility μ of the sample were 2.0×10^{18} cm^{-3} and 1440 cm^2/Vs, respectively. On the other hand, the sample grown by using the solution of Sn:In=3:1 by volume under the following growth conditions, T_s=550

°C, ΔT=2 °C, R=0.2 °C/min, t_g= 60 min, shows n=1.2×10^{19} cm^{-3} and μ=704 cm^2/Vs. Doping level was controlled by the ratio of Sn to In and the latter ratio was mainly used in the following experiments.

Figure 2.16 (a) shows a photograph of Sn-doped InP ELO stripes grown from Sn:In=3:1 solution on a (001) InP substrate whose line seeds are tilted 15° off the ⟨110⟩ direction. Each growth front is almost straight similarly to the undoped (001) InP case. The growth conditions were as follows: T_s=550 °C, ΔT=2 °C, R=0.2 °C/min, t_g=60 min; SiO_2 mask, width 6 μm, period 200 μm. The figure shows that ELO width and height are 45 μm and 4 μm, respectively. Then, the ELO ratio is about 11.3, which is much larger than that of the undoped (001) InP ELO. As a reference, fig.2.16 (b) shows a photograph of undoped InP ELO stripes grown from In solution on a (001) InP substrate whose line seeds are tilted 15° off the ⟨110⟩ direction. The growth conditions were as follows: T_s=550 °C, ΔT=3 °C, R=0.3 °C/min, t_g=60 min; SiO_2 mask, width 7 μm, period 200 μm. The growth condition was similar to that of the Sn-doped (001) InP ELO but ΔT and R were chosen a little large since In gives a low supersaturation. Fig.2.16 (b) shows that ELO width and height are 35 μm and 7 μm, respectively. ELO ratio is about 5.0, which is smaller than that of the Sn-doped (001) InP ELO. These two samples have almost the same width but the height of the samples differs more than two times. The result shows that Sn doping is effective to decrease the vertical growth rate of ELO.

Figure 2.17 shows the surface morphology of an Sn-doped InP ELO layer grown over parallel line seeds whose width and period are 2 μm and 10~30 μm, respectively. Some parts of ELO stripes were connected each other but the other parts of ELO were not connected in the upper half of the figure, when the period of the line seeds was 30 μm. On the other hand, all ELO stripes were connected and made a large flat area, where the period of the line seeds of 10 μm was used in the lower half of the figure. The large flat area is made from regions with conical shape, each of which has a screw dislocation near the center of it. These regions make a shape of Voronoi diagram. Each region was grown from the spiral step emerged from a

screw dislocation that belongs to the region. Figure 2.17 also shows the presence of stacking faults whose density is about 7000 cm^{-2}. The origin of these stacking faults is not understood now but high Sn doping may have some relation to generate these stacking faults because Si high doping is known to generate stacking faults in GaAs ELO layers[13].

Reproducibility of ELO was not good when narrow line seed was used whose width was less than 2 μm. The reproducibility was even worse when short line seed was employed. The use of Sn:In (3:1 by volume) solution resulted in no ELO growth as shown in fig.2.18. The cause of these phenomenons are interpreted as the poor wetting between melt and line seeds. In general, the wetting between In solution and SiO_2 mask is poor and this makes the melt separate from the line seeds. This brings poor reproducibility when narrow and short line seeds are used. The wetting between Sn:In solution and line seeds is worse than that between In solution and line seeds. Therefore, the use of Sn:In solution brings worse results. In order to improve the wetting, In thin layer was deposited on ELO substrates. Namely, before ELO growth, 3000$\sim$6000 Å In layer was deposited. The thin In layer covered both line seeds and SiO_2 masks. The In layer on line seeds helps the melt to wet the line seeds. Figure 2.19 shows excellent reproducibility of ELO growth. InP ELO layers perfectly grew from the solution of Sn:In=3:1 by volume over all line seeds although narrow and short line seeds were employed. The growth conditions were as follows: Sn:In (3:1 by volume), T_s=560 °C, ΔT=1 °C, R=0.1 °C/min, t_g=120 min; In film thickness of 5800 A, width of line seeds 2.5 μm, length of line seeds 10 μm $\sim$ 10 mm. With these conditions ELO is difficult without the predeposition of In.

2.7 ELO of InP on (111) InP Substrates

Figure 2.20 shows a photograph of InP ELO stripes grown from In solution with line seeds in star-like arrangements on a (111)B InP substrate. The growth condition of this sample is as follows: T_s=550 °C, ΔT=4 °C, R=0.15 °C/min, t_g=30

min; star-like line seed, width of line seeds 3.0 μm, length of line seeds 1 mm. It can be seen that the lateral growth depends on the orientation of the line seed. The lateral growth width takes the maximum if the line seed is oriented in $\langle 211 \rangle$ or in the equivalent orientations, whereas it takes the minimum if the line seed is opened in $\langle 110 \rangle$ or in the equivalent orientations. The relationship between the ELO width and the seed orientation is almost the same as that in the case of GaAs ELO on a (111)B GaAs substrate [2]. Similarly, facets which appear on the growth front of each stripe are identified as $\{111\}$ or $\{001\}$ faces by measuring the angle of each face to the substrate surface.

Figure 2.21 shows a photograph of InP ELO stripes grown again from In solution on a (111)B InP substrate whose line seeds were tilted 15° off from the $\langle 110 \rangle$ direction. The growth condition of this sample is as follows: T_s=500 °C, ΔT=4 °C, R=0.3 °C/min, t_g=60 min; width of line seeds 7.0 μm, length of line seeds 10 mm, period 200 μm. Every growth front took a shape of almost straight-line similarly in the (001) InP case. ELO ratio was about 40 at T_s of 500 °C, which was much larger than that in the (001) InP case. It is understood that the supersaturation was suitably chosen for ELO in this case and, moreover, the low growth rate of (111)B facets brought larger ELO ratio. The (111)B ELO layer can be widened by the extension of the growth time until facets appear on the lateral growth fronts. The growth time of 300 min led to the width of 140 μm and the ELO ratio of 47 but these ELO stripes have facets which terminate the growth front. The growth condition of this sample is as follows: T_s=500 °C, ΔT=4 °C, R=0.3 °C/min, t_g=300 min; width of line seeds 6.5 μm, length of line seeds 10 mm, period 200 μm.

Figure 2.22 shows a spiral step on a surface of a (111) InP ELO layer. The shape of this spiral step is not round but triangular. This shape probably reflects crystal symmetry, since InP (111)B face has 3-fold axis. Surface steps move with the fastest velocity in $\langle \bar{2}11 \rangle$ and its equivalent directions while they move with the slowest velocity in $\langle \bar{1}\bar{1}2 \rangle$ and its equivalent directions. As a result, a triangular spiral was formed. This figure also shows that the distance between steps is about

40 μm, which is more than four times larger than that of previously mentioned (001) ELO case. The growth condition of this sample is as follows: T_s=600 °C, ΔT=4 °C, R=0.5 °C/min, t_g=300 min; width of line seeds 6.5 μm, length of line seeds 10 mm, period 50 μm. The supersaturation of this condition is not largely different from that of the (001) ELO case. Therefore, the difference in the distance of spiral steps can be ascribed to the difference in the surface free energy for the side surface of the steps. The difference may bring a slow vertical growth rate of (111)B InP ELO, as predicted by BCF theory. Figure 2.22 also shows that the distance of steps in right hand side of the spiral is longer than that of steps in left hand side. This is probably because the edges of ELO stripes obstruct the motion of the steps. In other words, the steps are less movable in narrower ELO stripe. Therefore, narrow line seeds have short distance of the surface steps.

Figure 2.23 shows that macro steps exist on the (111)B InP ELO layer. These macro steps tend to appear at low growth temperature and with Sn doping etc. Sn atoms on the ELO surface are able to pin surface steps, therefore, the Sn doping helps the surface steps to bunch. The pinning is enhanced at low temperature because thermal energy, which is necessary for step going over pinning sites, is insufficient at low temperature.

2.8 Dislocations in ELO Layers

Figure 2.24 shows photographs of (111)B and (001) ELO layers after etching. It can be seen that etch pits appear only in the region over the seed area on the ELO stripe in both cases. These etch pits are due to the dislocations propagated from the substrate through the seed opening. No etch pit was observed in the lateral overgrowth regions, because the SiO_2 film between the lateral overgrowth layer and the substrate prevented the propagation of the dislocations from the substrate to the lateral overgrowth layer. A lot of etch pits observed in the outside of ELO (fig.2.24a) exhibits a high dislocation density present in the substrate. Here, the deposited SiO_2 film was removed before etching and InP substrate was exposed.

From above results, ELO is understood to have a stopping ability of dislocations from InP substrates. Atomically flat epitaxial InP layers with few dislocations can be obtained by using ELO.

There found two types of dislocations in ELO growth. One is named here as a type A dislocation which produces the vertical growth of ELO and the other is named as a type B dislocation which does not produce the vertical growth. The typical example of the former is a dislocation with screw component and the typical example of the latter is a pure edge dislocation. Type A dislocation is especially important for the study of ELO. If all type A dislocation can be eliminated, the vertical growth of ELO will be effectively suppressed and large ELO ratio will be achieved even if the ELO layer contains many type B dislocations. This is one of the reasons why an etch pit density of a ELO layer is always much larger than a density of growth spirals on ELO.

2.9 Summary

In this chapter, the principle of ELO is described at first. Then, ELO growth by LPE is explained. InP ELO with LPE has two problems which must be solved. One is the etching of wafers just before the growth and the other is the surface protection of InP substrates at high temperature. The solutions for these problems are presented and InP ELO was successfully performed.

A systematic investigation of the InP ELO by LPE has been conducted for the first time. The growth behavior of InP ELO was found, in principle, to be similar to that of GaAs ELO. A wide and flat ELO layer of InP on a (001) InP substrate can be obtained if the aligned seed is tilted away from the ⟨100⟩, ⟨110⟩ and their equivalent orientations. On the other hand, the lateral growth fronts are soon covered with {111} and {001} facets and the width of the lateral growth was minimum when the seed was aligned just in the above directions. It becomes clear that there was no etch pit on the lateral overgrowth regions except over the seed area. Nearly etch pit free lateral epitaxial layers of InP were also successfully

obtained on (111)B InP substrates. It is concluded that ELO is an excellent method to obtain an extremely flat and dislocation-free epitaxial layer grown on insulator.

Surface steps of ELO layer were also studied by using N-DICM and AFM. These surface steps played an important role in ELO growth. The vertical growth rate was controlled by the motion of the steps. Furthermore, AFM measurements show that these steps are monatomic.

The improvement of ELO ratio was performed by using Sn-doping. Nevertheless, Sn-doping brought low reproducibility of ELO layers. The reason of this low reproducibility was also investigated and it was found that predeposition of In was very effective to improve the reproducibility.

Bibliography

[1] S.Zhang and T.Nishinaga, J.Crystal Growth **99** (1990) 292.

[2] T.Nishinaga, T Nakano and S.Zhang, Japan.J.Appl.Phys. **27** (1988) L964.

[3] Y.Suzuki and T.Nishinaga, Japan.J.Appl.Phys. **28** (1989) 440.

[4] for example S.M.Sze,*Physics of Semiconductor Devices* (John Wiley & Sons, New York,1981) 2nd ed., p.704.

[5] I.P.Kaminow, R.E.Nahory, M.A.Pollack, L.W.Stulz and J.C.Dewinter, Electron. Lett. **15** (1979) 763.

[6] U.K.Mishra, A.S.Brown, S.E.Rosenbaum, C.E.Hooper, M.W.Pierce, M.J.Delany, S.Vaughn and K.White, IEEE Electron Device Lett. **EDL-9** (1988) 647.

[7] K.Nummila, M.Tong, A.Ketterson, I.Adesida, C.Caneau and R.Bhat, Electron Lett. **29** (1993) 274.

[8] R.J.Malik, J.R.Hayes, F.Capasso, K.Alavi and A.Y.Cho, IEEE Electron Device Lett. **EDL-4** (1983) 383.

[9] T.Won, C.K.Peng, J.Chyi and H.Morkoc, IEEE Electron Device Lett. **EDL-9** (1988) 334.

[10] R.Chin, N.Holonyak,Jun., G.E.Stillman, J.Y.Tang and K.Hess, Electron Lett. **16** (1980) 467.

[11] F.Capasso, W.T.Tsang, A.L.Hutchinson and G.F.Williams, Appl. Phys.Lett. **40** (1982) 38.

[12] Y.Suzuki, T.Nishinaga and T.sanada, J. Crystal Growth **99** (1990) 229.

[13] Wu-yih UEN, Doctor Thesis (1993)

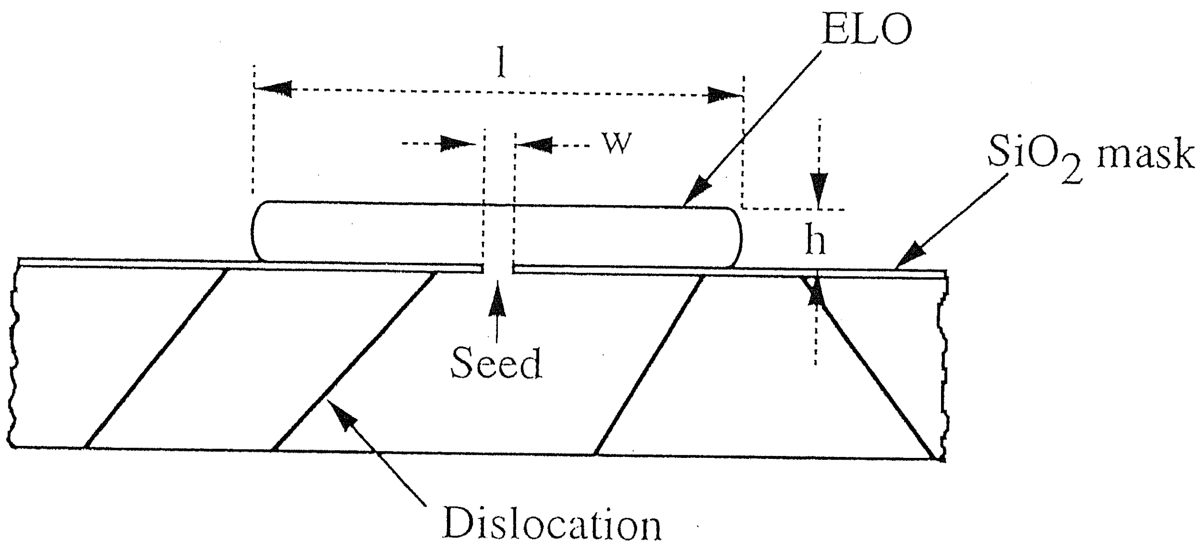

Figure 2.1: Schematic illustration of ELO.

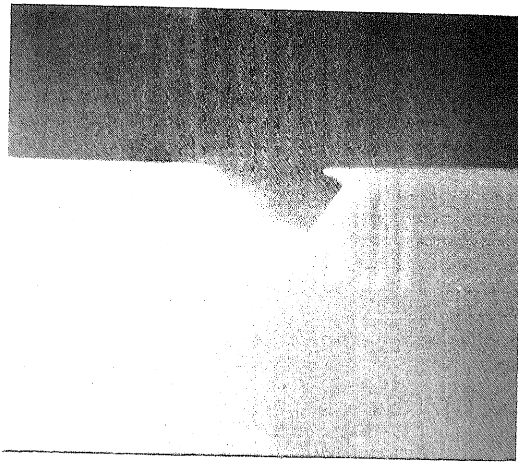

(a)

(b)

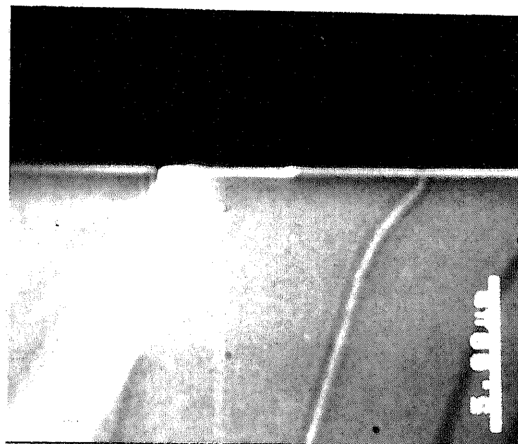

(c)

Figure 2.2: Cross-sectional SEM images of (a) a damaged line seed with overetching, (b) a damaged line seed with a bent SiO_2 mask and (c) a line seed with proper etching.

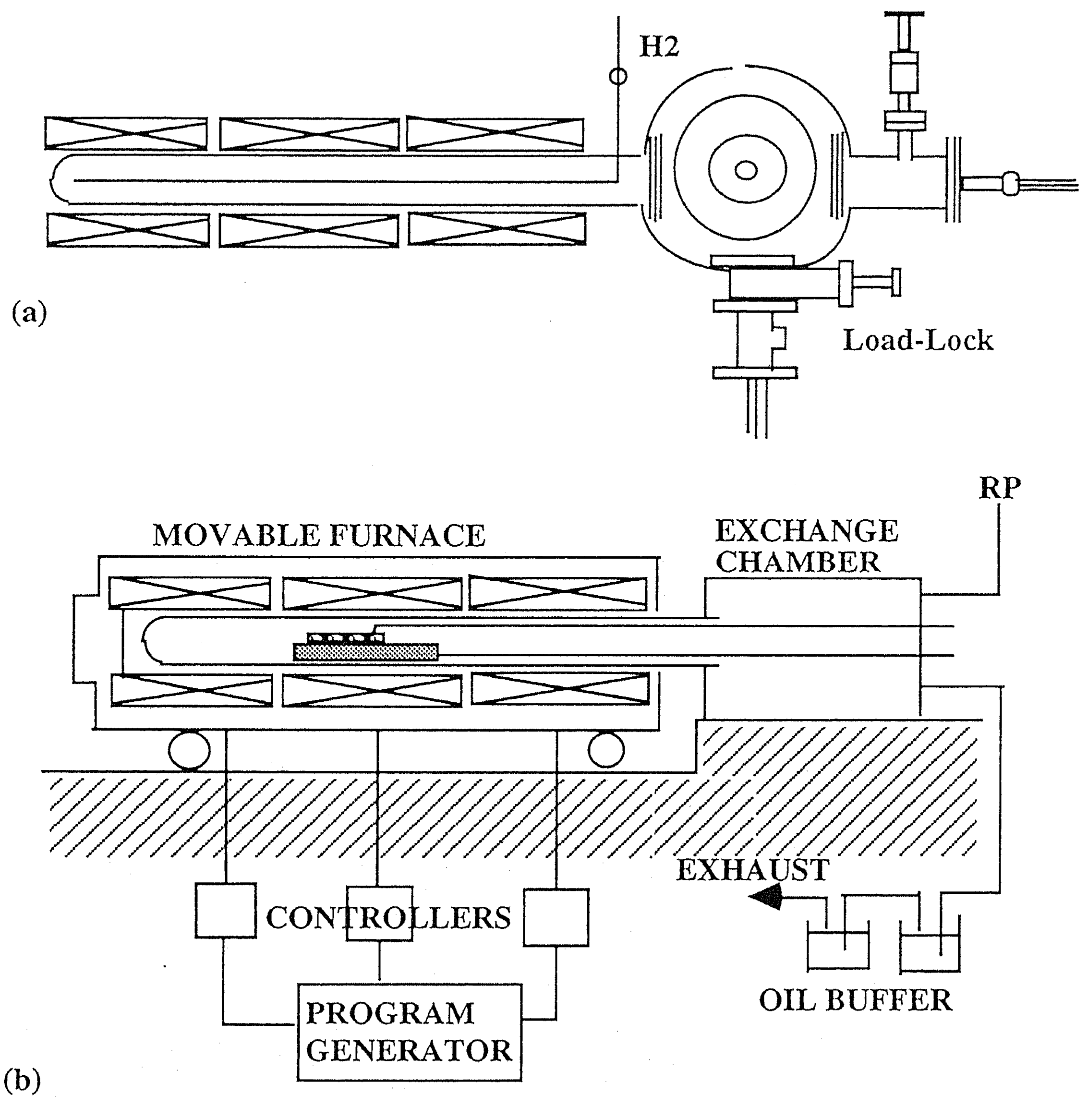

Figure 2.3: Schematic drawing of an LPE growth apparatus: (a) top view and (b) cross-sectional view.

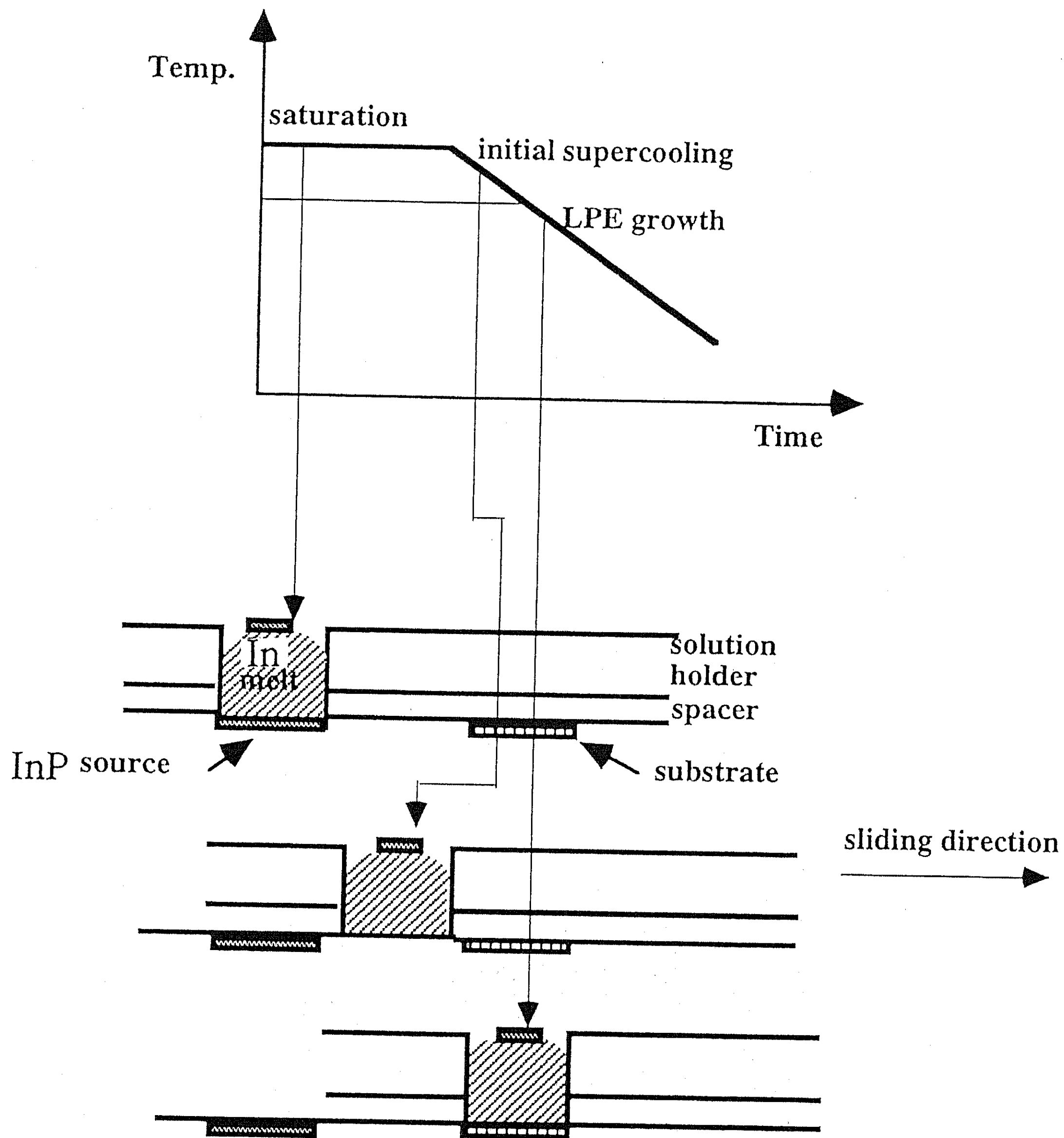

Figure 2.4: Schematic illustration of a LPE growth process and the corresponding slide of boat during LPE growth.

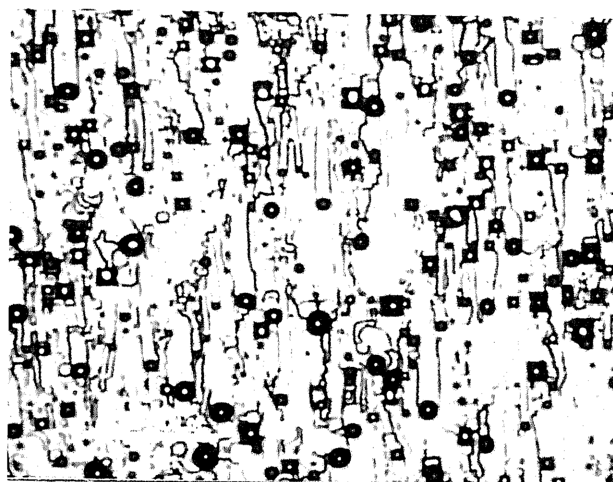

(a)

(b)

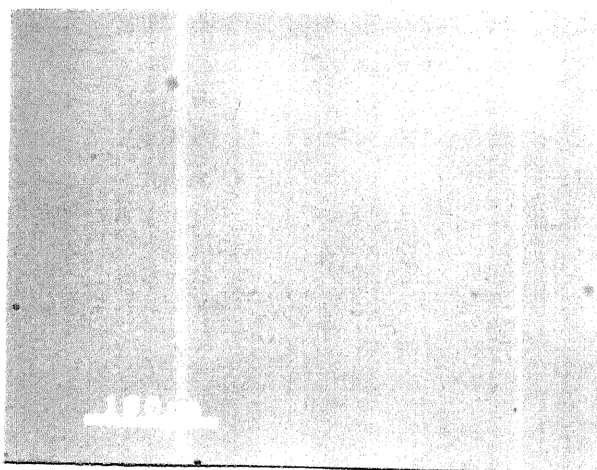

(c)

Figure 2.5: Surfaces of annealed InP substrates (a) without protection, (b) protected by the graphite sliding boat and (c) protected by an InP polycrystal.

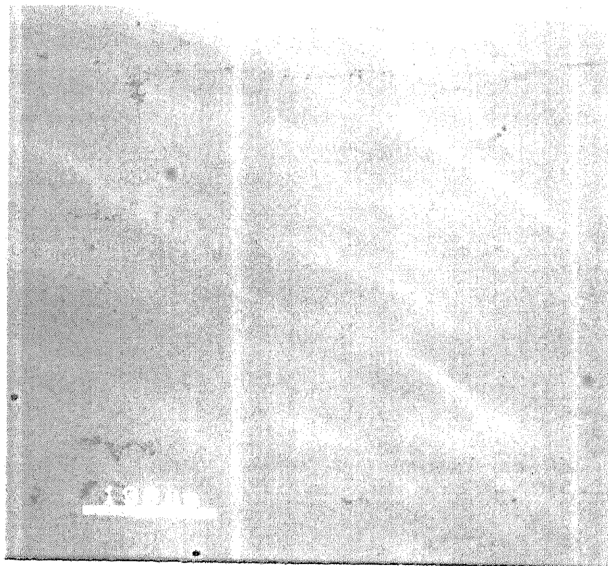

Figure 2.6: Surface morphology of an InP LPE layer grown on a (001) InP substrate.

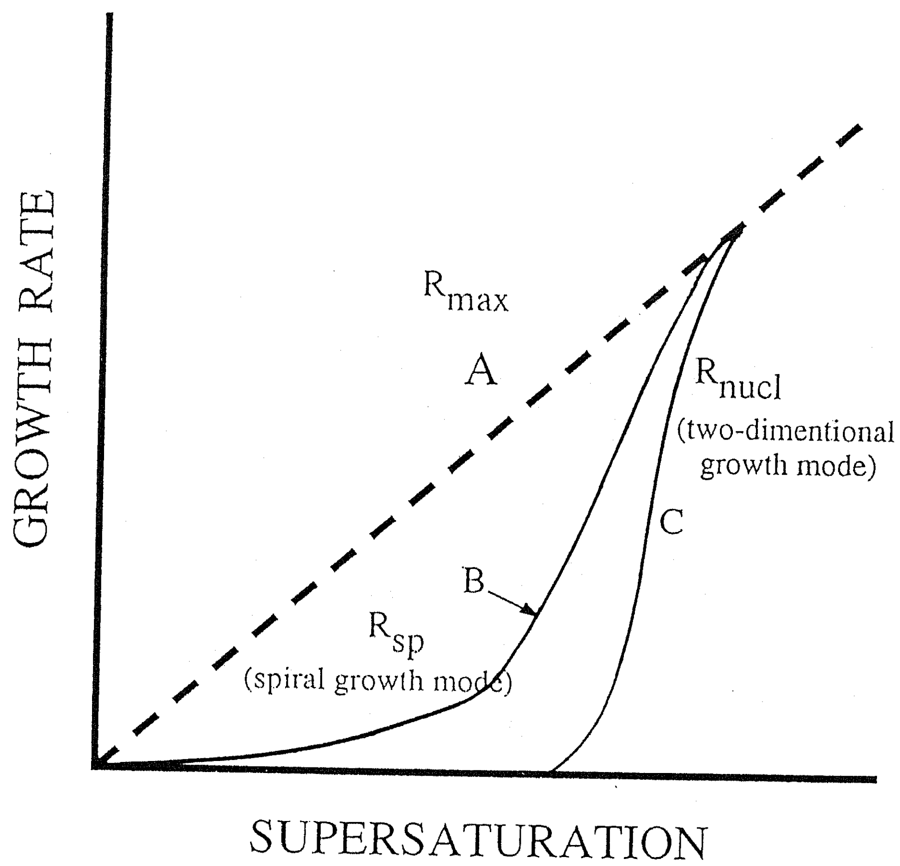

Figure 2.7: Relationship between growth rate and supercooling for LPE.

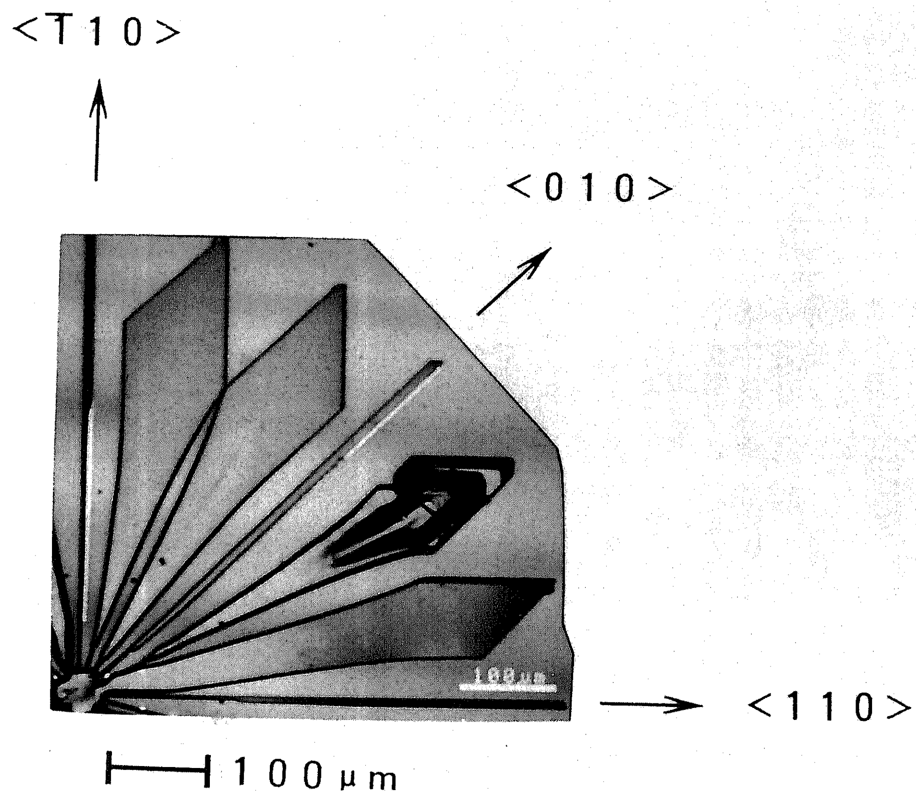

Figure 2.8: InP overgrowth with a star-like line seed on a (001) InP substrate.

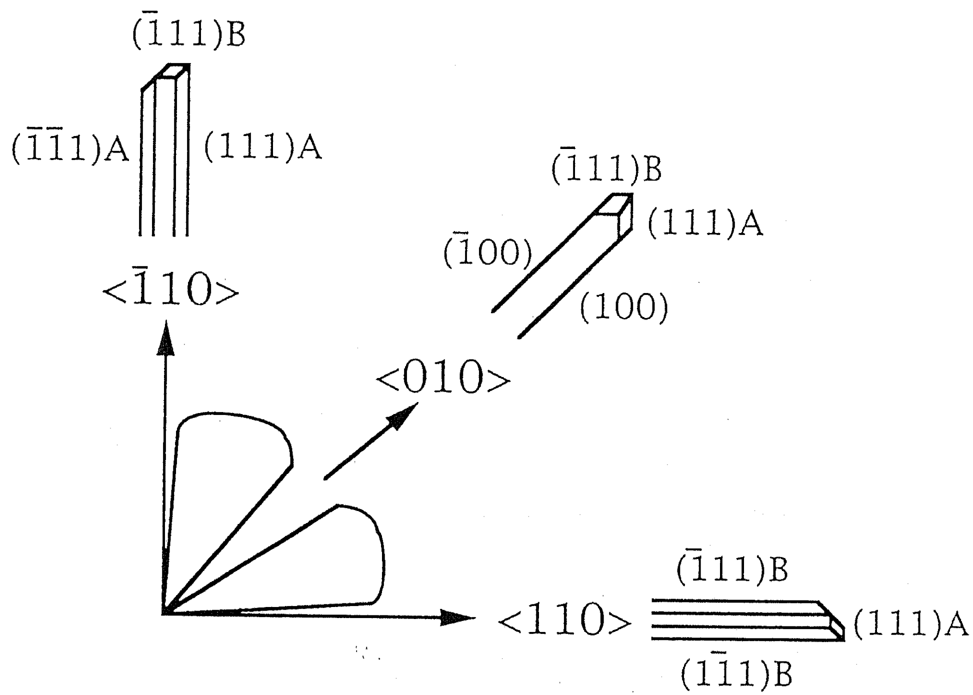

Figure 2.9: Lateral growth rate given in radial direction as a function of seed orientation and a sketch of the facets that appeared on the lateral growth front.

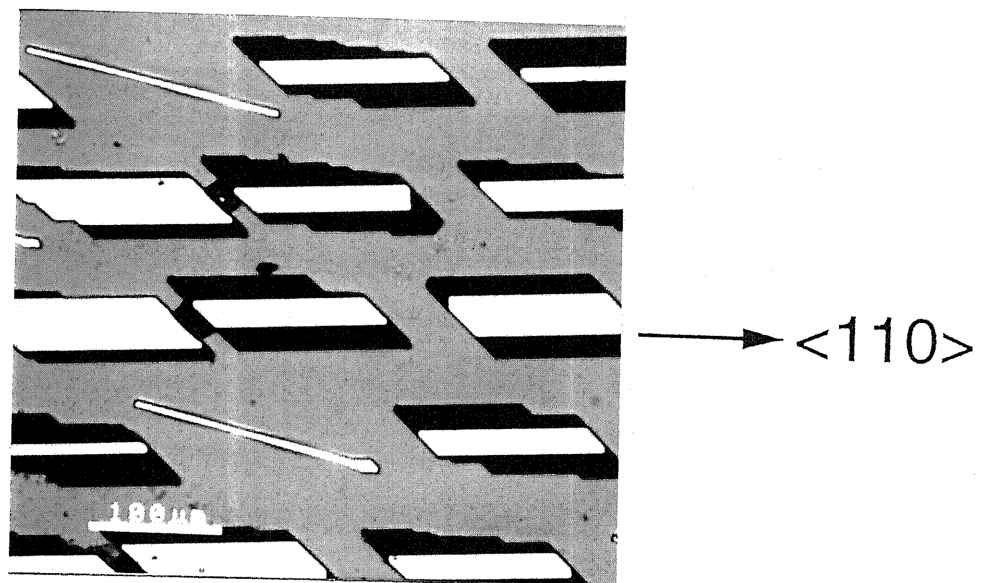

Figure 2.10: InP overgrowth of a short line seeds on a (001) InP substrate. The length of the line seeds is 200 μm and the width of them is 6.5 μm.

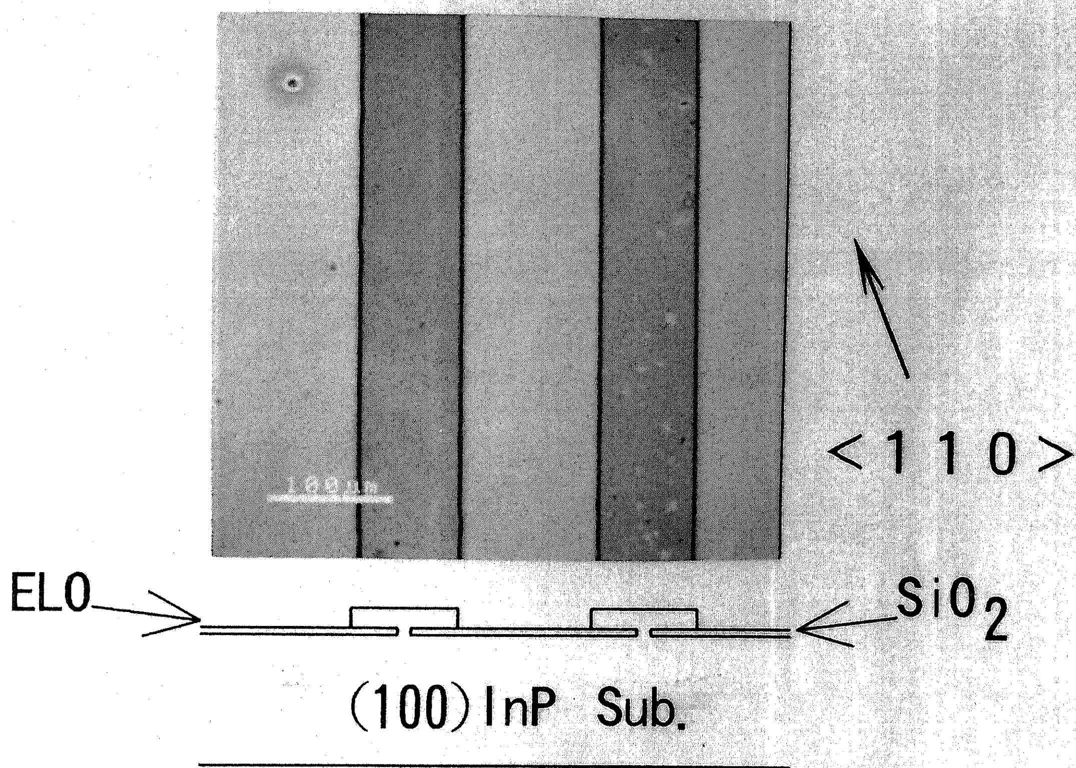

Figure 2.11: InP overgrowth of parallel line seeds on a (001) InP substrate. The width of line seeds is 6.5 μm and their periods are 200 μm.

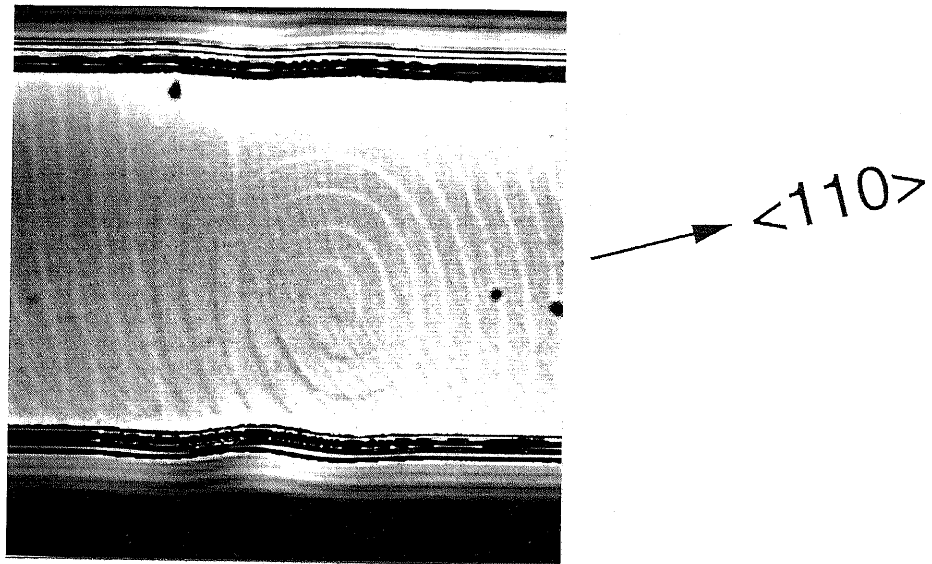

Figure 2.12: N-DICM photograph of a spiral step pattern on a (001) InP ELO layer.

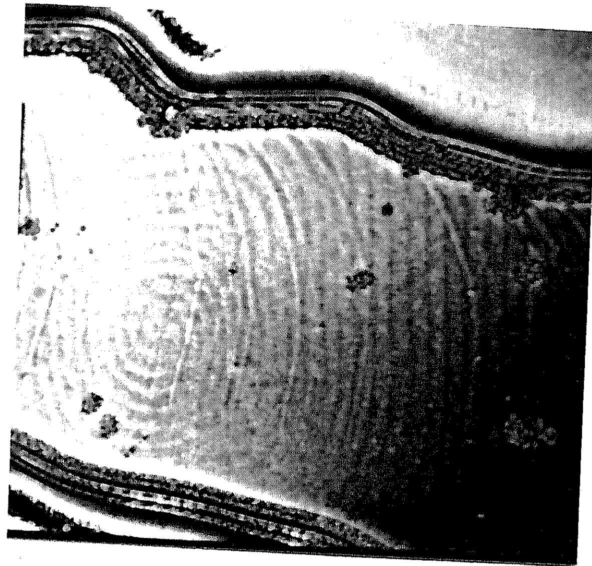

→ <110>

(a)

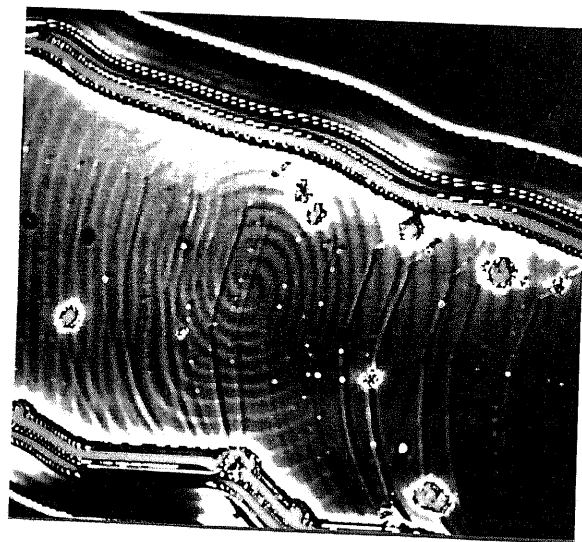

→ <110>

(b)

Figure 2.13: N-DICM photographs of spiral step patterns on (001) InP ELO layers (a) with double spirals and (b) with triple spirals.

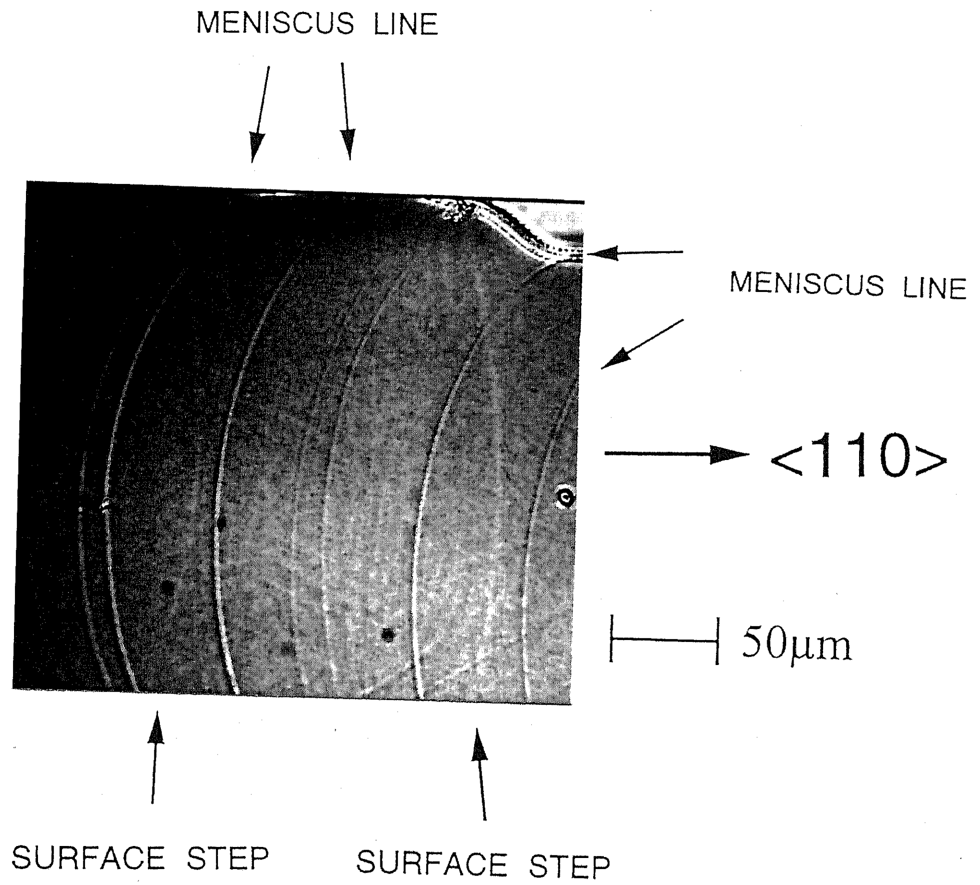

Figure 2.14: N-DICM photograph of surface steps on a (001) InP ELO layer with large separation.

InP

EXPLORER

HAR MODE

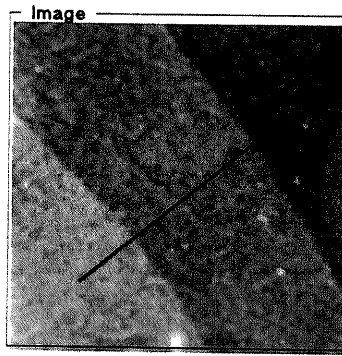

Report

#	Distance	Height
1	1.10 µm	0.19 nm
2	0.96 µm	0.21 nm

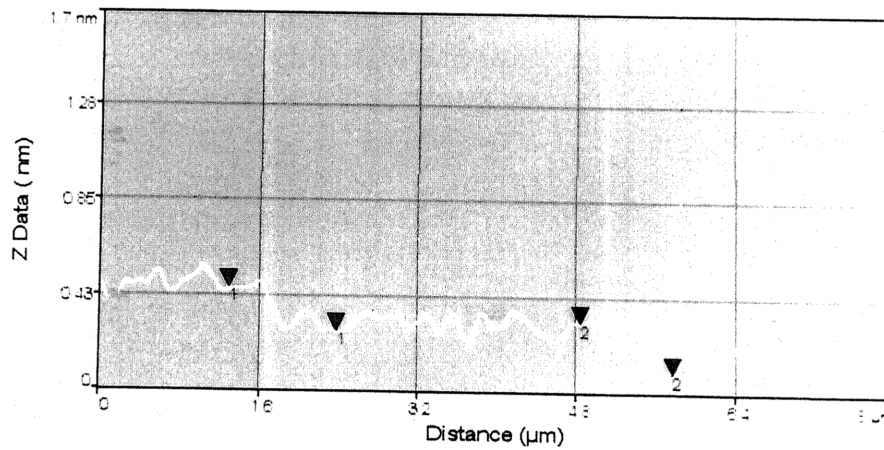

Figure 2.15: AFM image of a (001) InP ELO surface and its height profile.

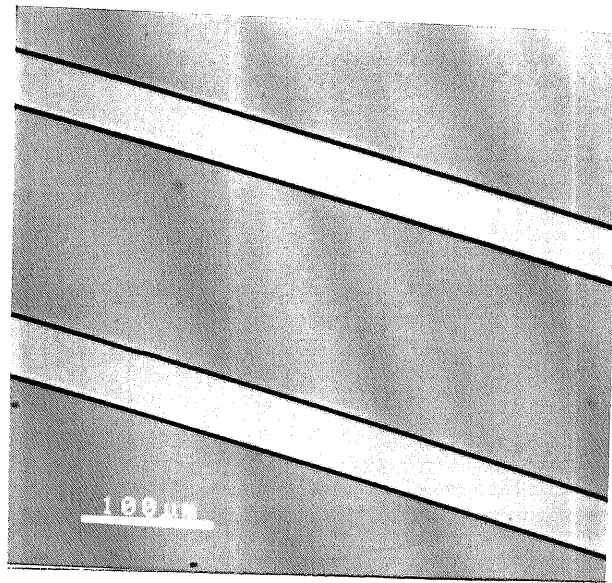

→ <110>

(a)

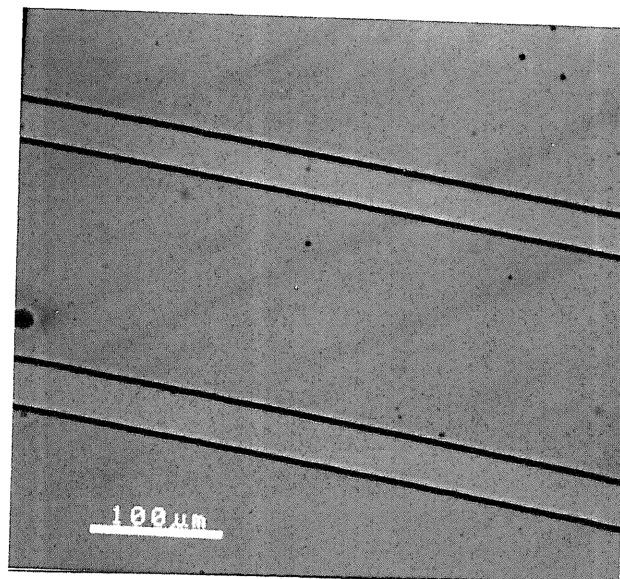

→ <110>

(b)

Figure 2.16: InP overgrowth of parallel line seeds on a (001) InP substrate (a) with Sn doping and (b) without doping.

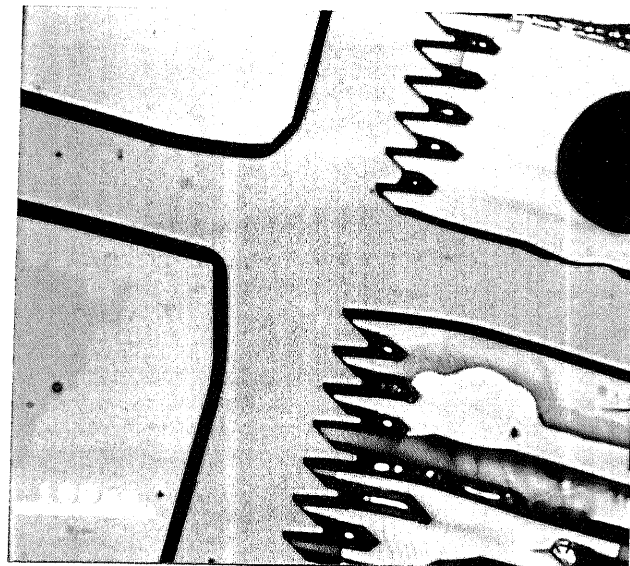

(a)

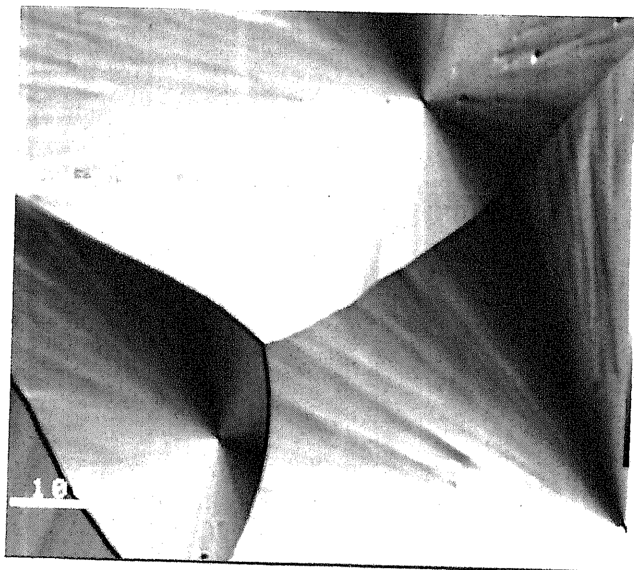

(b)

Figure 2.17: InP overgrowth of parallel line seeds on a (001) InP substrate with Sn doping. Period of line seeds (a) 10 and 30 μm and (b) 10 μm only.

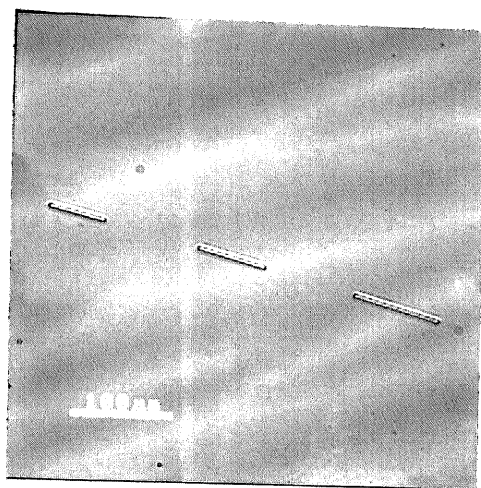

Figure 2.18: (001) InP ELO substrate with short line seeds after growth. The width of the line seeds is 2 μm.

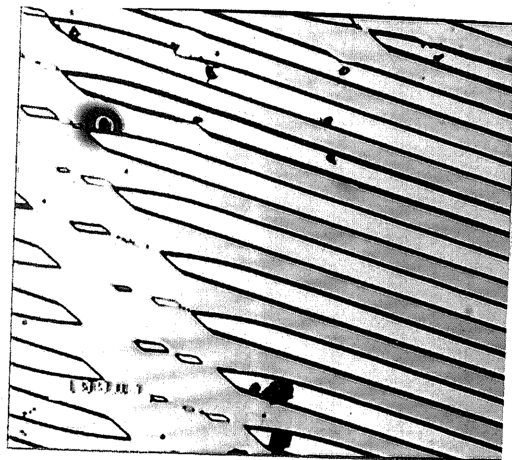

Figure 2.19: InP overgrowth of parallel line seeds on a (001) InP substrate. The width of line seeds is 2.5 μm.

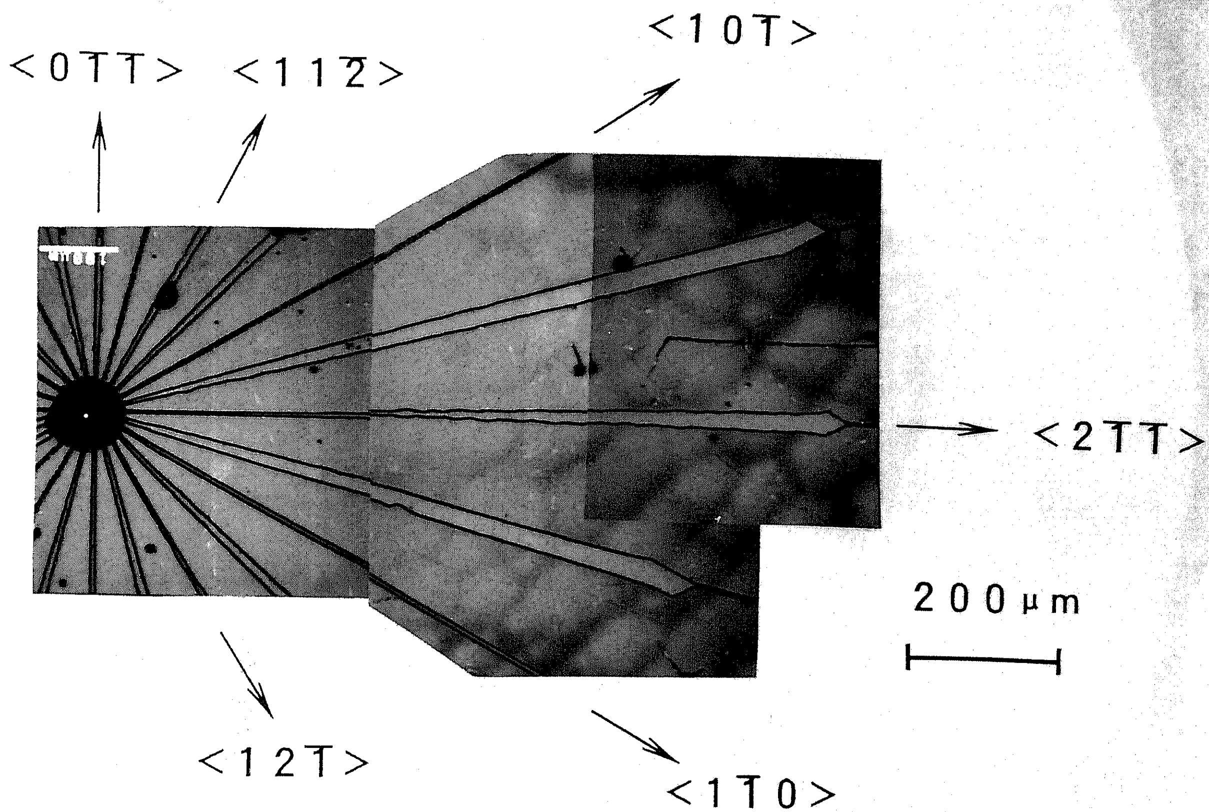

Figure 2.20: InP overgrowth of a star-like line seed on a (111)B InP substrate.

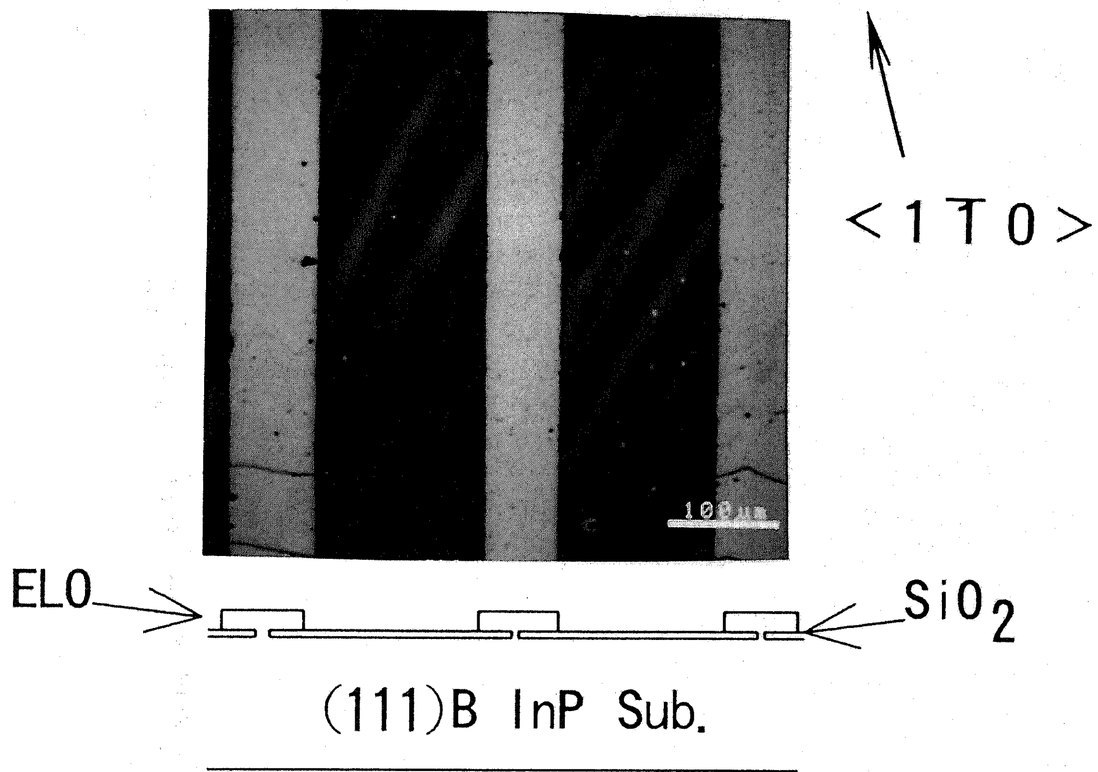

Figure 2.21: InP overgrowth of parallel line seeds on a (111)B InP substrate. The width of line seeds is 7μm and their periods are 200 μm.

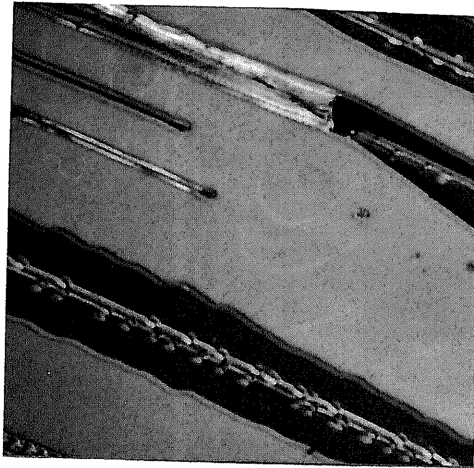

$\longrightarrow \langle 1\bar{1}0 \rangle$

Figure 2.22: N-DICM photograph of a spiral step pattern with triangular shape on a (111) InP ELO layer.

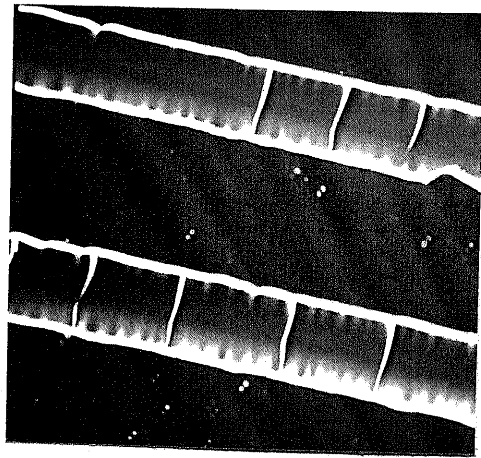

→ $\langle 1\bar{1}0 \rangle$

Figure 2.23: N-DICM photograph of macrosteps on a (111) InP ELO layer.

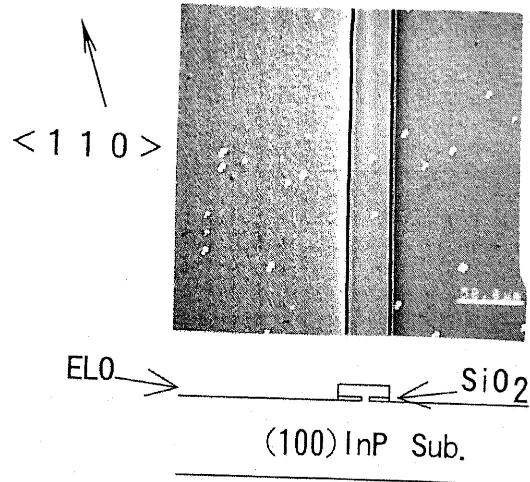

(a)

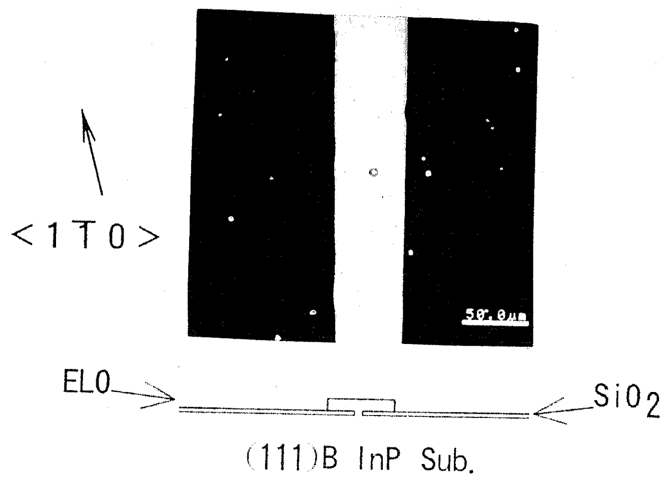

(b)

Figure 2.24: InP stripes after etching, (a) grown on a (001) InP substrate and (b) grown on a (111)B InP substrate.

Chapter 3

Epitaxial Lateral Overgrowth of InP on InP-coated Si Substrates

3.1 Introduction

It is believed that not only InP-based electric devices but also the opto-electronic integrated circuit (OEIC) will open a new field of application of InP. InP growth on Si is one of the most promising technologies for expanding this field. InP-based laser diodes, photodiodes, and solar cells have been fabricated on Si substrates[1~5]. In particular an InGaAsP laser diode reported by Sugo et al. [6] was one of the most successful ones. The laser diode showed excellent life characteristics but its DC characteristics were still inferior to those of diodes fabricated on InP substrates. The reason is probably because of the high density of generated dislocations and the residual stress in the grown films due to the large lattice mismatch (8%) and the large difference in the thermal expansion coefficient between InP films and Si substrates. It is reported that more than 10^6 cm^{-2} dislocation and about 0.4×10^{-3} strain exist in these layers. Though InP growth on Si has been investigated for several years, further crystallinity improvement is necessary to realize performance and reliability levels high enough to enable commercial applications.

Epitaxial lateral overgrowth (ELO) by liquid phase epitaxy (LPE) is known as a very promising technique to provide atomically flat epitaxial layers with few

dislocations for Si, GaAs and GaP alloy[7~12]. We also demonstrated that a remarkable reduction of the dislocation density is realized in InP ELO on InP substrates in chapter 2 [13]. It has been shown that a drastic decrease of dislocation density is possible even for a heteroepitaxy system with large lattice mismatch such as GaAs on Si where GaAs-coated Si substrate was used instead of Si substrate itself to prevent melt-back during LPE[14~16] These results encourages us to use the ELO technique for the growth of InP on InP-coated Si to obtain high quality InP layers on Si with low dislocation density. InP ELO on InP-coated Si substrates differs from homoepitaxial InP ELO on InP substrates in the following two respects. (1) Stress and strain will be produced in InP-coated Si substrates by both the lattice mismatch and the large difference in thermal expansion coefficient between InP films and Si substrates. (2) An InP-coated Si substrate has a rough surface and a high dislocation density which is more than one hundred times that of InP substrates. Therefore, these difficulties must be overcome in order to grow high-quality InP ELO layers on InP-coated Si substrates.

In this chapter, the ELO procedure was first modified for the growth on InP-coated Si substrates. Then, InP ELO layers were grown on InP-coated substrates by using the modified ELO procedure. InP ELO growth on InP-coated substrates is studied to attain atomically flat and nearly dislocation-free InP layers. The mechanism of ELO growth on InP-coated Si substrates is also discussed in comparison with that of ELO growth on InP substrates.

3.2 Modification of ELO for InP-coated Si Substrate

In the present study, a (001) surface was chosen for the substrate orientation because the (001) surface was not only convenient for device fabrications but also suitable for ELO growth as shown in chapter 2. Although it is best to grow InP directly on a Si substrate, but this is difficult since Si substrates are meltbacked by In solution during LPE growth. As the results line seeds will be damaged.

Moreover, InP grown layer contains much Si and this will bring a lot of defects in the ELO layers. To prevent the meltback, a InP thin layer was deposited by VME(Vapor Phase Epitaxy) [17] first in NTT Opto-electronics Laboratories [18] and then ELO by LPE was performed. VME is a kind of a hydride vapor phase epitaxy (VPE). In VME, InCl vapor and PH_3 vapor are mixed just before the substrate to grow InP films at low substrate temperature.

VME of InP is carried out on epi-Si substrates with the misorientation of 2° toward $\langle 1\bar{1}0 \rangle$. Here, epi-Si substrate mean an epitaxial Si wafer which consist of 5 μm-thick epitaxial Si layer doped with P and 500 μm-thick (001) Si wafer doped with Sb. Hereafter, we call this wafer as an "epi-Si substrate". In VME, off-angled substrates are used because a just (001) Si substrate gives a large number of hillocks on the surface of the InP grown layer. The structure of the InP-coated Si substrate is shown in fig.3.1. The etch pit density and X-ray full width at half-maximum of the InP layer are about 5×10^6 cm^{-2} and 65 arcsec, respectively. It is reported that the strain in InP-coated Si substrate is about $4x10^2$ [19]. The surface morphology of an InP-coated Si substrate is shown in fig.3.2. The substrate is macroscopically mirror like but there are wavy-hillocks all over the surface. It also has defects, which are longer than 200 μm as shown in fig.3.2 (b). On the other hand, fig.3.2 (c) shows small round defects and stacking faults. Non-flatness of surface brings difficulties in photolithography, in other words, narrow lines can not be cut since the rough surface scatters the light from a Hg lamp. Therefore, we used a resist suitable for a scattering condition (TSMR-CR B, Tokyo Ohka Kogyo Co. Ltd.). Line seed as narrow as 2 μm can be obtained with this resist.

The substrate preparation procedure for InP ELO on InP-coated Si substrates is basically similar to that of InP ELO on InP substrates described in chapter 2. The difference in the thickness of substrates was adjusted by changing a spacer of a well for a substrate. We also used line seeds in parallel and star-like arrangements, the latter of which has a line opening every 15 degrees. The width of the line seed was varied from 3 to 7 μm and the 10 mm and 500 μm-long line seeds was used for parallel arrangement and the star-like arrangement, respectively. An In solution

or a solution of In:Sn=1:3 was used in LPE. The latter is effective to enhance the lateral growth rate [16]. During the saturation, the substrate was also covered with an InP polycrystal wafer to protect its surface from thermal degradation.

As InP-coated Si substrates have the dislocation density of more than 10^6 cm^{-2}, the surfaces may be weak for the thermal degradation. Therefore, we checked whether the protection with an InP polycrystal was sufficient.To check this, an InP-coated Si substrate was annealed at 600°C for 2 hours. The surface morphology of the annealed substrate is shown in fig.3.3. The figure shows that there is no thermal damage of the surface. The use of an InP polycrystal is sufficient to protect the surface of an InP-coated Si substrate. Then an InP plycrystal was used for the protection before LPE growth.

In a typical growth process the following growth conditions were used: the saturation temperature (T_s) was between 500 and 600 °C, the initial supersaturation (ΔT) was between 0 and 4 °C, the cooling rate (R) was between 0.1 and 0.3 °C/min. The growth time was typically 60 min.

The morphology of the ELO layer was investigated with a Nomarski differential interference contrast microscope (N-DICM) and a scanning electron microscope (SEM). The dislocation density of ELO layers was characterised by chemical etching (H_3PO_4:HBr=2:1) at room temperature for 20s [20].

3.3 ELO of InP on InP-coated Si Substrates

A N-DICM photograph of an InP ELO sample which was grown from In solution with a star-like pattern on an InP-coated (001) Si substrate is shown in fig.3.4. The growth conditions of this sample are as follows: T_s=550 °C, ΔT=4 °C, R=0.3 °C/min, T_g=60 min. It can be seen that the width of ELO was the largest when the stripe was 15° and 30° off-oriented from the $\langle 110 \rangle$ and $\langle 010 \rangle$ directions or their equivalent directions, while it was the smallest when the stripe was oriented almost exactly in the $\langle 110 \rangle$ and $\langle 010 \rangle$ directions or their equivalent directions because a facet formation on the front edge of the ELO largely reduces the growth rate.

The facets on the front edge of the ELO are identified as {111} and {001} planes by measuring the angle of each plane to the substrate surface. The relationships between the ELO and the seed orientation described above are almost the same as those in the case of InP ELO on a (001) InP substrate mentioned in chapter 2. The result shows that the growth mechanism of InP ELO on InP-coated (001) Si is almost the same as that of InP ELO on (001) InP. Although the dislocations from InP-coated Si substrates enhance the vertical growth rate of ELO layers [21], the overall growth behavior might remain unchanged by the presence of a low density of dislocations.

In fig.3.4 it is seen that a part of the ELO near the center of the star-like pattern has no facet on the top. This is because the substrate is tilted toward $\langle 1\bar{1}0 \rangle$. A faceted ELO should become thicker in the direction of $\langle 1\bar{1}0 \rangle$ in fig.3.4. On the other hand, the growth rate which determines layer thickness decreases with a decrease in distance from the center, since the surface supersaturation decreases with the decrease in distance from the center of the star-like pattern [15]. Therefore, near the center of the pattern the growth rate is not high enough to produce a facet. It is also found that the length of (001) facets tends to become short with the increase of the angle between the $\langle 110 \rangle$ direction and the line seed. The cause for this phenomenon will be discussed in the following.

The InP-coated Si substrate with the misorientation of 2° toward $\langle 1\bar{1}0 \rangle$ is not suitable for ELO growth because the top surfaces of ELO stripes incline to the surface of the substrate. As shown in fig.3.4, the thickness of ELO layers is not uniform and, moreover, the region where a (001) facet is formed on the top is restricted on a part of a line seed as mentioned above. This is because the thickness of ELO layer can not exceed the total growth thickness of LPE and a facet can not be formed out of the region. Figure 3.5 shows the schematic illustration of the facet formation on an ELO stripe. The angle (ψ) between a line seed direction and the misorientation direction of the substrate decides the maximum length (L) of the facet formed on the ELO stripe. L is expressed as

$$L = \frac{d}{\cos(\psi)\tan(\theta)}, \tag{3.1}$$

where d is the difference in thickness of the faceted region and θ is the substrate misorientation angle. L takes a maximum value when ψ closes 90°. But ψ=90° should not be chosen as a direction of line seeds since the ELO stripe does not widen. In the case, the line seed directs just toward $\langle 1\bar{1}0 \rangle$.

Figure 3.6 shows InP ELO stripes grown from In solution on an InP-coated Si substrate with ψ=175°. The growth conditions for this sample is as follows: T_s=600 °C, ΔT=4 °C, R=0.3 °C/min, T_g=65 min; SiO_2 mask with 5 μm width and 200 μm period. L of this sample is as short as 200 μm and there are facets only at the end of stripes. On the other hand, InP ELO stripes grown from In solution on an InP-coated Si substrate with ψ=105° have long (001) facets whose length is as long as 1 mm as shown in fig.3.7. The growth conditions for this sample is as follows, which is almost same as above mentioned sample: T_s=600 °C, ΔT=4 °C, R=0.3 °C/min, T_g=60 min; SiO_2 mask with 7 μm width and 200 μm period. In this case, the top surfaces of the ELO stripes incline to the surface of the substrate toward $\langle \bar{1}10 \rangle$ direction, because of the substrate misorientation. The thickness of the stripe is 14 μm at the left and it is 22 μm at the right of the facet. The difference between these two values is 8 μm which agrees well with the value of 9 μm calculated from equation (3.1). Anyhow, misoriented substrates are not suitable to ELO growth since facets can not extend all over the long line seed.

To overcome the inconvenience and to enlarge the area of ELO, a short line seed (SLS) whose length was less than 1mm was proposed. When the line seed is shorter than 1mm, a facet can spread all over the line seed. Figure 3.8 shows an InP ELO layer grown from In solution on an InP-coated Si substrate using SLS. The growth conditions are as follows: T_s=550 °C, ΔT=0 °C, R=0.08 °C/min, T_g=180 min; SiO_2 mask and 5 μm width and 700 μm length, 22° off-oriented from the $\langle 110 \rangle$ direction. The line seed orientation was chosen to obtain widest ELO layers[22]. The ELO layers were broken in middle points probably because the line seeds were damaged in this sample. The shape of ELO expected in a successful

case is shown by a broken line in this figure. The width and thickness of the sample are 44 μm and 18 μm. Then, the ELO ratio becomes 2.4, which is not large. This is because InP-coated Si substrate has a lot of dislocations which are effective to increase the vertical growth rate by supplying surface steps.

In some samples, the width of ELO is large. For example, fig.3.9 shows an InP ELO Layer grown from In solution on InP-coated substrate, whose width is as large as 100 μm. The growth conditions are as follows: T_s=560 °C, ΔT=2 °C, R=0.3 °C/min, T_g=90 min; SiO_2 mask with 6 μm width and 200 μm length, 15° off-oriented from the $\langle 110 \rangle$ direction. The thickness of the grown layer is 5-8 μm and ELO ratio is about 15. The ratio is considerably large. The reason of the large ratio will be discussed in chapter 4 using the results of photoluminescence measurements. Si-doping is the most probable candidate for this broadening, whose Si comes from the Si substrate.

Detailed observation of ELO surfaces with N-DICM shows the existence of spirals. Figure 3.10 shows one spiral on the upper ELO stripe and two spirals on the lower ELO stripe. The growth conditions for this sample is as follows: T_s=560 °C, ΔT=2 °C, R=0.2 °C/min, T_g=90 min; SiO_2 mask with 6 μm width and 200 μm period, 15° off-oriented from the $\langle 110 \rangle$ direction. An In was used as a solution. These spiral of surface steps are emerged from screw dislocations. Two of them lie over the line seed but one of them exists out of the line seed region and on the lateral growth region. These screws are thought to come from the substrate through line seeds. Therefore, it seems that the latter screw was bent during the growth. But our result can not exclude the probablity that these screws were generated at the interface between SiO_2 mask and the grown layer. Since the screw dislocations supply steps for growth, the spirals made large effects on the vertical growth of ELO. The N-DICM photograph, however, does not show each step of the spirals. It only shows the contrast of a conical shape on the surface, which corresponds to a spiral. This is probably because the interstep distance of the spiral is so small that N-DICM can not resolve each step. In general, the interstep distance is determined by the supersaturation. Such a small interstep

distance indicates that the supersaturation of the growth was high.

Then, we tried to observe these steps using AFM. Figure 3.11 shows a center of the spiral observed by AFM. Two spiral steps are emerged from the center. These spirals have oval shape, which is similar to the case of InP ELO layers grown on InP substrates. The long axis of this spiral directs toward $\langle\bar{1}10\rangle$. The intervals between each two steps are about 3250 Å toward $\langle\bar{1}10\rangle$ direction and 2700 Å toward $\langle110\rangle$ direction. Here the average values are not described because the intervals of two spirals are not uniform. One spiral is accompanied by the other with the separation of about 1000 Å. The ratio of these values is 3250 Å/2700 Å = 1.20, which is almost equal as that of InP ELO layers on InP substrates (8.3 μm/6.7 μm=1.24). This suggests that the mechanism which decides spiral shape is the same in both cases, in other words, the difference between "A" step and "B" step does. Ordinary screw has Burgers vector of a lattice constant **a**, which is two atomic-layer in zinc blend structure. Then, it is easily understood that two spirals emerge from one screw which has a Burgers vector of **a**. As shown in fig.3.12, the height of the spiral step is 0.24 $\sim$ 0.29 nm, which indicates that these are monolayer steps. The interstep distance of the ELO grown on InP-coated Si substrate is more than 50 times smaller than that of the ELO grown on InP substrates. The supersaturation of these two samples did not differ so much. Therefore, this is probably due to the Si-doping in the InP ELO layer grown on InP-coated Si substrate. Though the area of the substrate used in this experiment was smaller than the area of the well for the In solution, there must be a part that the solution touched a side of the Si substrate and Si atoms were dissolved into the In solution and doped into the ELO layer. As Si atoms on the ELO surface make it difficult for the motion of the surface steps, the interval of the steps becomes small in this case.

3.4 Doping Effects

As mentioned in previous section, the doping of Si are useful to suppress vertical growth rate and to improve ELO ratio. In this section, effects of Sn doping on InP

ELO layer grown on InP-coated substrate are investigated.

To avoid the formation of side facets, we have chosen the line seed orientation of 15°off-oriented from the ⟨110⟩ direction to obtain wide and long ELO layers. Line seeds of 7μm wide were parallel to each other width period of 200 μm. The growth conditions for this sample is as follows, T_s=550 °C, ΔT=1 °C, R=0.15 °C/min, T_g=60 min. An In and Sn mixture (In:Sn=1:3 by volume) was used as the solution for Sn doping. Figure 3.13 shows a cross-sectional micrograph of the ELO layer. As is seen in the figure, ELO with large width of about 90 μm and small thickness of about 6 μm is obtained. ELO ratio of the sample is 15, which is almost equal to that of homoepitaxial InP ELO [13].

The result shows that good InP ELO layers can be grown on InP-coated Si substrates if Sn doping and appropriate growth conditions for ELO are used. Moreover, since the ELO layer shows no sign of facet formation on the front edge of the ELO, even wider ELO is expected to be obtained simply by the extension of the growth time.

3.5 Dislocations in ELO layers

InP ELO layers grown on InP-coated Si substrates were chemically etched to measure the dislocation density. An ELO layer after etching is shown in fig.3.14, which is a part of the ELO layers shown in fig.3.4, whose thickness is about 7μm. It can be seen that most etch pits are observed over the line seed region. The result suggests that the dislocations represented by these pits originated from the InP-coated Si substrate through the line seeds. Figure 3.14 also shows that one etch pit exists on an edge of the ELO layer. One of the cause is a bending of the dislocation, which originated from the substrate through the line seed. Other parts of the etched ELO layers are shown in fig.3.15. These photographs show that most of the etch pits exist over the line seed region. Stacking faults are also found in figs. 3.15 (c) and (d).

Another example of ELO layer after etching is shown in fig.3.16. It can be

seen in the figure that etch pits align in two parallel lines, which may correspond to the two sides of the line seed. A few etch pits are observed on the lateral overgrowth regions. This figure also shows the presence of a stacking fault on an inclined {111}B plane, in other words, the line which shows a stacking fault points to ⟨110⟩ direction. No stacking fault on inclined {111}A planes was observed in all etched samples. The following types of dislocations in GaAs layers grown on Si substrates have been reported so far [23]: 30°-type dislocation, 60°-type dislocation and a screw-type dislocation. All these dislocations except the screw type glide on {111} planes, as shown in fig.3.17. A 60°-type dislocation lies on one of the four ridges of a pyramid which consists of four {111} planes (fig.3.17 (a)). On the other hands, a 30°-type dislocation lies on the center of a side face of the pyramid. From the similarity in dislocations between InP and GaAs, it is understood that the etch pits aligned in two lines in fig.3.16 imply the propagation of dislocations (30°-type or 60°-type) on {111} planes through the line seed (fig.3.17 (b)). The fact that there are rather few dislocations appearing in the area just above the line seed opening indicates that the density of screw-type dislocations and 30°-type dislocations on {111}A planes is low. If we calculate the average dislocation density of the ELO layer (fig.3.16) assuming that one etch pit corresponds to one dislocation, we obtain the value of 3.4×10^5 cm^{-2}. This is more than one order lower than the density of dislocations, 5×10^6 cm^{-2}, existing in InP-coated substrates. Figure 3.16 also shows that dislocation-free InP areas, whose width is about 30 μm, exist in the outer regions of the dislocation areas. This indicates that the SiO_2 film between the lateral overgrowth layer and the substrate effectively prevented the propagation of the dislocations from the substrate. Dislocation-free InP areas have been obtained on Si substrates for the first time and are expected to be used as a substrate on which various kinds of devices can be fabricated.

Figure 3.18 shows other ELO layer after etching. The growth conditions for this sample is as follows: T_s=550 °C, ΔT=1 °C, R=0.1 °C/min, T_g=60 min; SiO_2 mask with 6.5 μm width and 200 μm period. An In and Sn mixture (In:Sn=1:3 by volume) was used as the solution for Sn doping.It can be seen from this figure

that etch pits align in a straight line in the right part of the figure and that etch pits start to align in two parallel lines. This change ascribes to the difference in the thickness of the ELO layer, whose thickness is about 7 μm at the right and gradually increases to 12 μm at the left. Since the dislocations (30°-type or 60°-type) propagate on {111}B planes as mentioned above, two {111}B planes which originates from the line seed play an important role for deciding the distribution of dislocations. When the ELO layer is thin, the separation between two {111}B planes is small and the crossing lines between the {111}B panes and the surface of the ELO layer look like one line. When the thickness of the ELO layer increases, the separation of two {111}B planes increases and two crossing lines are separated. Four stacking faults are also observed in this figure. The dislocation and the stacking faults in this figure can be ascribed to the defects which originated from the InP-coated Si substrate through the line seed because of the coincidence in their densities.

3.6 Summary

At first the procedure of ELO was modified to be suitable for InP-coated Si substrate, which has a rough surface. Then, InP ELO growth on InP-coated Si substrates was investigated.

An InP epitaxial layer with a dislocation-free area was obtained for the first time on a Si substrate by using the ELO technique. The growth behavior of the ELO layer on Si substrates was found, in principle, to be similar to that of homoepitaxial growth of InP ELO. A wide and flat ELO layer of InP on a (001) InP-coated Si substrate was achieved if the line seed is tilted around 15° away from ⟨100⟩, ⟨110⟩ and their equivalent directions. On the other hand, the lateral growth fronts are soon covered with {111} and {001} facets and the lateral growth is minimum when the line seeds are prepared almost exactly in the above directions.

Spirals of surface steps were observed on InP ELO layers grown on InP-coated Si substrates by N-DICM and AFM, similarly to the case grown on InP substrates.

This indicates that ELO mechanism is almost the same in both case. Atomically flat InP layers were obtained also on Si substrates.

The ELO ratio of InP ELO layers grown on InP-coated Si substrates was increased by doping. Sn doping was effective to increase ELO ratio, which was increased to be as large as 15. On the other hand, we should prevent a Si unintentional doping from Si substrates. If an In melt touches with the side of a Si substrate, Si is dissolved into the In melt and is doped into the grown layer. Though the Si doping brings a large ELO ratio, the increase is not controllable. The unintentional doping will be avoided with the use of a large InP-coated Si substrate, which is larger than the size of the well for the In solution.

Though a small number of etch pits were observed on the lateral overgrowth regions, most of the etch pits were observed above the line seeds. This indicates that the SiO_2 film between the lateral overgrowth layer and the substrate is useful to prevent the propagation of the dislocations from the substrate to the ELO layer. ELO is an excellent method to obtain dislocation-free InP layers on Si substrates with extremely flat surfaces. Therefore InP ELO layers grown on Si substrates are expected to realize high performance of the devices fabricated on them.

Bibliography

[1] D. G. Deppe, N. Holonyak, Jr., D. W. Nam, K. C. Hsieh, G. S. Jackson, R. J. Matyi, H. Shichijo, J. E. Epler and H. F. Chung: Appl. Phys. Lett. **51** (1987) 637.

[2] T. Egawa, H. Tada, Y. Kobayashi, T. Soga, T. Jimbo and M. Umeno: Appl. Phys. Lett. **57** (1990) 1179.

[3] J. Paslaski, H. Z. Chen, H. Morkoc and A. Yariv: Appl. Phys. Lett. **52** (1988) 1410.

[4] W. Dobbelaere, J. De Boeck, P. Heremans, R. Mertens, G. Borghs, W. Luyten and J. Van Landuyt: Appl. Phys. Lett. **60** (1992) 3256.

[5] Y. Itho, T. Nishioka, A. Yamamoto and M. Yamaguchi: Appl. Phys. Lett. **49** (1986) 1614.

[6] M. Sugo, H. Mori, Y. Itoh and Y. Sakai: *Ext. Abstr. 1992 Int. Conf. on Solid State Devices and Materials* (Japan Society of Applied Physics, Tsukuba,1992) P656.

[7] T. Nishinaga, T. Nakano and S. Zhang: Jpn.J.Appl.Phys. **27** (1988) L964.

[8] S. Zhang and T. Nishinaga: J.Cryst.Growth **99** (1990) 292.

[9] Y. Suzuki and T. Nishinaga: Jpn.J.Appl.Phys. **28** (1989) 440.

[10] R. Bergmann, E. Bauser and J. H. Werner: Appl. Phys. Lett. **57** (1990) 351.

[11] R. Bergmann: J.Cryst.Growth **110** (1991) 823.

[12] S. Zhang and T. Nishinaga: Jpn.J.Appl.Phys. **29** (1990) 545.

[13] S. Naritsuka and T. Nishinaga: J.Cryst.Growth **146** (1995) 314.

[14] Y. Ujiie and T. Nishinaga: Jpn.J.Appl.Phys. **28** (1989) L337.

[15] S. Sakawa and T. Nishinaga: J.Cryst.Growth **115** (1991) 145.

[16] S. Sakawa and T. Nishinaga: Jpn.J.Appl.Phys. **31** (1992) L359.

[17] H.Mori, M.Ogasawara, M.Yamamoto and M.Tachikawa, Appl. Phys. Lett **51** (1987) 1245.

[18] M. Tachikawa, T. Yamada, T. Sasaki, H. Mori and Y. Kadota: Jpn.J.Appl.Phys. **34** (1995) L657.

[19] M.Sugo, N.Uchida, A.Yamamoto, T.Nishioka and M. Yamaguchi, J. Appl. Phys. **65** (1989) 591.

[20] A. Huber and N. T. Linh: J.Cryst.Growth **29** (1975) 80.

[21] W. Burton, N. Cabrera and F. C. Frank: Philos. Trans. R. Soc. London **A243** (1951) 299.

[22] Wu-yih Uen, Doctor Thesis (1993).

[23] M. Tamura, A. Hashimoto and N. Sugiyama: J.Appl.Phys. **70** (1991) 4770.

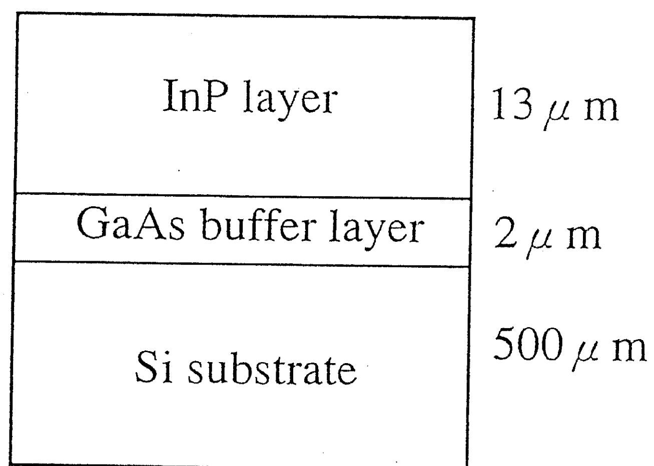

Figure 3.1: Schematic illustration of an InP-coated Si substrate.

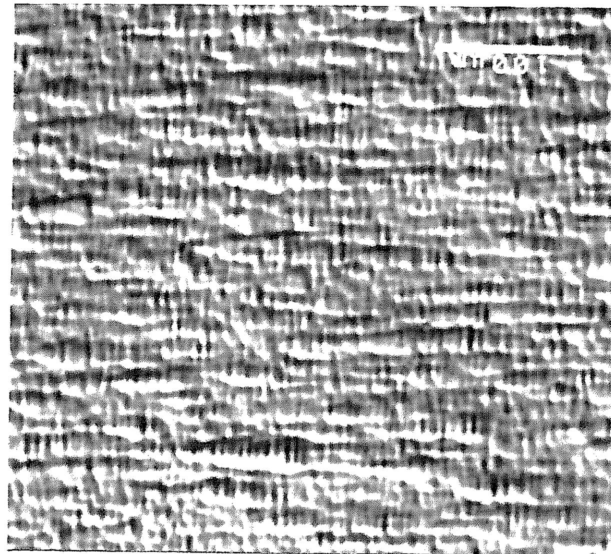

(a)

<1$\bar{1}$0>

100 μm

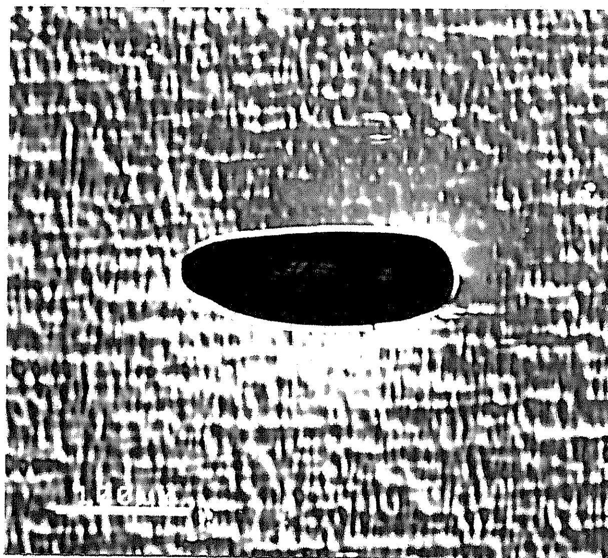

(b)

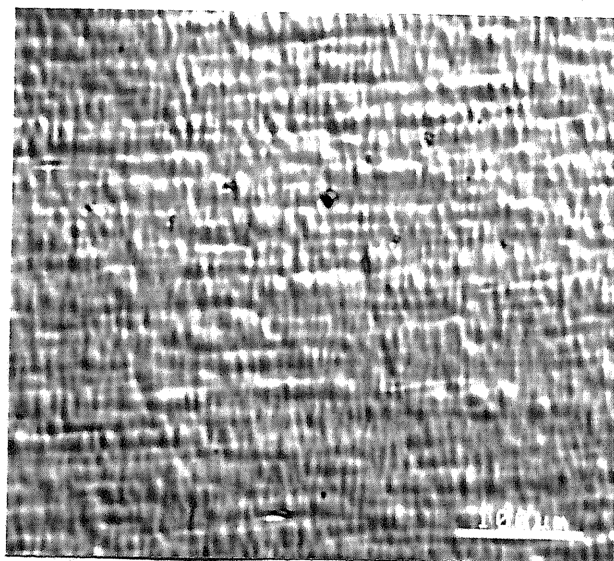

(c)

Figure 3.2: Surface morphology of an InP-coated Si substrate.

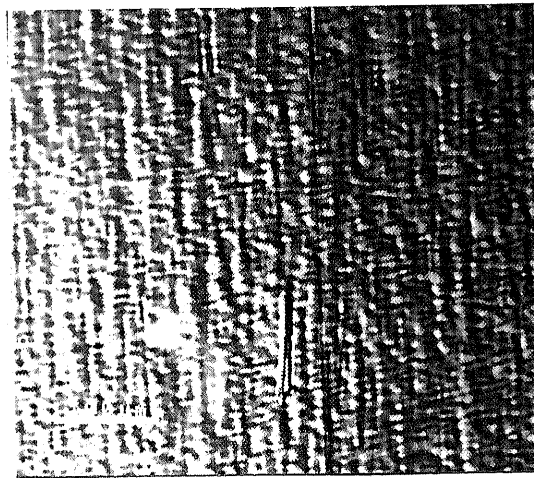

Figure 3.3: Surface morphology of an annealed InP-coated Si substrate.

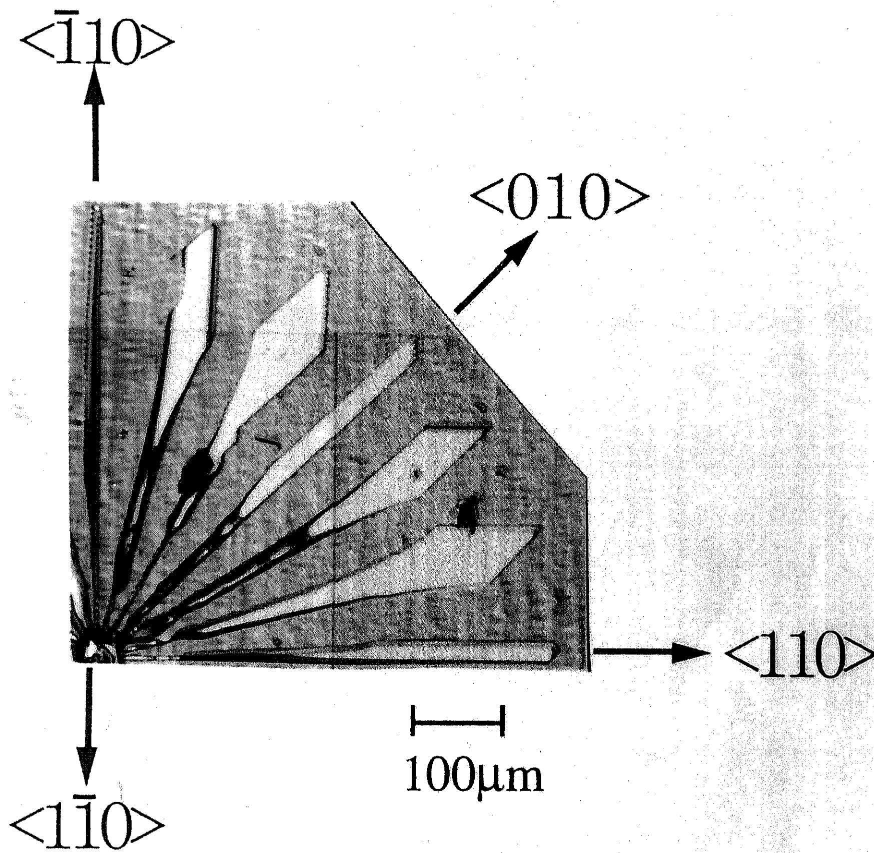

Figure 3.4: InP overgrowth with a star-like line seed on an InP-coated (001) Si substrate.

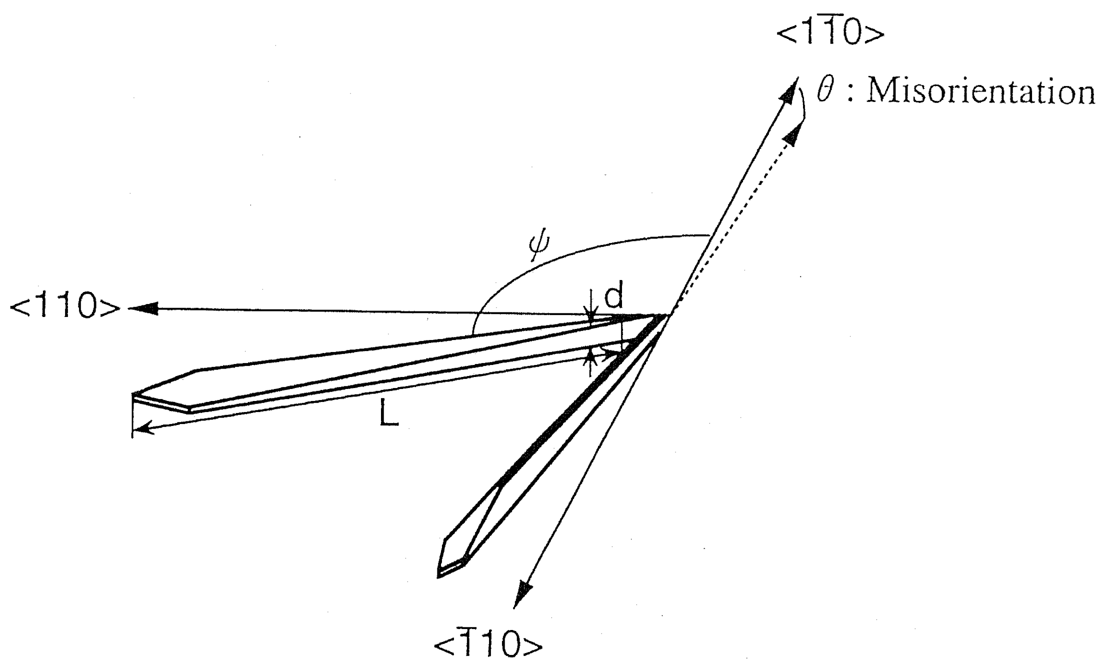

Figure 3.5: Schematic illustration of the facet formation on an ELO stripe.

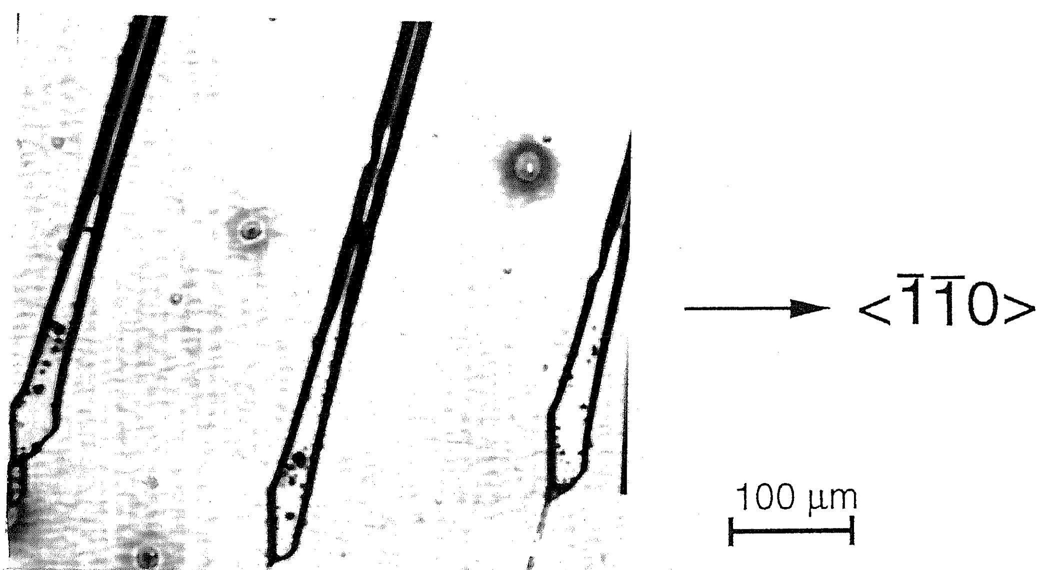

Figure 3.6: InP overgrowth with parallel line seeds on an InP-coated (001) Si substrate: $\psi = 175°$.

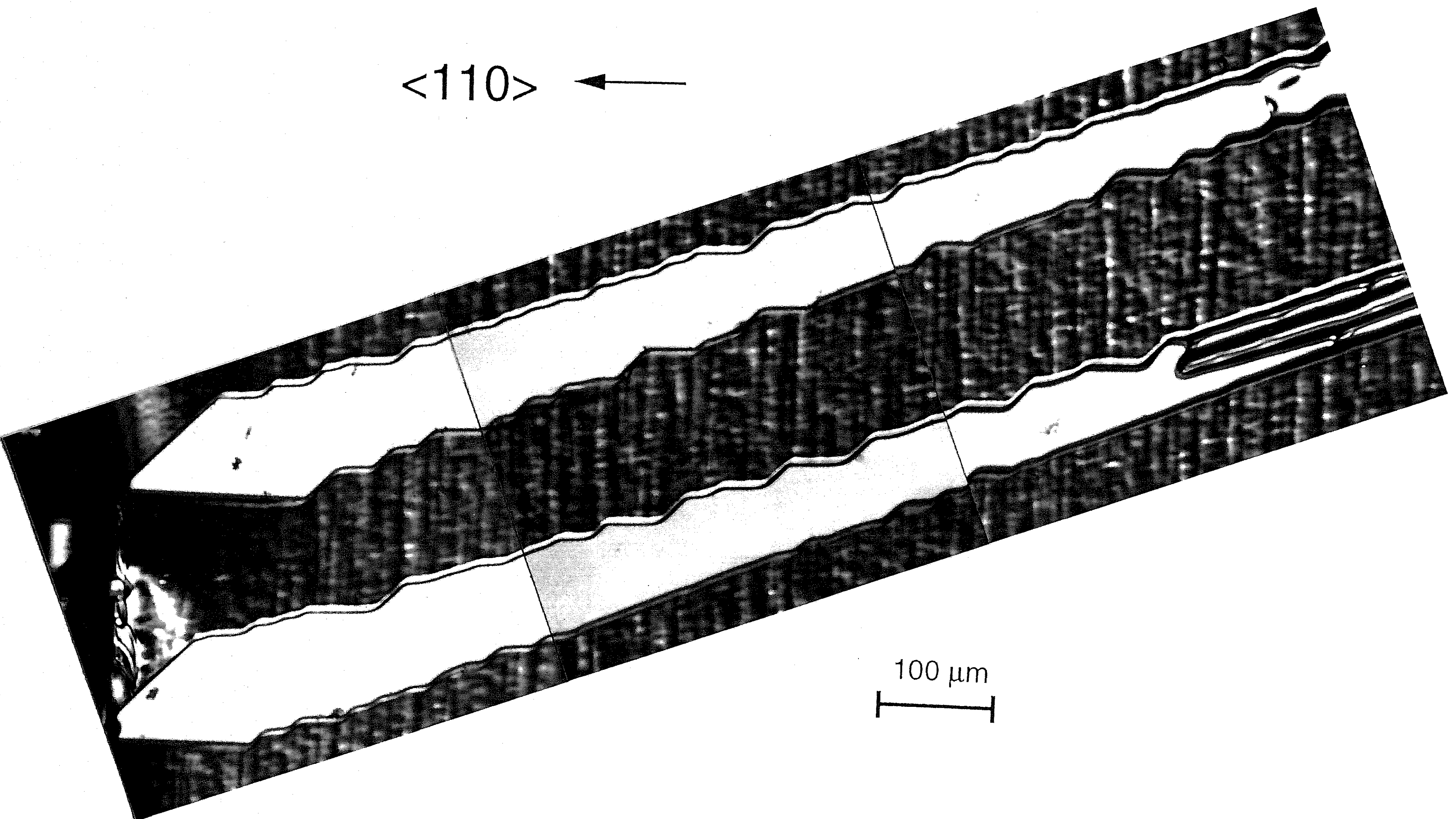

Figure 3.7: InP overgrowth with parallel line seeds on an InP-coated (001) Si substrate: $\psi = 105°$.

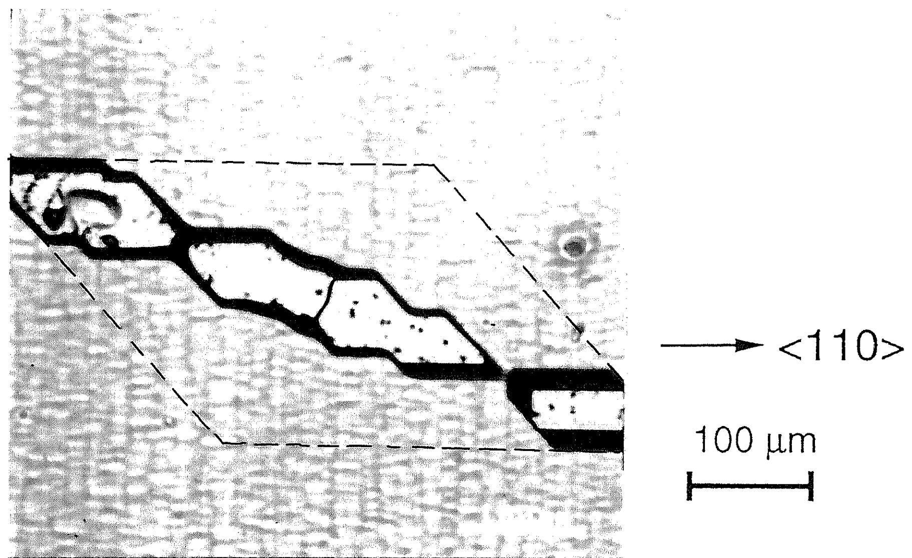

Figure 3.8: InP overgrowth with parallel line seeds on an InP-coated (001) Si substrate.

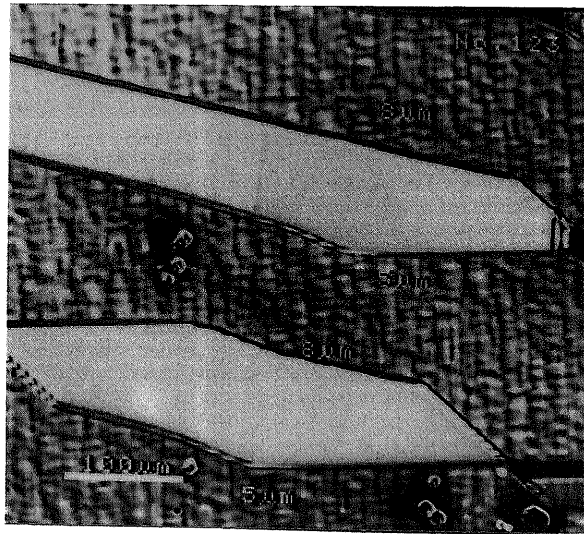

Figure 3.9: InP overgrowth with short line seeds on an InP-coated (001) Si substrate with unintentionally Si doping.

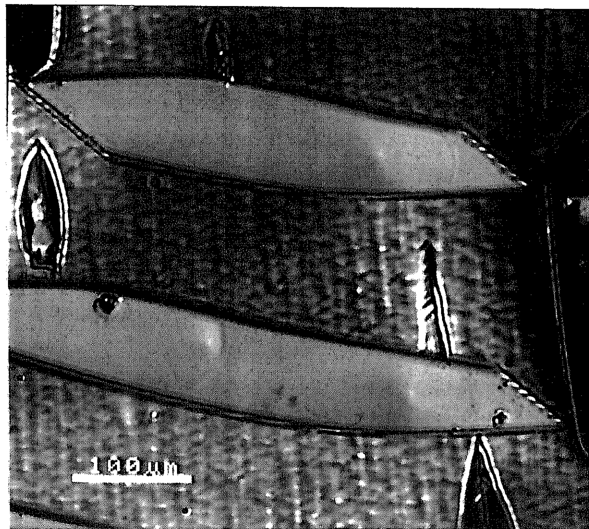

Figure 3.10: N-DICM photograph of an InP ELO layer grown on an InP-coated Si substrate, which shows the existence of spirals on the surfaces.

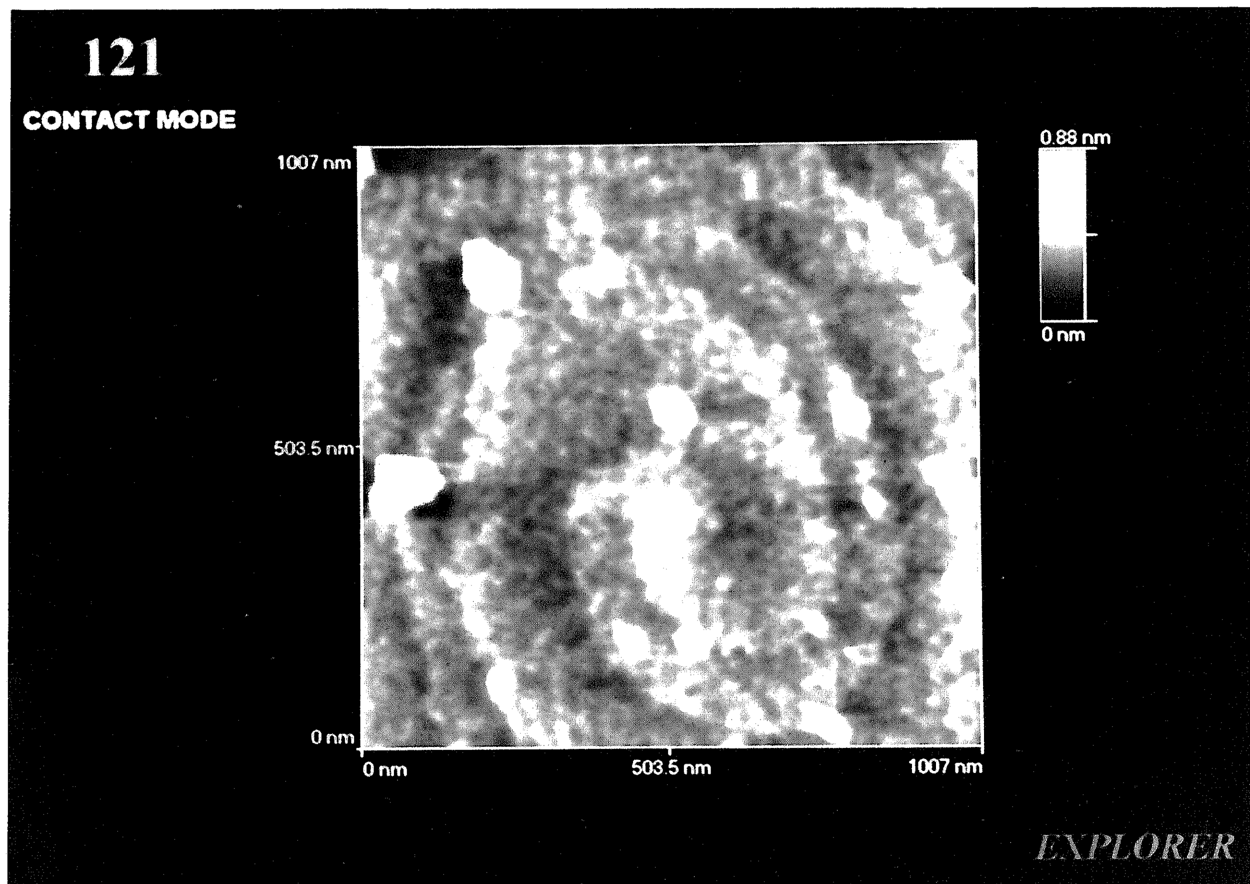

Figure 3.11: AFM image of a spiral step on a (001) InP ELO layer grown on an InP-coated Si substrate.

121

CONTACT MODE

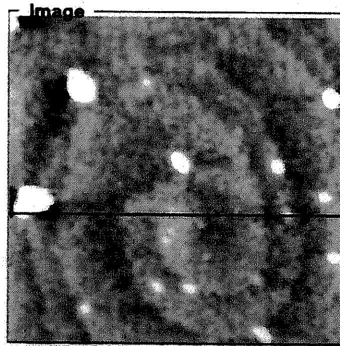

Report

#	Distance	Height
1	105.02 nm	0.26 nm
2	53.58 nm	0.29 nm
3	62.16 nm	0.24 nm

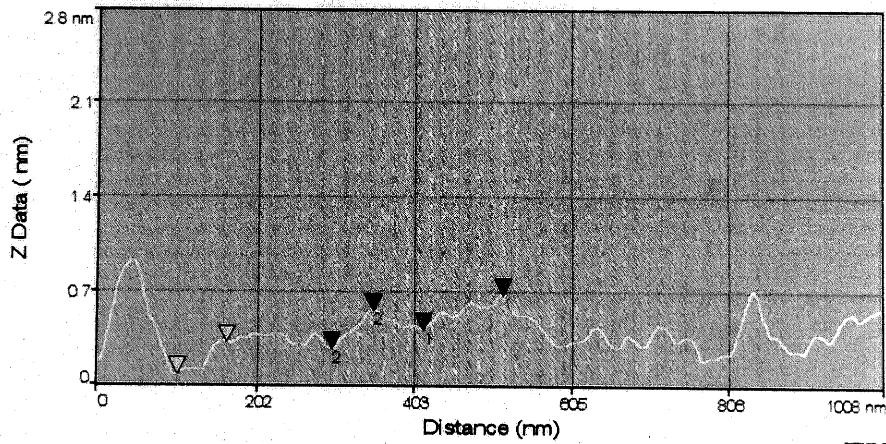

EXPLORER

Figure 3.12: AFM image of a spiral step on a (001) InP ELO layer grown on an InP-coated Si substrate and its hight profile.

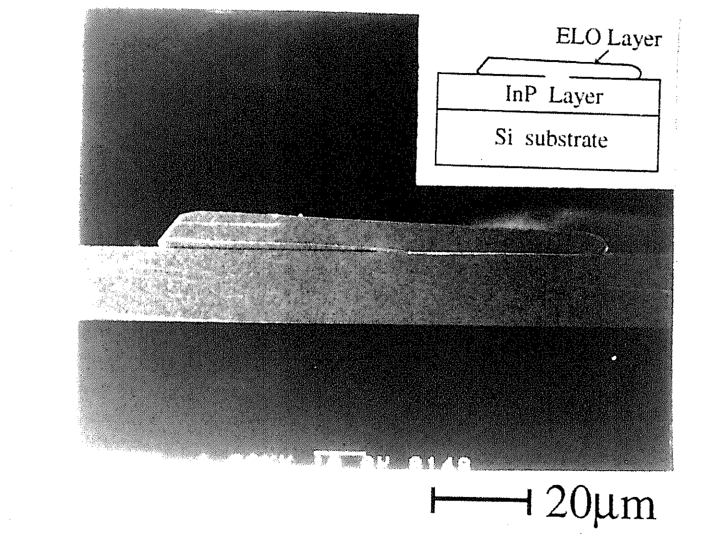

Figure 3.13: Cross-sectional SEM image of a (001) InP ELO layer grown on an InP-coated Si substrate with Sn doping.

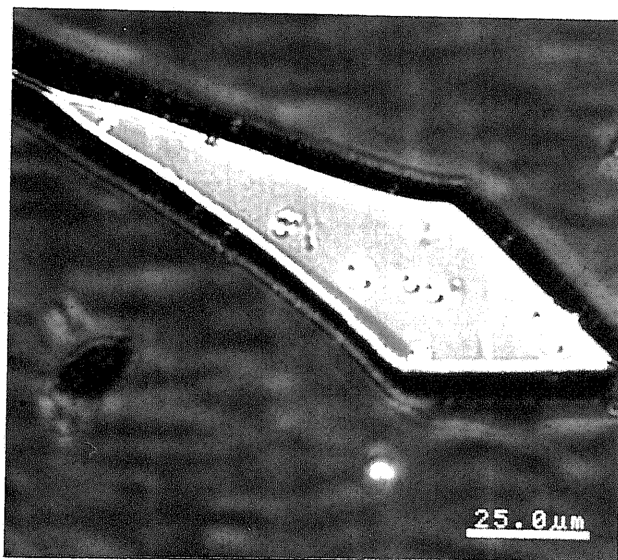

Figure 3.14: InP stripe after etching grown on a (001) InP-coated Si substrate with a star-like line seed.

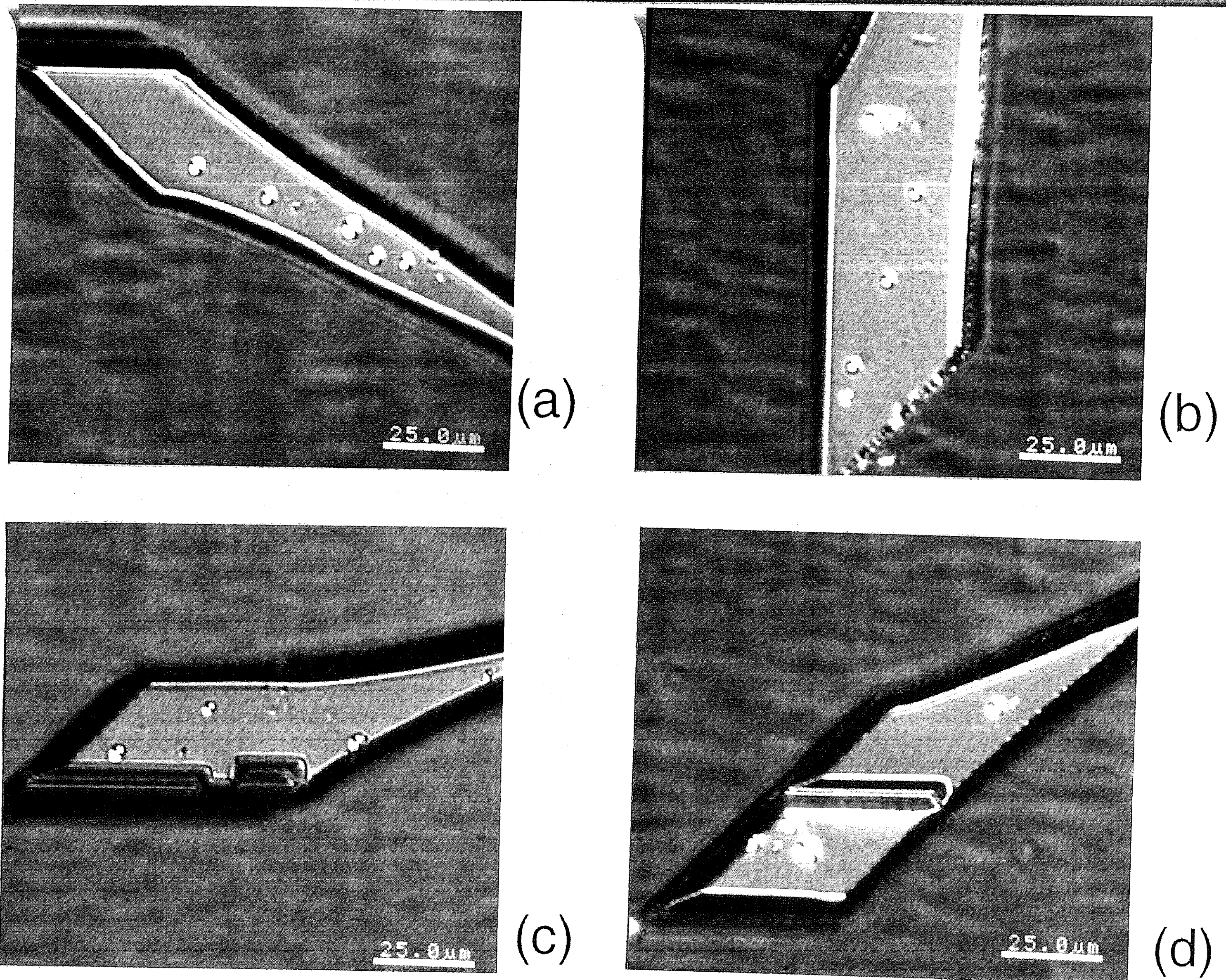

Figure 3.15: InP stripes after etching grown on a (001) InP-coated Si substrate with a star-like line seed. (a) $\psi = 75°$, (b) $\psi = 165°$, (c) $\psi = 105°$ and (d) $\psi = 150°$.

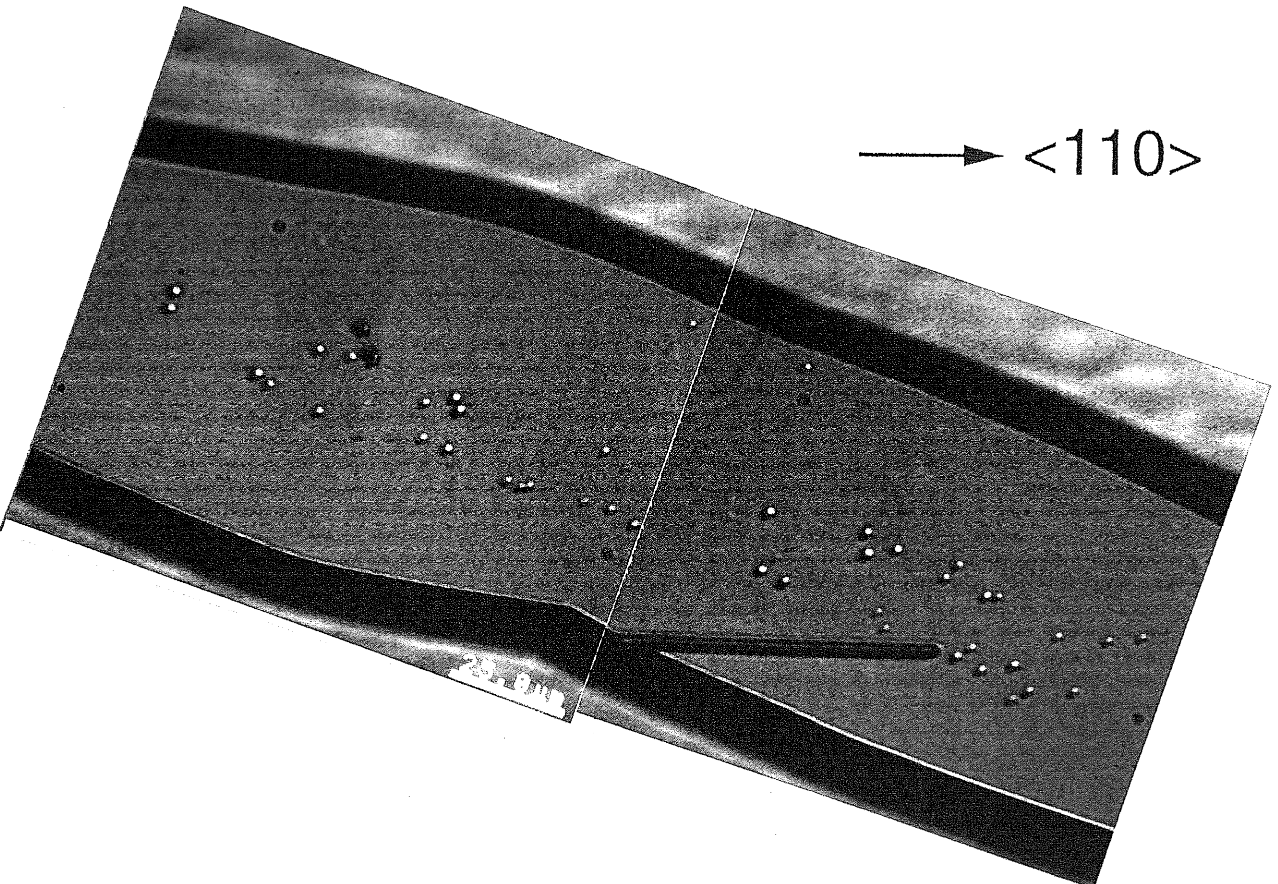

Figure 3.16: InP stripe after etching grown on a (001) InP-coated Si substrate with a parallel line seed.

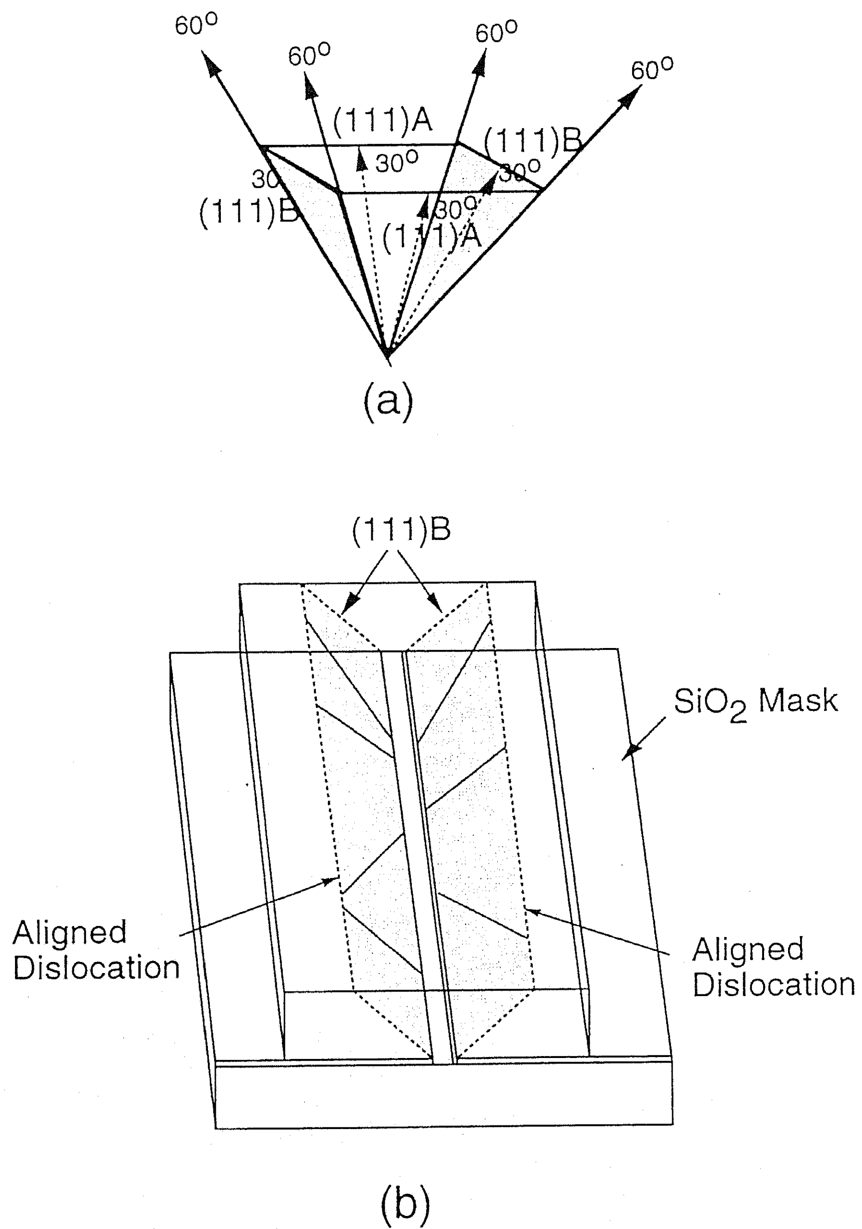

Figure 3.17: (a) Schematic illustration of the propagation directions of dislocations and (b) dislocation propagation in an ELO layer and the formation mechanism of two parallel lines of etch pits.

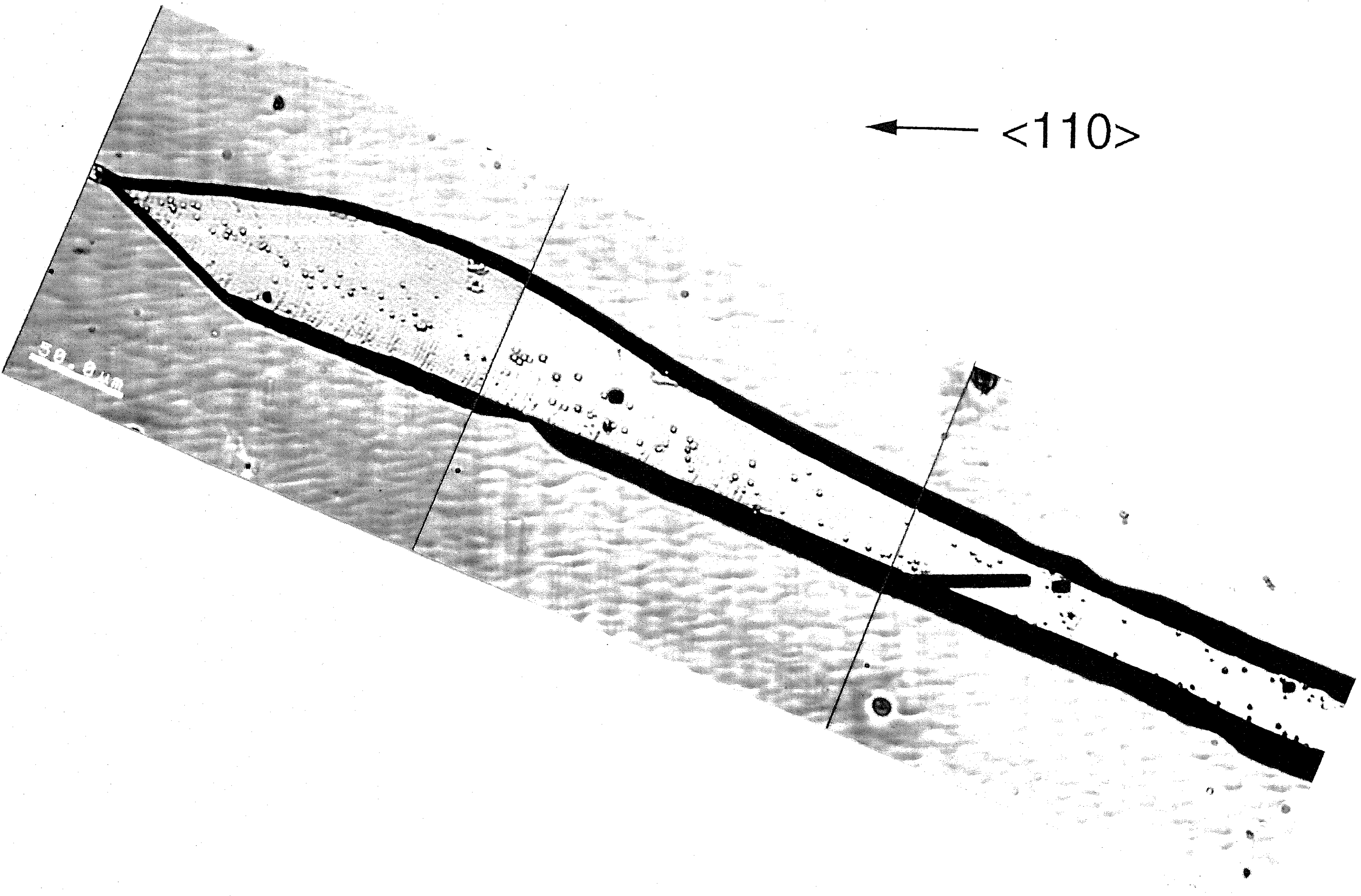

Figure 3.18: InP stripe after etching grown on a (001) InP-coated Si substrate with a parallel line seed.

Chapter 4

Characterization by Spatially Resolved Photoluminescence

4.1 Introduction

We have so far dealt with the ELO growth to improve crystallinity of InP layers grown on Si substrates. Dislocation-free areas have been realized on InP-coated Si substrate. One of the subjects of our study is to fabricate optical devices such as laser diodes on Si substrates to step forward to the way for OEIC. The fabrication of optical devices with excellent qualities requires grate improvement in the optical property of InP layers grown on Si substrates. Optical quality of InP layers can be characterized by photoluminescence measurements[1, 2]. An ordinary PL system, however, finds it difficult to characterize small 3-dimensional structures of ELO layers. Therefore, we tried to use spatially resolved photoluminescence (SRPL) system to characterize ELO layers[3, 4]. A high spatial resolution of SRPL system, which will be described in the subsequent section, makes the characterization possible.

Residual stress in grown layers is another extremely important factor in heteroepitaxial growth. Stress makes a shift and a broadening of photoluminescence spectra since stress redegenerates two radiational peaks which are originated from light holes and heavy holes[5∼7]. Then, stress in InP layers grown on Si sub-

strates were investigated by photoluminescence[8~11]. Wuu et al. estimated the stress in InP layers grown on Si substrates from their PL peak shifts[8]. They reported that thin InP layers grown on Si substrates, which were thinner than 0.8 μm, showed compressive stress and ones, which were thicker than 1 μm, showed tensile stress as a result of difference in thermal contraction during the cooling process after growth. Sugo et al. reported a similar result[9]. Because ELO layers have 3-dimensional structure, stress in the layers is expected not to be uniform and may have some distributions. Therefore, study for the distribution of stress is necessary for more understanding of ELO growth. We also tried to investigate stress distribution in ELO layers using SRPL technique.

Two causes for residual stress in ELO layers are considered: one is the differences between InP and Si in lattice constant and thermal expansion coefficient and the other is the difference between SiO_2 mask and InP in thermal expansion coefficient, which produces residual stress during cooling process after growth. In this chapter the cause for the stress is discussed about with the results of SRPL measurements.

A multi quantum well (MQW) structure is grown on an InP ELO layer on an InP-coated Si substrate to prepare for the fabrication of optical devices. The optical properties of the MQW layer are characterized using SRPL.

Stress simulation is another important approach to study stress in heteroepitaxial layers. An analytical way of simulation of the stress in heteroepitaxial layers was proposed by Feng et al.[12], which was one application of bi-metal stress simulation. A calculated stress in GaAs/Si was also reported[13]. However those works dealt only using 2-dimensionally flat structure. Since ELO layers have 3-dimensional structures, a special method will be needed for the simulation of their stress. We try to simulate these stresses numerically. Finite element method (FEM) is a very effective way to simulate stress numerically. Therefore, stress in ELO layers are simulated by a computer using FEM. The simulated results are used in the discussion of the stress distributions in ELO layers.

The critical width of line seeds not to form misfit dislocations are also estimated

about GaAs on Si and InP on Si in order to see the possibility of ELO.

4.2 SRPL Measurement

SRPL measurements were performed at 98 K using a SRPL system. Figure 4.1 shows a SRPL system which consists of a laser, a microscope, a monochrometer and other optical parts. The output light emitted from an Ar^+ laser is chopped at 1000 Hz by a chopper and is introduced into a microscope by a half mirror. This 488 nm light from the laser is focused on a sample, which is in a cryostat evacuated by a rotary pump. The sample is cooled with a flow of liquid nitrogen until 98 K. The temperature of the sample is measured by a thermocouple installed in the sample holder. Luminescence light from the sample is gathered by a lens of the microscope and is introduced into a monochrometer (Nippon Bunkou, CT-100). The focal length of the monochrometer is 1000 mm. The out put signal of the monochrometer is detected by a photomultiplier (R712, Hamamatsu-photonics Co.). A direct beam from the laser is cut by a filter, which is put before the monochrometer to decrease noise. Lock in amplifier is used to increase a signal to noise ratio. A pinhole in the microscope, whose diameter is 200 μm, is used to improve spatial resolution of the measurement. The spatial resolutions of 5 μm and 20 μm are obtained by the use of objective lenses whose magnification is 40$\times$ (Nikon OPTIPHOT-POL, numerical aperture : 0.50) and 10$\times$ (Nikon OPTIPHOT-POL, numerical aperture : 0.25). The x–y position of the sample is precisely controlled by micrometers.

4.3 SRPL of InP ELO on InP Substrates

FWHM of photoluminescence spectra is influenced by the impurities and perfection of crystal structures of samples. The effect of impurity on FWHM was investigated from the dependence on run number. Here run number indicates the number of growth runs after renewal of an In solution. In all experiments, a solution was not

baked before growth. A solution and an InP source were prepared with the method described in chapter 2. A solution was etched with HCl for 2 minutes and dipped in Di H_2O five times. An InP source was etched with H_2SO_4:H_2O_2:H_2O after chemical degreasing with organic solvents. Therefore, some impurities are not removed by this process and they are brought into growth system. Volatile components of the impurities are evaporated during growth runs and even nonvolatile components are also consumed to be doped into grown layers. Then, impurities concentrations in the solution gradually decrease with growth runs. In other words, the more the run number increases, the purer the grown crystal becomes.

Figure 4.2 shows the dependence of FWHM of PL spectra on growth number. The figure shows that the FWHM decreases from 27 to 20 meV and eventually saturates to 19 meV. Since FWHM of PL spectra is wide in a sample with high carrier density, the decrease in FWHM indicates that the carrier density, in other words, impurity concentration decreases with growth runs.

Figure 4.3 shows SRPL spectra of an InP ELO layer grown on an InP substrate for 5 positions across the ELO stripe. The ELO layer was grown from In solution with the growth conditions as shown in following: T_s=550 °C, ΔT=0 °C R=0.05 °C/min, t_g=60 min; line seed with 3 μm in width and 700 μm in length. The shapes of these spectra are almost similar and the intensity of these spectra decreased a little in both edges. The optical property of this ELO layer is nearly uniform. The FWHM of these spectra is as narrow as 19 meV and the peak wavelengths of these spectra are about 882 nm. These values are almost the same as those of a flat InP ELO layer grown directly on an InP substrate in a similar growth condition: T_s=600 °C, ΔT=4 °C R=0.3 °C/min, t_g=60 min. The peak wavelength and FWHM of the layer are 880.7 nm and 15.7 meV, respectively. The difference in thermal expansion coefficient between SiO_2 and InP may bring some residual stress in those layers during the cooling process after growth. The SRPL results, however, indicate the SiO_2 mask causes almost no stress in the ELO layer. The thickness of the SiO_2 mask of about 1000 Å and/or the ELO structure itself, which is effective to release stress, seem to bring extremely low residual stress.

The dependence of peak wavelength, FWHM and intensity of SRPL spectra on their measured positions on the ELO stripe are shown in fig.4.4 (a), (b) and (c), respectively. Peak wavelengths of the PL spectra of the ELO layer are 882.5±0.5 nm as shown in fig.4.4 (a). The emission is ascribed to a band edge emission because the band gap of InP is 1.407 eV (881.2 nm) at 100 K, calculated from the equation: $Eg = 1.421 - 3.63 \times 10^{-4}T^2/(T + 162)$ [14]. The good coincidence between the peak wavelengths and the band gap energy of InP suggests that no residual stress exists in this layer. Fig.4.4 (b) also shows that the FWHM of PL spectra is as narrow as 19 meV and has uniform distribution over the stripe, though the intensity of PL spectra decreases a little at both sides as shown in fig.4.4 (c).

A broadening of PL spectra is caused by a doping of impurities. Therefore, we should keep the carrier concentrations in mind when we discuss about the broadening of SRPL spectra. On the other hand, residual stress makes the peak wavelengths shift. Therefore, strain can be estimated from the photoluminescence peak shift using a deformation-potential model[6]. The calculated energy gap change ΔE under stress is given by[15, 9]

$$\Delta E = [\frac{2a(C_{11} - C_{12})}{C_{11}} \pm \frac{b(C_{11} + 2C_{12})}{C_{11}}]\epsilon_{||} \tag{4.1}$$

where C_{ij} are the elastic stiffness constants, a is the hydrostatic deformation potential, b is the shear deformation potential. and $\epsilon_{||}$ is defined to be positive for tensile stress. The distribution of residual stress in ELO layers can be estimated from SRPL measurement using the above equation.

4.4 SRPL of InP ELO on InP-coated Si Substrates

A SRPL spectrum of an ELO layer grown from In solution on an InP-coated Si substrate is shown in fig.4.5. The growth conditions of this sample is as follows: T_s=550 °C, ΔT=4 °C R=0.3 °C/min, t_g=60 min; line seed 3 μm in width. The figure also shows SRPL spectra of an InP-coated Si substrate and an InP reference

sample grown directly on an InP substrate under a similar growth condition by LPE. The peak wave length of the ELO layer was about 882 nm, which was almost the same as that of the reference sample. This indicates that the stress in the ELO layer was very low. In other words, the ELO is able to decrease the stress caused by both the lattice mismatch and the difference in thermal expansion coefficient. The strong SRPL intensity, which was rather stronger than that of the reference sample, and the narrow FWHM of the SRPL spectrum (18.5 meV) show that the optical quality of the ELO layer is almost as good as that of the reference sample. It can also be said that ELO is beneficial not only for the reduction of the dislocation density but also for the relief of the stress, which results in good optical quality of ELO layers.

The spatial resolution of the SRPL measurement is as small as 5 μm in diameter as mentioned in previous section. The distribution of PL spectra was also investigated by using SRPL measurements. Figure 4.6 shows SRPL spectra for each measured position, which aligned across the ELO stripe. The shapes of these spectra are almost equal. This indicates that the optical property of the ELO layer is quite uniform over the stripe. The intensity of these spectra is as large as those of homoepitaxial grown ELO layers and FWHM of these spectra are also narrow. These large and narrow PL spectra show that InP ELO layers grown on InP-coated Si substrates have a good crystal quality as good as homoepitaxially grown layers. Moreover, the peak wavelengths of these spectra are about 882 nm, which is the same as those of InP homoepitaxial layers. Since there is no residual stress in homoepitaxially grown layers, the ELO layer is thought to be free from the stress which may be produced by both the lattice mismatch and the large difference in thermal expansion coefficient between InP films and a Si substrate.

The dependence of peak wavelength, FWHM and intensity of these SRPL spectra on their measured positions on the ELO surface are shown in fig.4.7 (a), (b) and (c), respectively. The peak wavelengths are 882$\pm$1 nm as shown in fig.4.7 (a). These emissions can be ascribed to a band edge emission from their wavelength. The good coincidence between these peak wavelengths and the band gap energy

of InP indicates that there is almost no residual stress in the layer. On the other hand, the PL peak wavelength of an InP-coated Si substrate was measured as 885 nm, which was about 3 nm longer than this value. The longer peak wavelength indicates the existence of tensile stress. Sugo et al. also reported the existence of tensile stress in a InP-coated Si substrate[9]. Figure 4.7 (b) shows that the FWHM of PL spectra is uniform and narrow (~23 meV) over the stripe. The intensity of PL spectra is also uniform as shown in fig.4.7 (c). These values are equvalent to that of the InP ELO layers homoepitaxially grown on InP substrates. These results show that almost all residual stress in the InP-coated Si layer is released in the InP ELO layer. The ELO structure is effective to decrease not only dislocations but also stress. Therefore, ELO is promising technique to fabricate III-V devices with excellent characteristics.

Though the above mentioned SRPL spectra are excellent, broad and weak SRPL spectra are obtained in some samples. A typical spectrum of this is shown in fig.4.8. An In solution was used as a solution and the growth conditions of this sample is almost the same as above mentioned one. They are as follows: T_s=550 °C, ΔT=0 °C R=0.08 °C/min, t_g=165 min; line seed with 7.5 μm width and 700 μm length. FWHM of this spectrum is more than 100 meV and peak wavelength is as short as 850 nm. This spectrum is inconsistent with above mentioned ones. There are two possible reasons for this broadening: one is large residual compressive stress and the other is unintentionally doping. In order to determine the mechanism of this broadening, the SiO_2 mask was removed with buffered HF (NH_4F:H_2O:HF=85 g: 56 ml:35 ml) for 2 days at room temperature. The elimination of SiO_2 mask will influence the residual stress in ELO layers since the InP ELO layer will be isolated from the InP-coated Si substrate. Figure 4.9 shows the cross sectional SEM photograph of the InP ELO layer after the elimination of SiO_2 mask. This figure shows that the SiO_2 mask under the ELO layer was perfectly eliminated. Figure 4.9 also shows the SRPL spectrum without SiO_2 mask, which is almost the same as the SRPL spectrum with SiO_2 mask. The elimination of SiO_2 mask made no change in SRPL spectra. Then, it is thought that the broadening

of SRPL spectra is caused by unintentionally doping and not by residual stress.

As mentioned above, high carrier concentration makes PL spectra shift and widen. Figure 4.10 shows a SRPL spectrum of highly Sn-doped InP layer, whose carrier concentration is more than 10^{19} cm^{-3}. The peak wavelength is about 800 nm and the FWHM of this spectrum is more than 300 meV. This is the typical example of the peak broadening and peak shifting caused by a high doping.

Here we will discuss about where the dopant comes from. Most possible candidate of this doping is the Si substrate as described in chapter 3. When the area of the substrate used in the experiment is smaller than the area of the well for the solution, the solution certainly touches the side of the Si substrate and Si dissolves into the solution to be doped into the ELO layer. To solve this problem, we used a large InP-coated Si substrate which was put the proper position not to touch the solution at both sides. When the position is not correct, the solution does not come the center of the substrate and touches either of the sides. Narrow and large SRPL spectra were obtained as shown previously in fig.4.6 without unintentionally doping.

4.5 SRPL of MQW

A multi quantum well (MQW) structure was fabricated on an InP ELO layer grown on an InP-coated Si substrate by using MOCVD. The MQW structure is shown in fig.4.11, which is almost the same as the laser structure except for doping.

SRPL of the MQW structure are shown in fig.4.12. Figure 4.12 (a) shows the dependence of the peak wavelength of SRPL spectra on the measured position on the ELO stripe. The peak wavelength is a little bit longer at the both sides of the stripe. This is probably due to the edge effect of the MOCVD growth, which brings a change in composition of the grown layers. Figure 4.12 (a) also shows that the peak wavelength of the center of the stripe is almost the same as that of a MQW structure grown directly on an InP substrate. This confirms the above speculation of the mechanism for the peak shift. Figure 4.12 (b) indicates that

the FWHM of the SRPL spectra of the MQW structure are almost uniform on the stripe, whose value is about 50 meV which is as narrow as that of the MQW structure grown directly on an InP substrate. Intensity dependence of the SRPL spectra on the measured position is shown in fig.4.12 (c). The intensities of the SRPL spectra from the MQW structure are equivalent to that of the layer grown directly on an InP substrate but the intensity increases at the right side of the stripe. The enhancement of the SRPL intensity is probably due to the reflection of the luminescence from the interface between the ELO layer and the SiO_2 film. The high reflection might enhance the intensity of the SRPL spectra at the right side of the stripe.

4.6 Stress Calculation by Finite Element Method

The stress in ELO layers was simulated using finite element method (FEM). The simulation was performed on a model ELO structure shown in fig.4.13. As ELO stripes have a uniform cross section in the stripe direction, plane strain conditions are realized. Therefore, only a two-dimensional finite element calculation is required to obtain a stress distribution in a ELO layer. As shown in fig.4.13 there is a ELO stripe on a InP-coated Si substrate, which consists of a 15 μm-thick InP buffer layer and a 500 μm-thick Si substrate. The surface of the InP-coated Si substrate is covered with a 0.1 μm-thick SiO_2 mask. There is a line seed opening, whose width is 2 or 6 μm, in the SiO_2 mask. A ELO layer, whose thickness and width are 10 μm and 200 μm, respectively, covers this line seed and the SiO_2 mask.

Fine element calculations[16] were performed by PC98 personal computer. The elastic constants used in the calculation were given in table 4.1.

Finite element meshes and their dimensions are shown in fig.4.14. The small elements were used around the line seed to increase the accuracy of the simulation. In this simulation, stress is assumed to be caused mainly by the difference in the thermal expansion coefficient between InP and Si. At growth temperature, all stress is assumed to be accommodated with the nucleation of misfit-dislocation at

Table 4.1: Elastic constants of materials

	InP	Si	SiO_2
E (Young's modulus)	0.7×10^{11} (N/m^2)	1.3×10^{11}	0.7×10^{11}
ν (Poisson's ratio)	0.3	0.28	0.2
$\Delta\alpha$ (Thermal expansion coefficient)	4.5×10^{-6} (K^{-1})	2.4×10^{-6}	0.5×10^{-6}

the interface between the InP-coated layer and the Si substrate. Then, stress is assumed to be produced by the cooling process from the growth temperature to room temperature. We assumed that the ELO structure was cooled from 550 °C to 0 °C during the cooling process. The SiO_2 mask is assumed to stick firmly to the InP layers.

Figure 4.15 shows the simulated stress in an ELO layer grown on an InP-coated Si substrate. In this figure, the length of the arrow indicates the strength of a stress and the direction of the arrowhead indicates whether the stress is compressive or tensile. The width of the line seed is 2 μm in fig.4.15 (a). There is compressive stress both in the ELO layer and in the InP buffer layer. This compressive stress is thought to be generated by a bi-metal action mainly caused by the difference in the thermal expansion coefficient between InP and Si. The compressive stress in the ELO layer shows a slight decrease in both sides. The decrease is due to the release of the stress at the corner of ELO. On the other hand, there is a large compressive stress near the line seed. The result suggests that the difference in elastic constants between InP and SiO_2 mask made large stress near the line seed. Besides this, there is a tensile stress in SiO_2 mask, which is thought to be caused by the difference in the thermal expansion coefficient between InP and SiO_2 mask.

Figure 4.15 (b) shows the simulated stress in an ELO layer grown on an InP-coated Si substrate with 6 μm-line seed. The stress distribution of this case is almost the same as the above mentioned case except the areas close to the line seed. These results suggest that not only line seed but also SiO_2 masks transmit

the stress of the InP buffer layer to the ELO layer. While the existence of the line seed effects the stress distribution only around it, the stress in the ELO layer apart from the line seed is transmitted through the SiO_2. Therefore, the increase in the width of line seed made small change in overall stress distribution and it caused increase of the stress only near the line seed.

Figure 4.16 (a) shows the contour of maximum principal stress, in the ELO layer grown from 2 μm-wide line seed and fig.4.16 (b) shows that of 6 μm-wide line seed. Here, maximum principal stress indicates the maximum stress on principal axes and the number in the figure indicates the strength of stress. These contours are almost equal except the area around the line seed below the SiO_2 mask. The result suggests that the change of the line seed width made small effect on the stress distribution in the ELO layer. The stress in the ELO layer is mainly determined by the stress transmitted from the InP buffer layer through SiO_2 mask. The assumption of no slip between the InP layers and the SiO_2 mask brings these results which contradicts with SRPL measurements. Moreover, the symmetries of these contours are not good as shown in fig.4.16 because the shape of the contours are influenced by the shape of meshes, which are triangular, used in these simulations.

As mentioned in previous section, SRPL results shows that there is almost no stress in ELO layers. Therefore, the experimented results are inconsistent with the FEM simulations. The inconsistency should be ascribed to the wrong assumption for the simulation. We assumed that there is no slip between the SiO_2 and the InP layers. The SiO_2 mask was deposited by a spin coating of OCD and an ELO layer only covers the SiO_2 mask during growth. Then, there is no guarantee in which the bonding between the SiO_2 mask and the InP layers is firm. Moreover, the elastic constants of SiO_2 mask may differ from the ideal ones, in other words, the SiO_2 mask may be softer than ordinary one because the SiO_2 mask was deposited by a spin coating. Therefore, the stress in ELO layers should be reduced by the slip between InP layers and the SiO_2 mask and/or the deformation of the SiO_2 mask. Then, we performed new stress calculation assuming that no stress was transmitted through SiO_2 mask, in other words, assuming that there was no SiO_2

mask between an InP buffer layer and an ELO layer. In this simulation, an ELO layer was divided into small meshes as shown in fig.4.17 to increase the accuracy of the simulation.

Figure 4.18 shows the simulated stress distribution in an ELO layer grown on an InP-coated Si substrate under the new assumption. The line seed width is 2 μm in fig.4.18 (a). While compressive stress exists in the InP buffer layer as described before, the stress in the ELO layer is very weak. Almost all stress in the InP buffer layer is thought to be released by this ELO structure. The result agrees well with the experiments. There is still a large compressive stress near the line seed. The deformation of this area absorbs the stress and relaxes the stress in the InP buffer layer. Figure 4.18 (b) shows the contour of the maximum principal stress in this ELO layer. The figure shows the relaxation of the stress. The stress near the line seed decreases drastically in the ELO layer. This stress becomes negligibly small within the distance of 3 μm. Except this region, almost no stress exists in the ELO layers. This contour is also not symmetrical because triangular meshes are also used in this simulation.

Figure 4.19 (a) shows the simulated stress in an ELO layer grown on an InP-coated Si substrate with 6 μm-wide line seed under the new assumption. The stress distribution of this result is almost the same as the above mentioned one except the areas close to the line seed. The area suffered from strong compressive stress is widened as the line seed width is increased. The result suggests that the change in the width of line seed only influenced the stress near the line seed and did not influenced the stress apart from the line seed. The contour of the maximum principal stress in the ELO layer with 6 μm-line seed is shown in fig.4.19 (b). This contour is almost equal to the result shown in fig.4.18 (b) but the stress region is expanded up to a distance of $\sim 5\mu$m. From this results, it can be said that the narrower the line seed is, the faster the stress decays in the ELO layer. Therefore, the narrower line seed is more effective to reduce residual stress in ELO layers.

4.7 Microchannel Epitaxy

We have so far shown that narrow line seeds bring decrease in residual stress in ELO layers. The density of dislocations originated from substrates also decreases with decreasing the width (W) of the line seeds. The number of dislocations passing through narrow line seeds is calculated as follows assuming the dislocation density (n_d) of a substrate is 1×10^7 cm^{-3}. The number of dislocations passed through a line seed per 1 cm which is given by $n_d W$ is 1000 for 1 μm-line seed. On the other hand, it is decreased to 1 for a 100Å-line seed. Almost all dislocations in ELO layers can be eliminated by using an extremely narrow line seed. Hereafter we call the extreme narrow line seed as "microchannel". Microchannel also relaxes residual stress in ELO layers, which is produced by both a lattice mismatch and the difference in thermal expansion coefficient between ELO layers and substrates. Moreover, microchannel can reduce or stop the formation of misfit dislocations at the heterointerface. We will discuss in the following about the critical width of line seeds above which misfit dislocations are introduced. Two examples, GaAs on Si and InP on Si are studied. At first, we estimate the critical thicknesses of these two heteroepitaxial systems on a flat substrate. The critical thickness (h_c) can be estimated from the equation reported by People and Bean[17]:

$$h_c \simeq (\frac{1-\nu}{1+\nu})(\frac{1}{16\pi\sqrt{2}})(\frac{b^2}{a})(\frac{1}{f^2})\ln(\frac{h_c}{b}), \qquad (4.2)$$

where ν is Poisson's ratio, b is slip distance, a is the bulk lattice constant of the film and f is the lattice mismatch. The constants used for the calculation are summarized in table 4.2. Substituting these constants in eq.(4.2), we get,

$$h_c \simeq 13.5\ln(\frac{h_c}{4.15}) \qquad \text{for GaAs/Si,} \qquad (4.3)$$

and

$$h_c \simeq 3.09\ln(\frac{h_c}{4.24}) \qquad \text{for InP/Si.} \qquad (4.4)$$

From above equations, h_c are calculated as 6.9 Å for GaAs/Si and as 5.0 Å for InP/Si, respectively. These critical thicknesses are very thin. Therefore, we can

Table 4.2: Material constance used in h_c calculation

Material	f	ν	a (Å)	b (Å)
GaAs/Si	0.041	0.31	5.65	4.15
InP/Si	0.081	0.36	5.87	4.24

not use so thin layer in ordinary applications, for examples, device fabrications. As ELO structure is thought to relax this limit, we will estimate the critical width of line seeds not to form misfit dislocation. The method reported by Luryi and Suhir[18] and Buryskiewicz[19] are used for the simulation.(See Appendix A.)

As the result, L_c for GaAs/Si = 440 Å and L_c for InP/Si = 40 Å are obtained. These values are much larger than the critical thickness (h_c) of the above mentioned for flat epitaxial layers. If we make a microchannel whose width is less than 440 Å, we can grow GaAs layers without misfit dislocations on Si substrates. A formation of this width of a microchannel is difficult but it is not impossible. A lithography with e-beam enables us to form lines whose width is less than 100Å. Moreover, even if we cannot get a microchannel which is as narrow as 440 Å, a narrow microchannel which is narrower than 1 μm will bring a low density of dislocations in an ELO layer. We can use a ELO structure as shown in fig.4.20, where the hight of the microchannel is larger than its width, to reduce residual stress and dislocation density effectively. To fabricate this structure, the narrow epitaxial layer, which is narrower than the thickness of the SiO_2 mask, is grown at first. These narrow stripes are not only useful to reduce residual stress but also useful to decrease dislocation density because most dislocations, which climb on (111) planes, can be eliminated by the shapes of this narrow stripes. Though some techniques should be developed to perform heteroepitaxial growth by LPE as shown in Appendix B, ELO technique gets more power to grow heteroepitaxial layers with excellent crystallinity by using microchannel.

4.8 Summary

Optical properties of ELO layers were studied by using SRPL technique. The optical properties of InP ELO layers grown homoepitaxially on InP substrates are as good as those of InP layers directly grown on InP substrates. The narrow SRPL spectra with high intensities were obtained, whose peak wavelength was the same as those of InP layers directly grown on InP substrates. The uniformity of the optical properties were also fine. This result suggests that there is almost no stress in InP ELO layers grown homoepitaxially on InP substrates. It seems that the stress caused by the difference in the thermal expansion between SiO_2 mask and InP layers is negligibly small. Though the purity of InP layers depends largely on the purity of the melt and source, the purification in LPE growth is also important to obtain high purity ELO layers with narrow FWHM.

The optical properties of InP ELO layers grown heteroepitaxially on InP-coated Si substrates are also investigated by SRPL. They are almost as good as those of InP ELO layers grown on InP substrates. Excellent and uniform optical properties of these layers indicates the stress in these ELO layers are also weak and these ELO layers are no less better than InP layers grown homoepitaxially on InP substrates on optical quality. This suggests that some mechanism acts to release residual stress in ELO layers. Occasionally a broad and weak SRPL spectrum was obtained, which was ascribe to the unintentional doping of Si from the Si substrate. To avoid this, In melt must be kept away from the Si substrate during growth.

A MQW structure was grown on an InP ELO layer grown on an InP-coated Si substrate to characterize the optical property. Though the MQW structure was suffered the edge effects of the MOCVD growth, the optical quality of the MQW structure is also as good as those grown on InP substrates. This result shows that these ELO layers are very promising for the use of optical devices because these layers can be expected to give excellent optical properties to the layers grown on them.

The stress in ELO structures were simulated using FEM. Then, the FEM

simulation was compared with the experimental results. As a result, there are possibly some mechanisms which release residual stress in ELO layers. The SiO_2 mask may slip from InP layers and the narrow line seed may release stress. The FEM simulation shows that the narrower the line seed is, the sooner the stress relaxes in the ELO layer. Therefore narrow line seed is a promising way to grow highly-mismatched (HM^2) heteroepitaxial layers.

To improve heteroepitaxial ELO, microchannel epitaxy is promising. Then we also discussed about microchannel epitaxy. Extremely narrow line seed brings not only both reduction of dislocation density and residual stress but also a perfect heterointerface without misfit dislocations. The critical width of microchannel which is necessary for the heteroepitaxial ELO not to form misfit dislocations is estimated by a theoretical simulation. The critical width for the GaAs ELO on Si substrates is obtained to be about 440 Å, which is able to be attained by an ordinary e-beam lithography.

Bibliography

[1] E.W.Williams, W.Elder, M.G.Astles, M.Webb, J.B.Mullin, B.Strraughan and P.J.Tuffton, J. Electrocehm. Soc. **120** (1973) 1741.

[2] M.Bugajski and W.Lewandowski, J. Appl. Phys. **57** (1985) 521.

[3] S.Zhang, Doctor Thesis

[4] S.Zhang and T.Nishinaga, Jpn. J. Appl. Phys. **29** (1990) 545.

[5] J.C.Hensel and G.Feher, Phys. Rev. **129** (1963) 1041.

[6] F.H.Pollak and M.Cardona, Phys. Rev. **172** (1968) 816.

[7] M.Chandrasekhar and F.H.Pollak, Phys. Rev. B **15** (1977) 2127.

[8] D.S.Wuu, R.H.Horng and M.K.Lee, Appl. Phys. Lett. **54** (1989) 2244.

[9] M.Sugo, N.Uchida, A.Yamamoto, T.Nishioka and M.Yamaguchi, J. Appl. Phys.**65** (1989) 591.

[10] O.Aina, M.Mattingly, J.R.Bates, A.Coggins, J.O'Connor, S.K.Shastry, J.P.Salerno, A.Davis, J.P.Lorenzo and K.S.Jones, Appl. Phys. Lett. **58** (1991) 1554.

[11] D.J.Olego, M.Tamura, Y.Okuno, T.Kawano and A.Hashimoto, J. Appl. Phys. **71** (1992) 4329.

[12] Zhe-chuan Feng and Hong-du Liu, J. Appl. Phys. **54** (1983) 83.

[13] K.Nakajima, J. Cryst. Growth **121** (1992) 278.

[14] J.R.Dixon and J.M.Ellis, Phys. Rev. **123** (1961) 1560.

[15] H.Asai and K.Oe, J. Appl. Phys. **54** (1983) 2052.

[16] Y.Ohura, K.Kobayashi and T.Kuroki, *CAE system of Finite Element Method* (Morikita Shuppan Co., Tokyo, 1993)

[17] R. People and J.C.Bean, Appl. Phys. Lett. **47** (1985) 322.

[18] S.Luryi and E.Suhir, Appl. Phys. Lett. **49** (1986) 140.

[19] T.Bryskiewicz, Appl. Phys. Lett. **66** (1995) 1237.

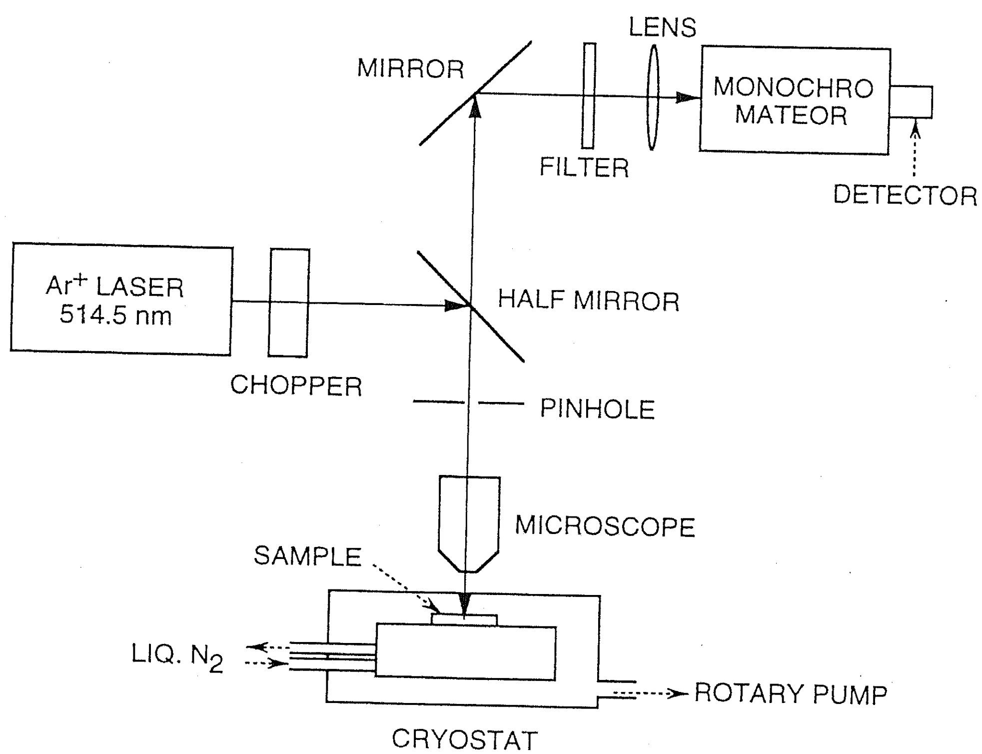

Figure 4.1: Schematic illustration of SRPL system.

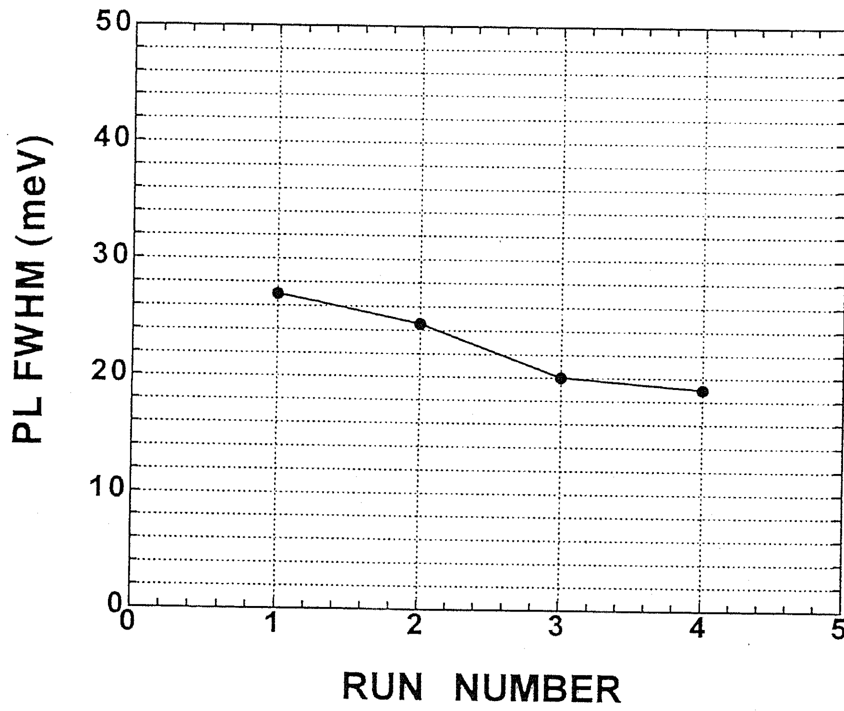

Figure 4.2: Run number dependence of FWHM of PL spectra.

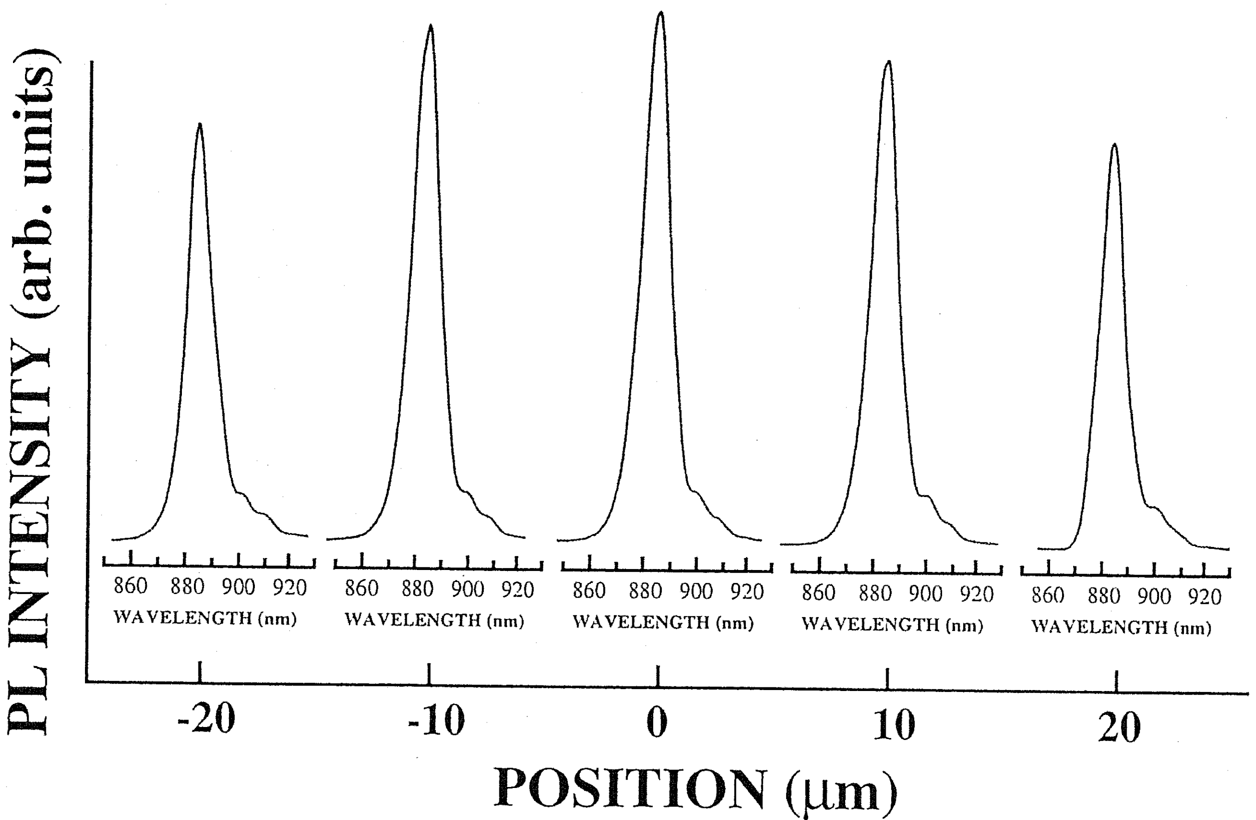

Figure 4.3: SRPL spectra of an InP ELO layer grown on a (001) InP substrate and their measured positions.

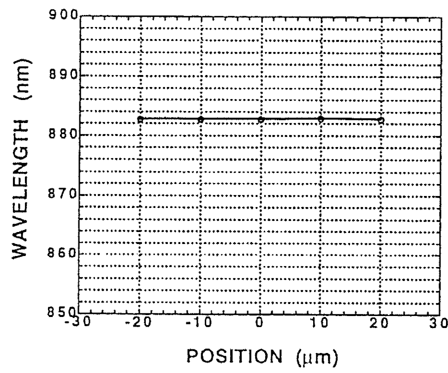

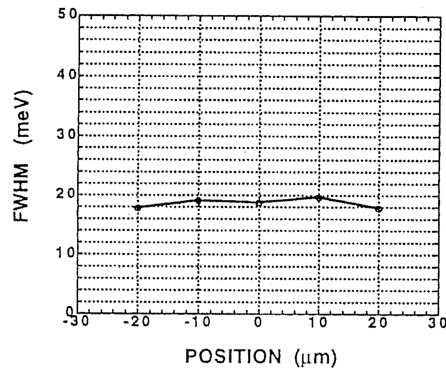

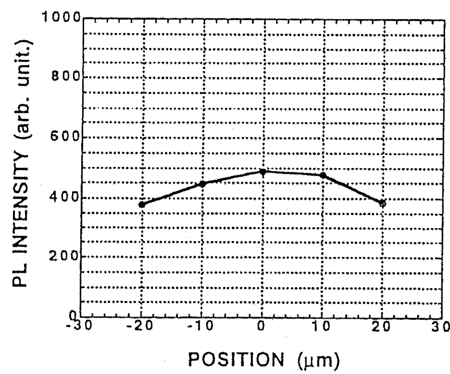

Figure 4.4: Dependence of (a) peak wavelength, (b) FWHM and (c) intensity of SRPL spectra on their measured positions on the ELO layer.

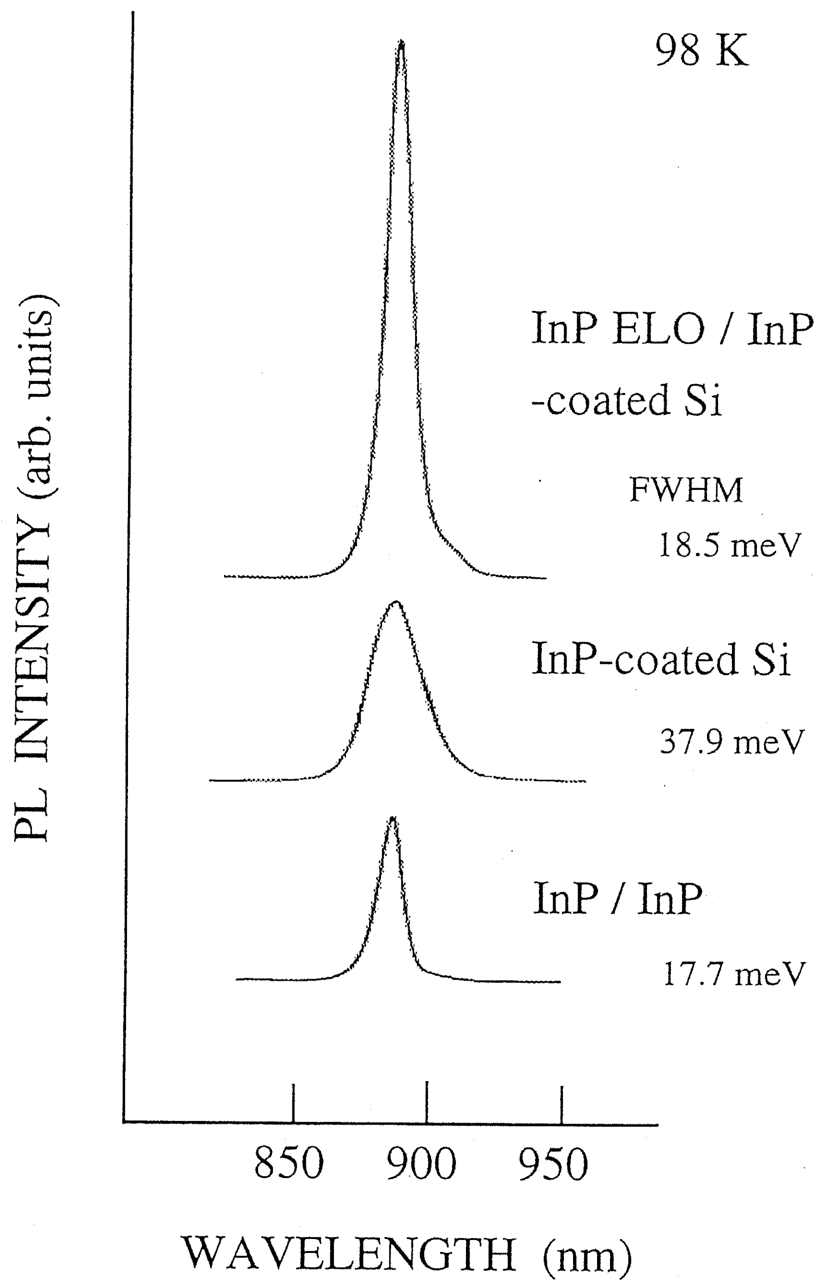

Figure 4.5: SRPL spectra at 98 K of InP ELO layer grown on an InP-coated (001) Si substrate, InP-coated Si substrate and homoepitaxial InP layer grown on a (001) InP substrate.

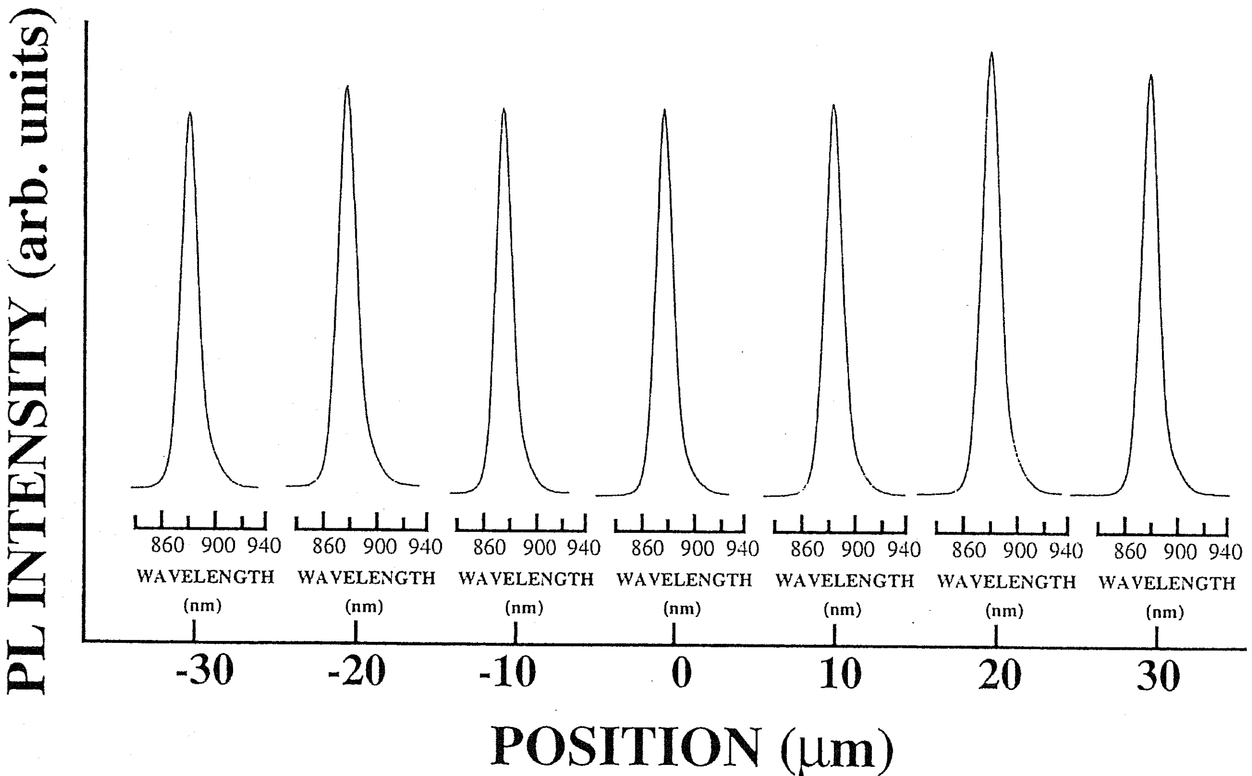

Figure 4.6: SRPL spectra of an InP ELO layer grown on a (001) InP-coated Si substrate and their measured positions.

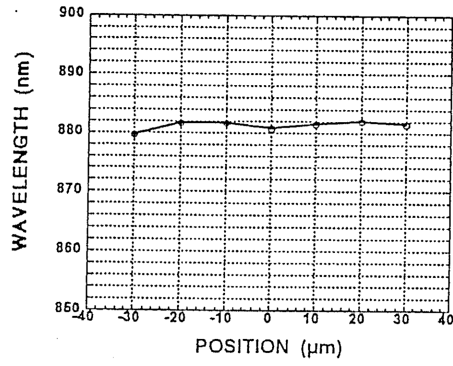

(a)

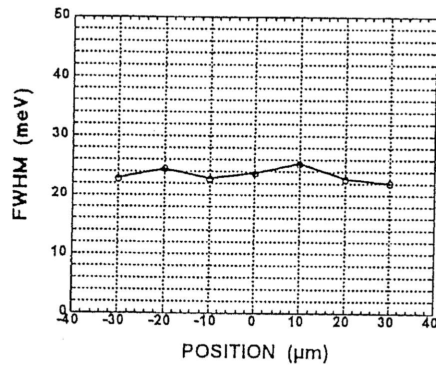

(b)

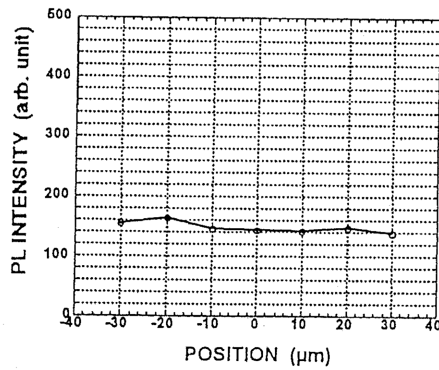

(c)

Figure 4.7: Dependence of (a) peak wavelength, (b) FWHM and (c) intensity of SRPL spectra on their measured positions on the ELO layer.

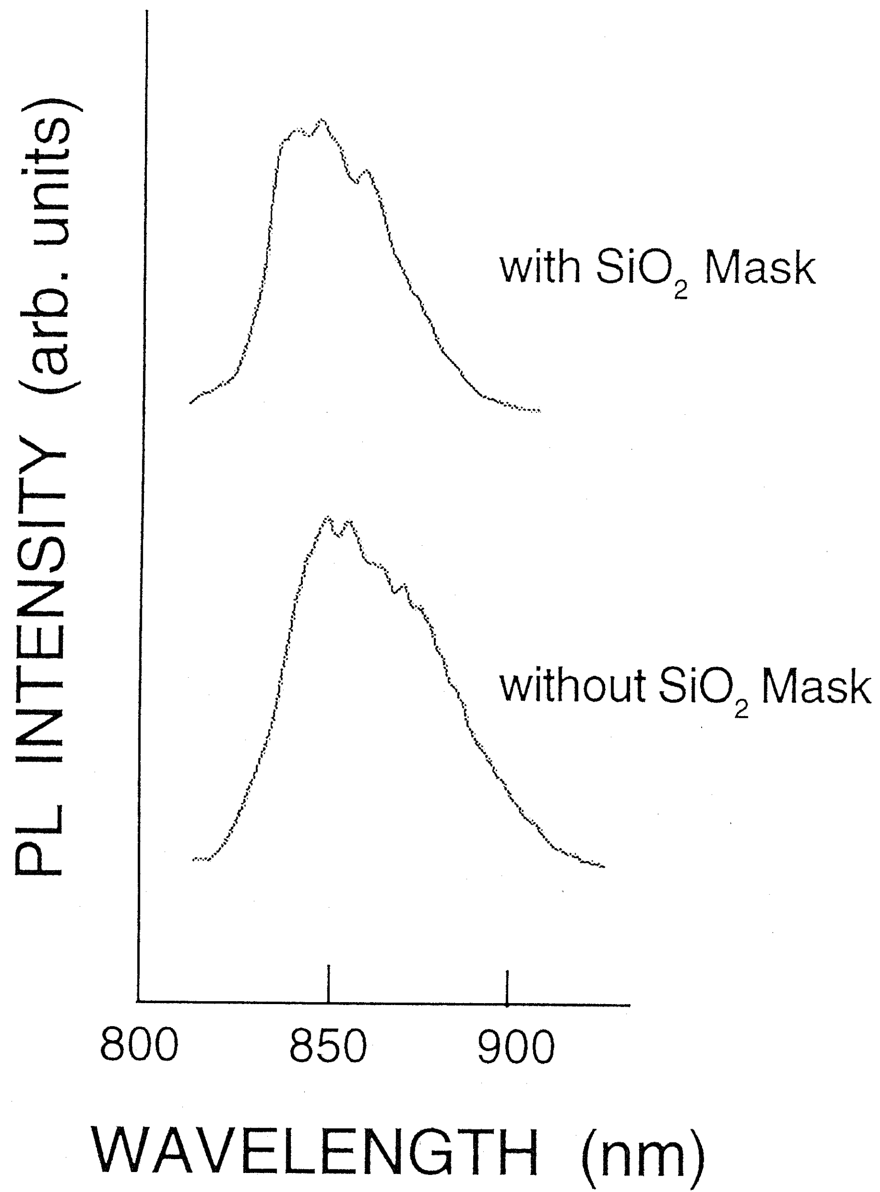

Figure 4.8: SRPL spectra of an InP ELO layer (a) with SiO_2 mask and (b) without SiO_2 mask.

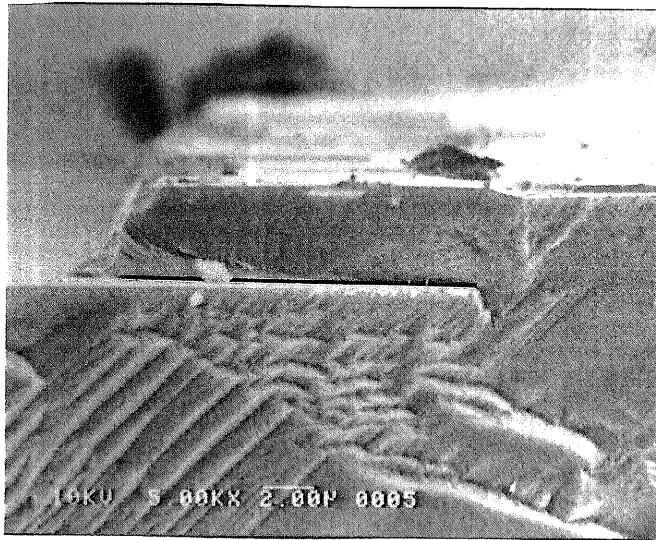

Figure 4.9: Cross-sectional SEM image of the InP ELO layer without SiO_2 mask shown in fig.4.8.

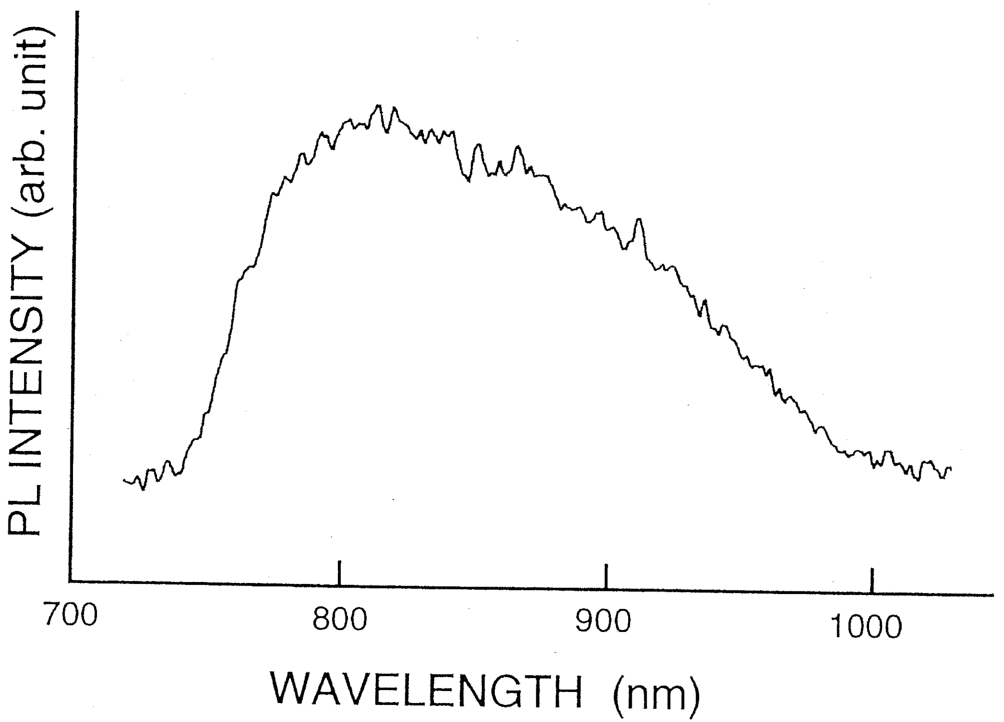

Figure 4.10: SRPL spectrum of an InP ELO layer grown with Sn doping.

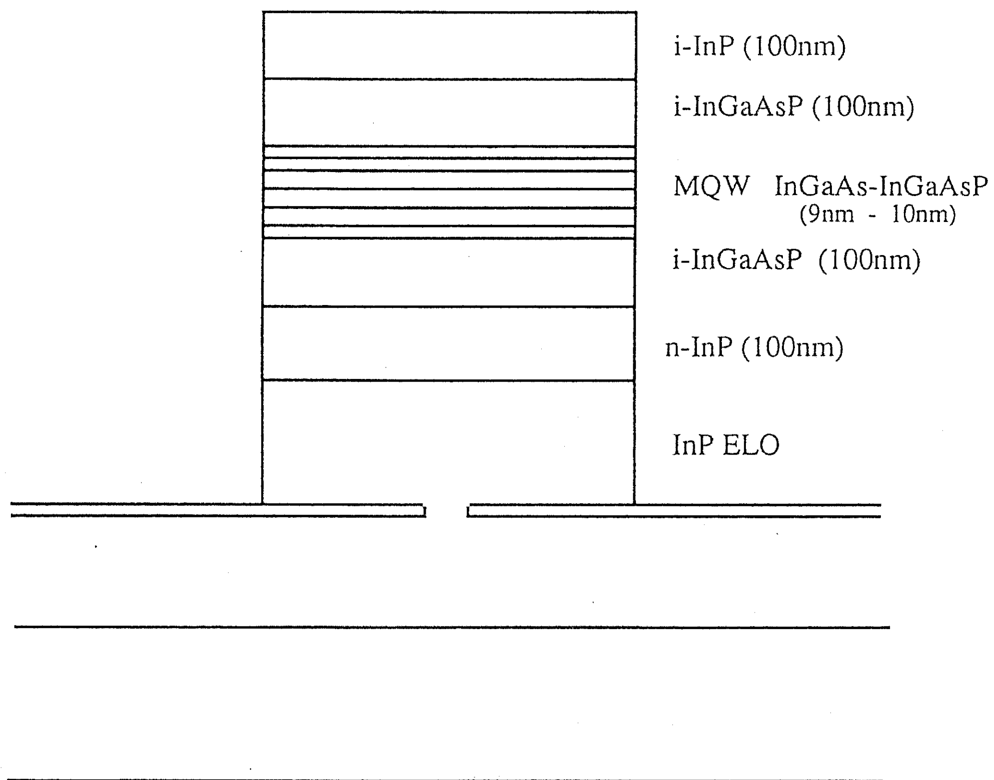

Figure 4.11: Schematic illustration of MQW structure.

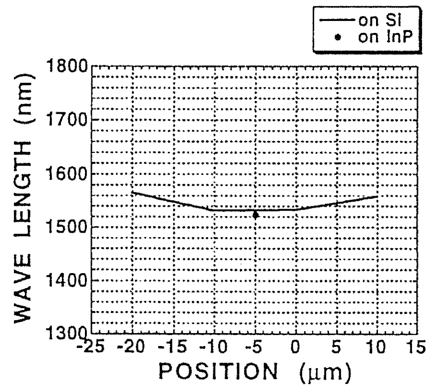

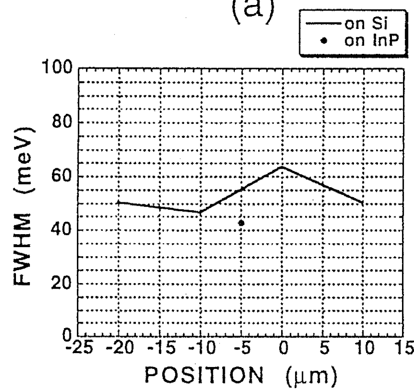

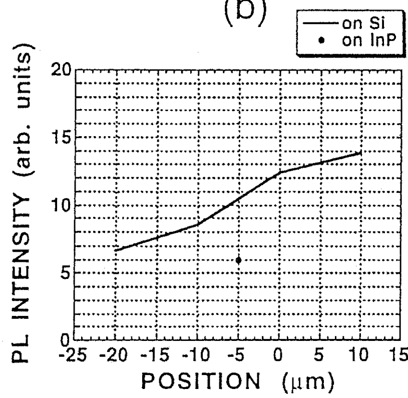

Figure 4.12: Dependence of (a) peak wavelength, (b) FWHM and (c) intensity of SRPL spectra of MQW on their measured positions.

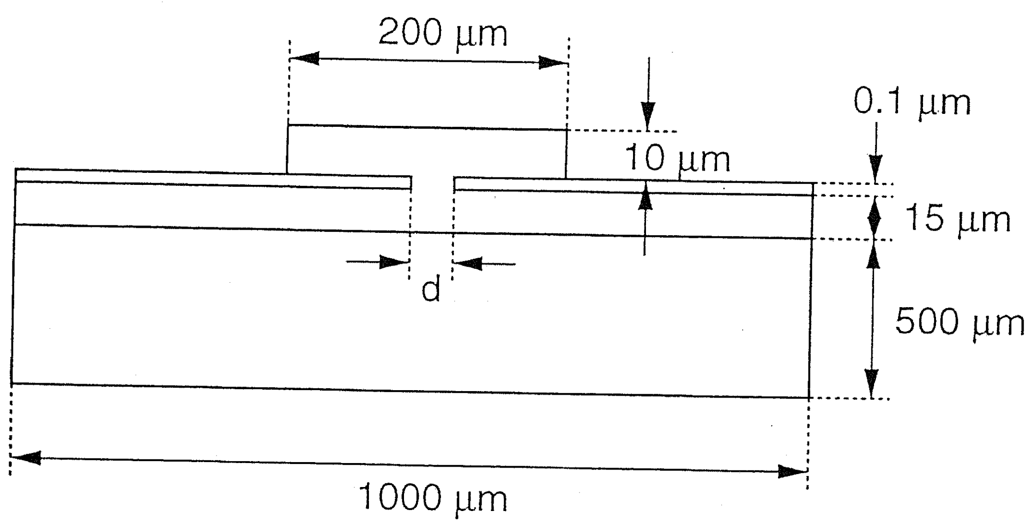

Figure 4.13: Schematic illustration of a model ELO structure used in calculation.

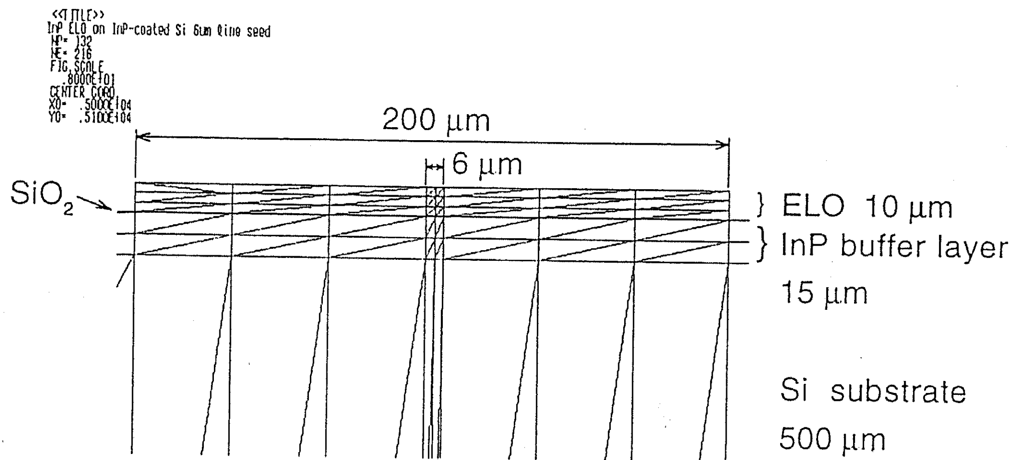

Figure 4.14: Schematic illustration of finite element meshes and their dimensions.

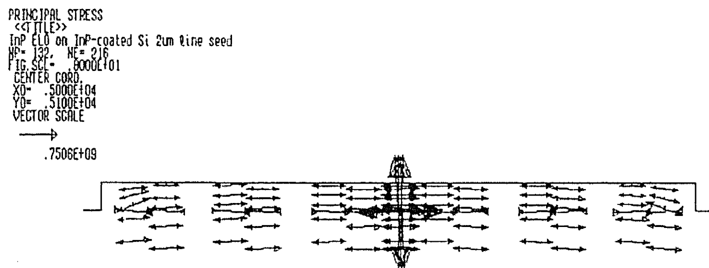

(a)

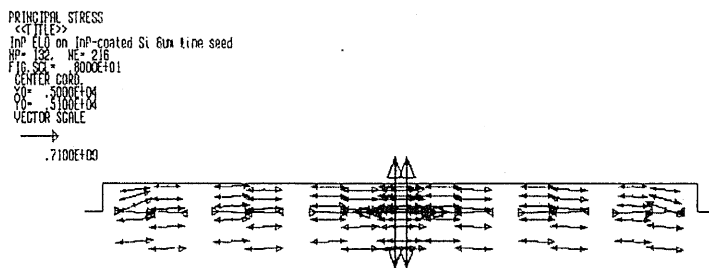

(b)

Figure 4.15: Simulated distribution of stress in an ELO layer grown on a (001) InP-coated Si substrate. The width of the line seed is 2 μm in (a) and 6 μm in (b). The length of the arrow indicates the strength of a stress and the direction of the arrowhead indicates whether the stress is compressive or tensile.

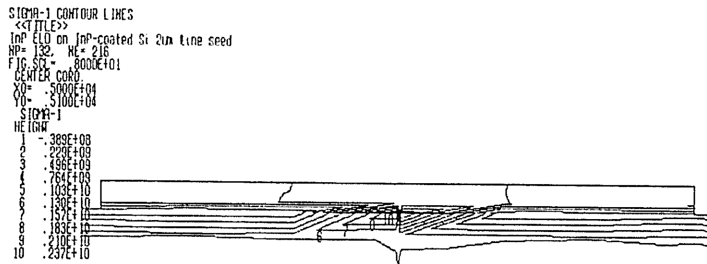

(a)

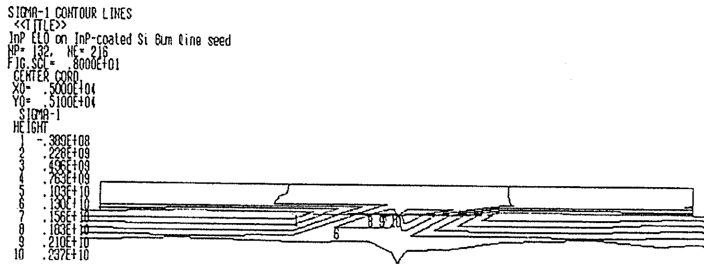

(b)

Figure 4.16: Simulated contour of maximum principal stress in an ELO layer grown on a (001) InP-coated Si substrate. The width of the line seed is 2 μm in (a) and 6 μm in (b).

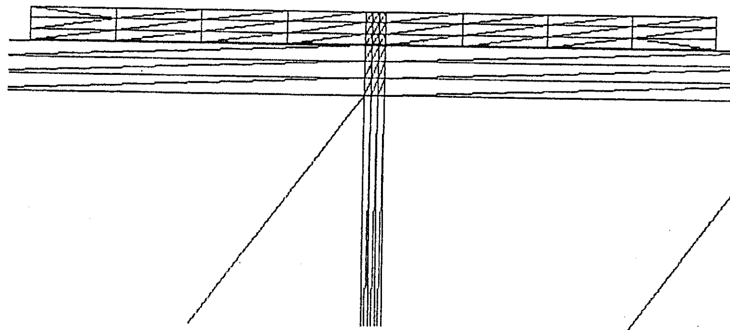

Figure 4.17: Schematic illustration of finite element meshes and their dimensions.

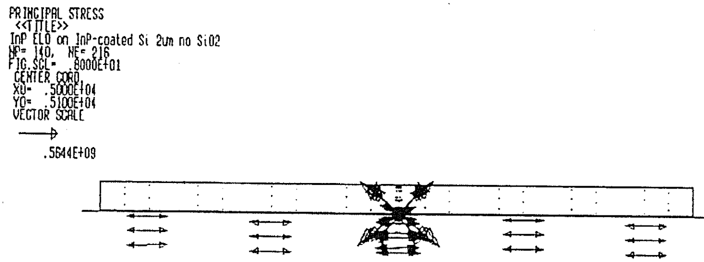

(a)

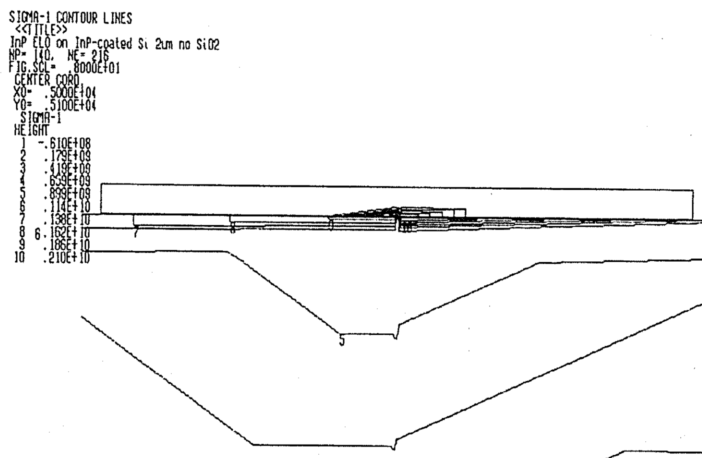

(b)

Figure 4.18: (a) Simulated distribution of stress and (b) simulated contour of maximum principal stress in an ELO layer grown on a (001) InP-coated Si substrate. The width of the line seed is 2 μm.

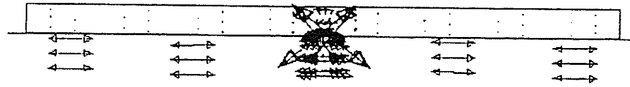

(a)

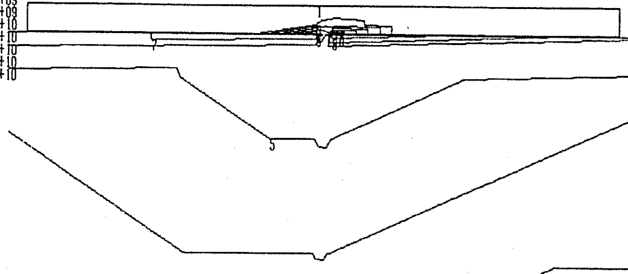

(b)

Figure 4.19: (a) Simulated distribution of stress and (b) simulated contour of maximum principal stress in an ELO layer grown on a (001) InP-coated Si substrate. The width of the line seed is 6 μm.

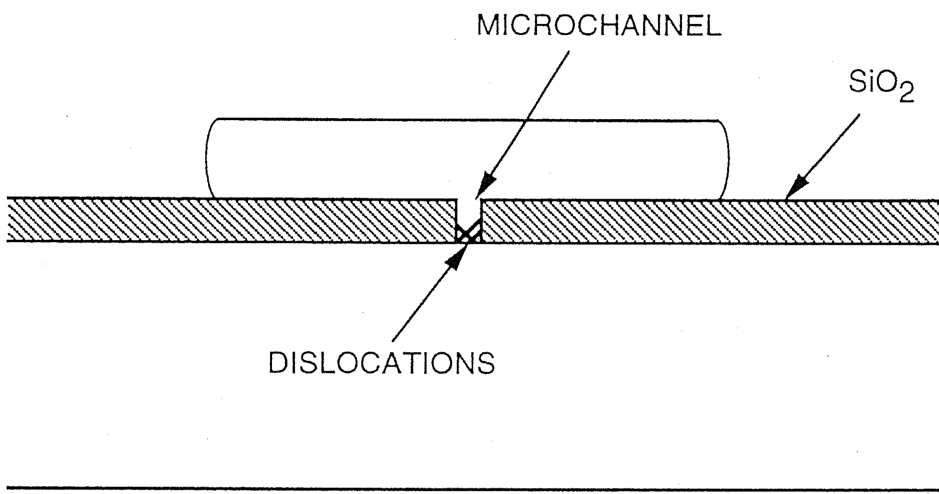

Figure 4.20: Schematic illustration of a ELO structure with a microchannel.

Chapter 5

Conclusions

In this thesis, ELO has been applied to InP growth on Si substrate to improve its crystallinity. Dislocation and stress-free InP layers with excellent optical properties have been obtained on Si substrates for the first time. The results obtained in this study are summarized as follows.

In chapter 2, a systematic investigation of the InP ELO by LPE has been conducted for the first time. A wide and flat ELO layer of InP on a (001) InP substrate can be achieved if the aligned seed is tilted away from the $\langle 100 \rangle$, $\langle 110 \rangle$ and their equivalent orientations. On the other hand, the lateral growth fronts are soon covered with $\{111\}$ and $\{001\}$ facets and the width of the lateral growth was minimum when the seed was aligned just in the above directions. It becomes clear that there was no etch pit on the lateral overgrowth regions except over the seed area. Nearly etch pit free lateral epitaxial layers of InP were also successfully obtained on (111)B InP substrates when a line seed was tilted away from the $\langle 110 \rangle$ and equivalent directions. On the other hand, the width of the lateral growth was minimum when it was aligned in the $\langle 110 \rangle$ and equivalent directions. It is concluded that ELO is an excellent method to obtain an extremely flat and dislocation-free epitaxial layer grown on insulator.

Surface steps of ELO layer were also studied by using N-DICM and AFM. Parallel steps and spirals were observed. These surface steps played an important role in ELO growth. The vertical growth rate was controlled by these steps. More-

over, AFM measurements show that these steps are monatomic in their height. To improve ELO ratio Sn-doping was used and a successful result was obtained.

In chapter 3, the procedure of ELO was modified suitable for InP-coated Si substrate, which has a slightly rough surface tilted 2° toward $\langle 1\bar{1}0 \rangle$ and InP ELO growth on InP-coated substrates was studied.

An InP epitaxial layer with a dislocation-free area was obtained for the first time on a Si substrate by using the ELO technique. The growth behavior of this ELO layer was found, in principle, to be similar to that of homoepitaxial growth of InP ELO. A wide and flat ELO layer of InP on a (001) InP-coated Si substrate can be achieved if the line seed is tilted around 15° away from $\langle 100 \rangle$, $\langle 110 \rangle$ and their equivalent directions. On the other hand, the lateral growth fronts are soon covered with $\{111\}$ and $\{001\}$ facets and the lateral growth is minimum when the line seeds are prepared almost exactly in the above directions.

Spirals of surface steps were observed on InP ELO layers grown on InP-coated Si substrates by N-DICM and AFM, as similar to the case of InP substrates. This indicates that ELO mechanism is almost the same in both two cases and atomically flat InP layers have been obtained on Si substrates for the first time.

The ELO ratio of InP ELO layers grown on InP-coated Si substrates can be increased by using doping. Sn doping was effective to increase ELO ratio, which was increased as large as 15. On the other hand, we should stop a Si unintentionally doping from Si substrates. If an In solution touches with the side of a Si substrate, Si is dissolved into the solution and the grown layer is doped. Though the Si doping also leads the increase in the ELO ratio, the increase can not be controlled. This unintentional doping can be avoided with the use of a large size InP-coated Si substrate, which is larger than the well size for the solution.

A small number of etch pits were observed on the lateral overgrowth regions and most of the etch pits were aligned in two lines on both sides of the line seed. This indicates that the SiO_2 film between the lateral overgrowth layer and the substrate can be useful to prevent the propagation of the dislocations from the

substrate to the ELO layer. ELO is an excellent method to obtain dislocation-free InP layers on Si substrates with extremely flat surfaces. Therefore InP ELO layers grown on Si substrates are expected to realize high performance of the devices fabricated on them.

In chapter 4, optical properties of ELO layers were evaluated by using SRPL technique. The optical properties of InP ELO layers grown homoepitaxially on InP substrates are shown as good as those of InP layers directly grown on InP substrates. The narrow SRPL spectra with high intensities were obtained, whose peak wavelength was the same as that of InP layers directly grown on InP substrates. The uniformity of the optical properties were also good. This result suggests that there is almost no stress in InP ELO layers grown homoepitaxially on InP substrates. It seems that the stress caused by the difference in thermal expansion between SiO_2 mask and InP layers is negligibly small. Though the purity of InP layers depends largely on the purity of the melt or source, the purification in LPE growth is important to obtain high purity ELO layers with narrow FWHM.

The optical properties of InP ELO layers grown heteroepitaxially on InP-coated Si substrates are also investigated by SRPL. They are almost as good as those of InP ELO layers grown on InP substrates. Excellent and uniform optical properties of these layers indicates the stress in these ELO layers are weak and the crystal quality of these ELO layers are equivalent to that of InP layers grown homoepitaxially on InP substrates. It is suggested that there is some unknown mechanism to release residual stress in ELO layers.

A MQW structure was fabricated on an InP ELO layer grown on an InP-coated Si substrate to characterize the optical property. Though the uniformity of the MQW was degraded by the edge effects of the MOCVD growth, the optical quality of the MQW structure is also as good as those grown on InP substrates. This result shows that these ELO layers are very promising for the use of optical devices because these layers can be expected to give excellent optical properties to the layers grown on them.

The stress in ELO structures were evaluated by using FEM simulation. By the simulation, a speculation is made on the mechanism by which the release of residual stress in ELO layers is made. The narrow line seed and the ELO structure itself may release stress. The FEM simulation shows that the narrower the line seed is, the shorter the stress relaxes in the ELO layer. Therefore it is thought that extremely narrow line seed is a promising way to grow highly-mismatched (HM^2) heteroepitaxial layers.

Extremely narrow line seed can also bring a growth of a perfect heterointerface without misfit dislocations. The critical width of microchannel which is necessary not to form misfit dislocations during heteroepitaxial ELO is estimated by a theoretical simulation. The critical width of microchannel for GaAs ELO on Si is about 440 Å, which is able to be attained by an ordinary e-beam lithography.

Although this work is only one step towards the final goal for the heteroepitaxial growth and the fabrication of OEICs, the author truly hopes this work may throw some light on the fields.

Appendix A

Critical Width for Michrochannel

Luryi reported a new approach to simulate the critical width of a structure illustrated in fig.A.1[1]. Since this structure is similar to ELO structure, critical width of microchannel can be calculated by this method. In a film loaded with a misfit strain f along a segment (-l,l) in y direction, the normal stress $\sigma_y \equiv \sigma$(y,z) can be approximately expressed in the form

$$\sigma(y,z) = f\frac{E}{1-\nu}\chi(y,z)e^{-\pi z/2l}, \tag{A.1}$$

where E is the young modulus of the film and the function χ, which characterizes the lateral stress distribution, is given by

$$\chi(y,z) = \begin{cases} 1 - \frac{\cosh ky}{\cosh kl} & z \leq h_e \\ 1 & z > h_e, \end{cases} \tag{A.2}$$

where h_e is the characteristic length of the decay of the stress. The interfacial compliance parameter k can be estimated by the following formula:

$$k = (\frac{3}{2}\frac{1-\nu}{1+\nu})^{1/2}\frac{1}{h_e} \equiv \frac{\zeta(\nu)}{h_e}. \tag{A.3}$$

For GaAs/Si ($\nu \approx 0.31$) and InP/Si ($\nu \approx 0.36$) one has $\zeta \approx 0.89$ and 0.84, respectively.

The maximum strain energy density per unit area is in the middle of the contact zone and is given by

$$\epsilon_S = \int_0^h \frac{E}{1-\nu}\sigma^2(0,z)dz \equiv \frac{E}{1-\nu} f^2 h_e. \quad \text{(A.4)}$$

In the integral in eq.A.4 we can extend the form of χ given by the top line of eq.A.2 to all values of z, since the range of $z > h_e$ gives a negligible contribution to the integral. The second equation in eq.A.4 defines h_e, viz.,

$$h_e = h[(1 - \text{sech}\frac{\zeta l}{h_e})^2(1 - e^{\pi h/l})\frac{l}{\pi h}]. \quad \text{(A.5)}$$

It can be seen from A.5 that h_e varies from $h_e \approx h$ when $h \ll l$ to

$$h_e = \frac{l}{\pi}[1 - \text{sech}(\zeta\pi)]^2 \equiv \frac{\xi^2 l}{\pi} \qquad h \gg l, \quad \text{(A.6)}$$

where for GaAs/Si $\xi \approx 0.878$ and InP/Si $\xi \approx 0.856$, respectively.

Following People and Bean[2], we can find the critical h (which we denote by h_c^l) for generating plasticity effects by comparing eq.A.4 with the areal energy density ϵ_D associated with a single linear dislocation located at a distance h from the free surface of the film,

$$\epsilon_D = \frac{E}{2(1+\nu)}\frac{b^2}{10\pi a\sqrt{2}}\ln\frac{h}{b}, \quad \text{(A.7)}$$

At critical thickness, $\epsilon_S = \epsilon_D$. In the limit $h \gg l$, substituting l instead of h in eq.A.7, using eq.A.6 in eq.A.4, we obtain

$$\frac{(\xi f)^2}{\pi} l \approx \frac{1-\nu}{1+\nu}\frac{1}{20\pi\sqrt{2}}\frac{b^2}{a}\ln\frac{l}{b}, \quad \text{(A.8)}$$

which is an equation determining $l = l_{min}$. We see that eq.A.8 is of the form of the People-Bean equation 4.2, but with a reduced $f_{eff} = \xi f/\sqrt{\pi}$. It follows that the value of l_{min} is given by

$$l_{min}(f) = h_c(\xi x/\sqrt{\pi}). \quad \text{(A.9)}$$

Then the critical width of the microchannel $L_c = 2l_{min}(f)$ is calculated by using material parameters. As the result, L_c for GaAs/Si = 440 Å and L_c for InP/Si = 40 Å are obtained.

Bibliography

[1] S.Luryi and E.Suhir, Appl. Phys. Lett. **49** (1986) 140.

[2] R. People and J.C.Bean, Appl. Phys. Lett. **47** (1985) 322.

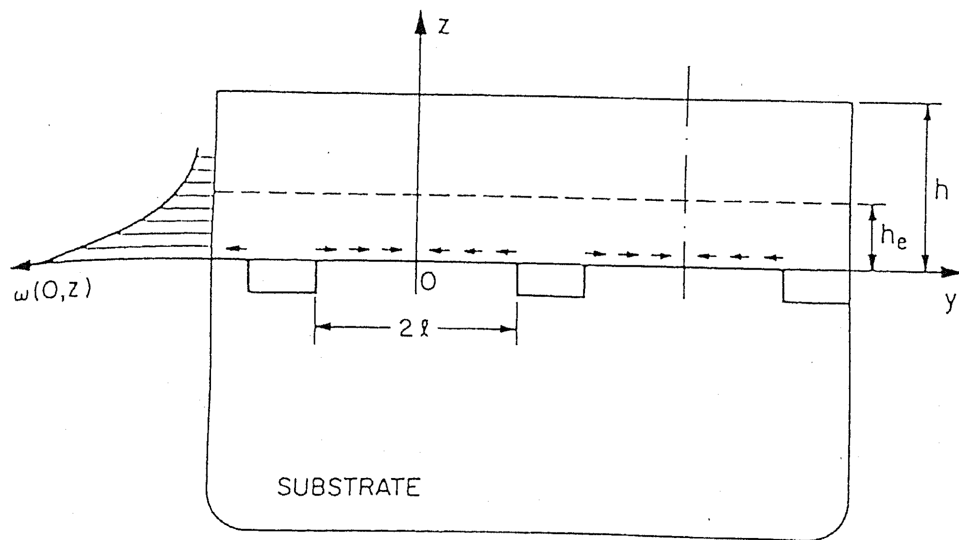

Figure A.1: Schematic illustration of the discontinuous boundary value problem.

Appendix B

Heteroepitaxial ELO of InP on InGaAs Layers

Heteroepitaxial ELO, which means an ELO growth of a material which is different from the substrate, is an important application field of ELO. In performing a heteroepitaxial ELO by LPE, a melt back is a major problem. An InP-coated Si substrate has been used so far to avoid the melt back of a Si substrate in the growth of InP ELO on Si. On the other hand, no buffer layer will be used in heteroepitaxial ELO. Therefore, a suppression of a melt back is a key technology for heteroepitaxial ELO.

Heteroepitaxial ELO has very wide application fields. Heteroepitaxial ELO is useful not only to reduce dislocation density but also to release residual stress originated from the lattice-mismatch and the difference in the thermal expansion coefficient between an ELO layer and a substrate. Moreover, heteroepitaxial ELO has big freedom in the choice of both an ELO layer and a substrate.

In this appendix, we describe a preliminary study about InP heteroepitaxial ELO on InGaAs layers. Two kinds of substrates were used to grow InGaAs layers. One is InP substrate with a 1.5 μm-thick InGaAs lattice-matched buffer layer. The other is Si substrate. To grow InGaAs layers on the latter substrate, a GaAs buffer layer with a super lattice (SL) or grading (GR) buffer layer was used. Moreover, the use of Si substrates has another important meaning. In InP ELO growth,

we use InP-coated Si substrates, which were supplied from NTT, to suppress the melt back. Though a low misorientation of substrates is beneficial for ELO to enlarge its width, this is prevented by the formation of high density of surface defects. Therefore, 2 ° off Si substrates must be used. If heteroepitaxial InP ELO on InGaAs can be performed, InGaAs will be used as a buffer layer which can be grown on 0.3 ° off epi-Si substrate and we will be able to grow all layers in our laboratory.

InGaAs growth on InP substrates is investigated at first. InP substrates are easily degraded since the vapor pressure of P is very high even at low temperature. Therefore, the substrate temperature must be quickly increased and the substrate surface must be protected by the irradiation of As beam when the surface oxide is removed. The condition for lattice match was obtained by changing the Ga cell temperature while the In cell temperature stayed constant. Figure B.1 shows surface morphologies and X-ray diffraction curves of 1.5 μm-InGaAs layers grown on (001) InP substrates at 500 °C in the vicinity of lattice-matched conditions. In the lattice-matched condition, the surface is very smooth and the X-ray diffraction curve from the InGaAs layer perfectly coincides with that of the InP substrate. In a Ga-rich condition, the surface has rough and wavy morphology, which can be ascribed to the formation of the misfit dislocations. The wide X-ray diffraction of this layer indicates that the composition of this layer is not uniform. A peak shift of the X-ray diffraction peak from a reference peak of InP substrate ($\Delta\theta$) of 1380" means 0.73 % Ga-rich condition. This figure also shows In-rich case. Since the lattice mismatch is as small as 0.10 %, the surface morphology is mirror-like.

InGaAs layers were also grown on Si substrates as previously shown. Two types of buffer layers were used. One is SL buffer layer and the other is GR buffer layer. The surface morphology and X-ray FWHM of the InGaAs layers grown with GR buffer layers are better than those of the InGaAs layers grown with SL buffer layers in our experiments. This is probably because the structure and the growth condition for the SL buffer layer were not optimized. Therefore, we use the GR buffer layers in the following experiments. The structure and the surface

morphology of a InGaAs layer grown on a Si substrate are shown in fig.B.2. This sample consists of a 0.1 μm GaAs buffer layer grown at 540 °C, a grading buffer layer, whose InAs content was gradually increased from 0 to 0.53, and a 2 μm InGaAs layer grown at 390 °C. The FWHM of the this sample is about 750" and the surface morphology is a little rough.

Heteroepitaxial ELO of InP was performed using an InGaAs buffer layer grown on an InP substrate. As shown in fig.B.3 a melt back of an InGaAs buffer layer was occurred in an ordinary growth condition. Almost all InGaAs buffer layer was melted off even in the regions where the InGaAs buffer layer was covered with a SiO_2 mask. The decrease of the growth temperature down to 350 °C is of no use to suppress the melt back. Thereby we change the melt from In to Sn because the supersaturation can be drastically increased by using Sn

Figure B.4 shows an InP layer grown on an InGaAs-coated InP substrate. The growth conditions were as follows: Sn melt; Ts=450 °C, ΔT=15 °C, R=0.3 °C/min, tg=5 min. The surface morphology of this layer shown in fig.B.4 (a) shows that no melt back was occured. Conical shapes are also observed, which indicate the existence of defects which lead the growth. Figure B.4 (b) shows the cross section. A 2.4 μm flat InP was grown on the InGaAs-coated InP substrate. A flat interface between the InP layer and the InGaAs layer suggests that no melt back occurred during the LPE growth. The use of a Sn melt brings no melt back of the InGaAs layer. Then we use this growth condition to grow an InP ELO layer on an InGaAs-coated InP substrate. The width of line seed is 2.5 μm and the period of them is 50 μm. The N-DICM photograph of the InP ELO layer grown on an InGaAs-coated InP substrate is shown in fig.B.5. This figure shows that ELO stripes are not strait and there are a lot of stacking faults (SF) on the stripes. The probable cause for SF is Sn-high doping. It is reported that Si high-doping brings SF in GaAs ELO layers[1]. The similar phenomenon may take place in the InP ELO growth on InGaAs since the Sn melt brings high doping of 10^{20} cm^{-3}. The imperfect shape of ELO stripes is possibly caused by the incompleteness of the removal of the surface oxide on the line seeds. As the etching rate of InGaAs is fast,

only 2 seconds H_2SO_4:H_2O_2:H_2O=5:1:1 etching at 28 °C was performed before the ELO growth. This short time of the etching might bring the incompleteness in the removal of oxide. A predeposition of 5800 Å also cause difficulties, for examples, a melt back of the surface of InGaAs layer, the growth of In-rich InGaAs layer at the first stage of the ELO. In order to know whole mechanism of this degradation, more detailed study is needed.

Bibliography

[1] Wu-yih Uen, Doctor Thesis (1993).

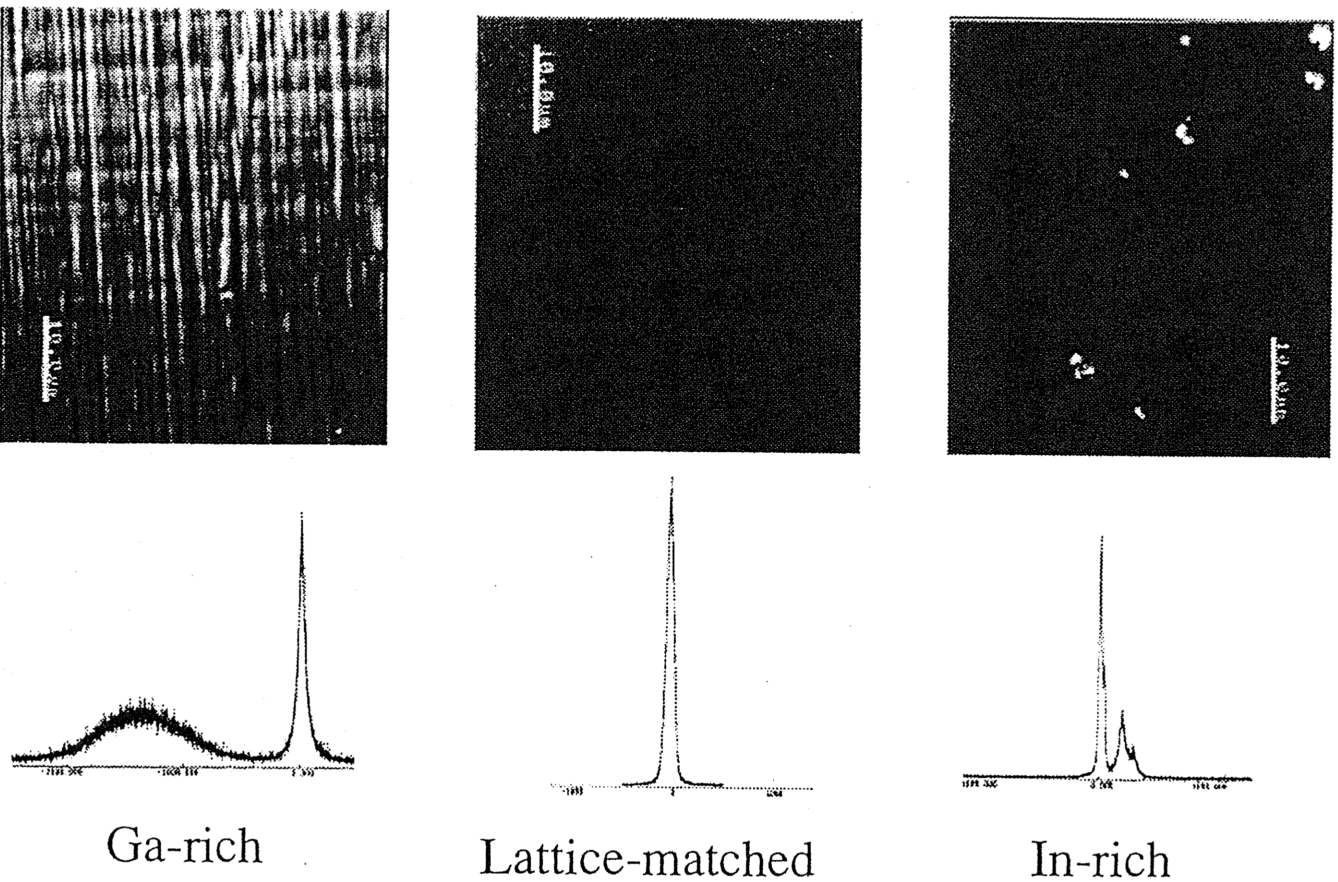

Figure B.1: Surface morphologies and X-ray diffraction curves of InGaAs layers grown on InP substrates.

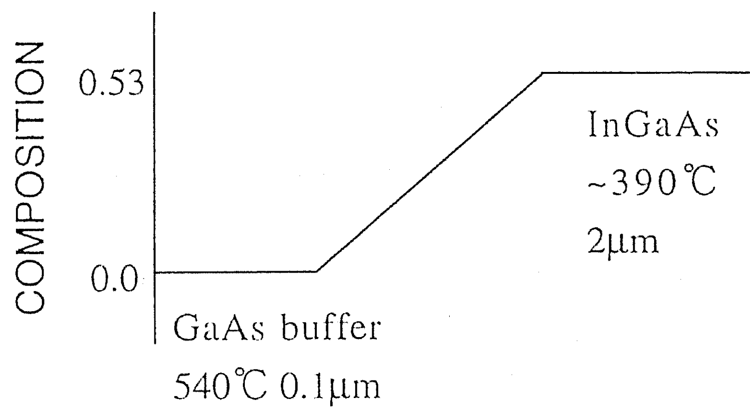

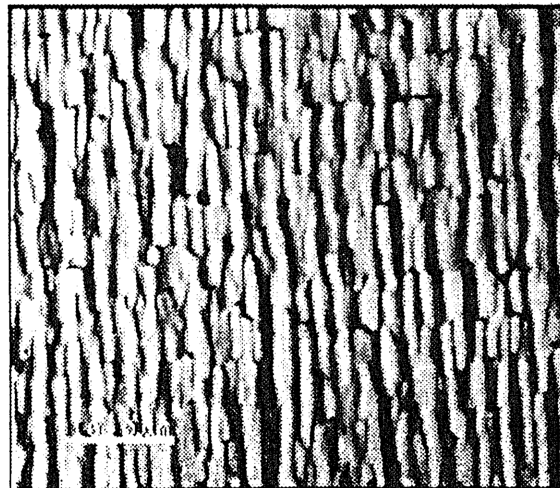

Figure B.2: Schematic illustration of a layer structure of a InGaAs layer grown on (001) Si substrate with a graded buffer layer and the surface morphology.

Figure B.3: Surface morphology of an InP layer grown on an InGaAs-coated (001) InP substrate.

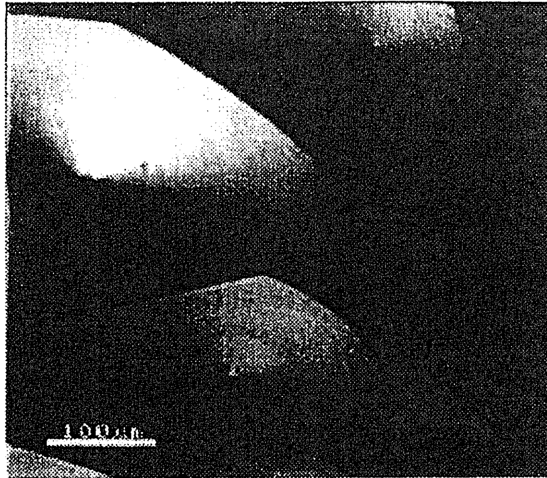

(a)

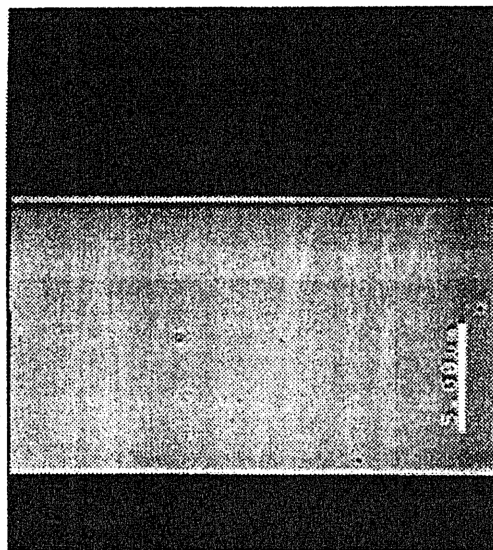

(b)

Figure B.4: (a) Surface morphology and (b) cross-section of an InP layer grown on an InGaAs-coated (001) InP substrate.

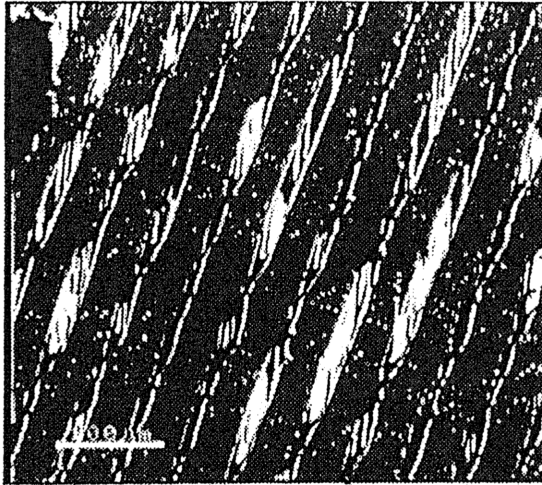

Ts=450℃
ΔT=15℃
R=0.3℃/min
tg=5min

(a)

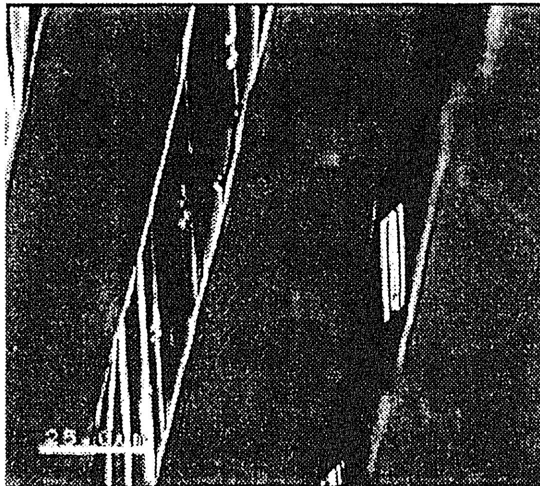

(b)

Figure B.5: (a) Surface morphology and (b) cross-section of an InP ELO layer grown on an InGaAs-coated (001) InP substrate.

Publication List

1. S.Naritsuka and T.Nishinaga,"Epitaxial lateral overgrowth of InP by liquid phase epitaxy" J. Cryst. Growth **146** (1995) 314.

2. S.Naritsuka, T.Nishinaga, M.Tachikawa and H.Mori, "InP Layer Grown on (001) Silicon Substrate by Epitaxial Lateral Overgrowth" Jpn. J. Appl. Phys. **34** (1995) L1432.

3. S.Naritsuka and T.Nishinaga,"Epitaxial lateral overgrowth of InP", The eighth international conference on vapour growth and epitaxy, Freiburg, Germany, July 24-29, 1994, LP11.

4. S.Naritsuka and T.Nishinaga,"Reduction of defects and stress in InP grown on (001) silicon substrate by Epitaxial Lateral Overgrowth" The 14th Electronic Materials Symposium, Izu-Nagaoka, July 5-7, 1995, E-10.

5. S.Naritsuka and T.Nishinaga, "Spatial resolved photoluminescence measurements of InP epitaxial lateral overgrowth layers grown on InP-coated Si" in preparation

International Conference

1. S.Naritsuka and T.Nishinaga, 8th International Conference on Vapour Growth and Epitaxy, 1994, Germany.